2000

Activation and Metabolism of P-Nitrosophenoland 2,2'-Thiobis-Ethanol by Horse Liver and Human Alcohol Dehydrogenase: Toxicological Implications.

Billy Fred Dudley Jr
Louisiana State University and Agricultural & Mechanical College

INFORMATION TO USERS

This manuscript has been reproduced from the microfilm master. UMI films the text directly from the original or copy submitted. Thus, some thesis and dissertation copies are in typewriter face, while others may be from any type of computer printer.

The quality of this reproduction is dependent upon the quality of the copy submitted. Broken or indistinct print, colored or poor quality illustrations and photographs, print bleedthrough, substandard margins, and improper alignment can adversely affect reproduction.

In the unlikely event that the author did not send UMI a complete manuscript and there are missing pages, these will be noted. Also, if unauthorized copyright material had to be removed, a note will indicate the deletion.

Oversize materials (e.g., maps, drawings, charts) are reproduced by sectioning the original, beginning at the upper left-hand corner and continuing from left to right in equal sections with small overlaps.

Photographs included in the original manuscript have been reproduced xerographically in this copy. Higher quality 6" x 9" black and white photographic prints are available for any photographs or illustrations appearing in this copy for an additional charge. Contact UMI directly to order.

Bell & Howell Information and Learning
300 North Zeeb Road, Ann Arbor, MI 48106-1346 USA
800-521-0600

UMI®

ACTIVATION AND METABOLISM OF *P*-NITROSOPHENOL AND 2,2'-THIOBIS-ETHANOL BY HORSE LIVER AND HUMAN ALCOHOL DEHYDROGENASE: TOXICOLOGICAL IMPLICATIONS

A Dissertation

Submitted to the Graduate Faculty of the
Louisiana State University and
Agricultural and Mechanical College
in partial fulfillment of the
requirements for the degree of
Doctor of Philosophy

in

The Department of Biological Sciences

by
Billy F. Dudley, Jr.
B.S., Louisiana State University, 1991
May 2000

ACKNOWLEDGMENTS

In acknowledging those who have given me great support and direction during my graduate career, I would first like to thank Dr. Gary Winston. While serving as my advisor, Dr. Winston was encouraging and showed great patience and effort in helping me to achieve my goals. In addition to Dr. Winston, I would like to thank the members of my graduate committee, Dr. Grover Waldrop, Dr. Barbara Shane, and Dr. Ezzat Younathan, for their help towards completion of my research and the requirements for the degree. Dr. Andy Deutsch was also instrumental in guiding me in the pursuit of my doctoral degree. I would like to also express my appreciation to Dr. Harold Silverman, Dr. Terry Bricker, and the faculty of the Department of Biological Sciences for their help in providing support, lab space, and equipment after my advisor moved to North Carolina. In particular, I'd like to thank Dr. Waldrop and the members of his lab for tolerating my frequent invasion of their lab space. I would also like to thank Dr. Thomas Hurley and Dr. William Bosron for providing purified human alcohol dehydrogenase during much of my graduate career.

There have been many people during the years who have had positive influence on my life, but few more than my friends in the lab and department. The members of the Winston Lab, Jose Castaneda, John Dugas, Susan Dobias, Robin Ertl, Robin Ertl, Zofia Maskos, Max Mayeaux, Caroline Metosh-Dickey, and Alex Tkachenko, have made many times enjoyable and have helped to keep me focused. I would especially like to acknowledge my lab mate, Linda Heffernan, for her freindship and help over the years.

Lastly I would like to thank my family for the love and support that they've given my over the years. My mother and brother Brice Dudley have been tremendous

sources of strength in helping to achieve my goals. And I thank my best friend David West for being an ear that listened when I was enjoying my work and when I wasn't. I am grateful to them all.

TABLE OF CONTENTS

LIST OF TABLES

LIST OF FIGURES

LIST OF ABBREVIATIONS

ADH	alcohol dehydrogenase
BQI	1,4-benzoquinoneimine
DC	dicumarol
DEA	diethanolamine
EDTA	ethylenediaminetetraacetic acid
HLADH	horse liver alcohol dehydrogenase
HLC	human liver cytosol
MES	2-(N-morpholino)ethanesulfonic acid
NAD^+	β-nicotinamide adenine dinucleotide
NADH	β-nicotinamide adenine dinucleotide, reduced
NADPH	β-nicotinamide adenine dinucleotide phosphate, reduced
NEA	N-ethylmorpholine
NQOR	NAD(P)H: quinone oxidoreductase
*p*AP	*p*-aminophenol
*p*N-OHAP	*p*-N-hydroxyaminophenol
*p*NSP	*p*-nitrosophenol
PDB	protein data bank
PYR	pyrazole
SD	standard deviation
TDG	thiodiglycol
Tris	tris(hydroxymethyl)aminomethane

ABSTRACT

C-nitroso compounds are reactive intermediates in the toxic sequelae of nitroarene metabolism. Alcohol dehydrogenase (ADH) contributes significantly to NADH-dependent C-nitroso reduction by cytosol relative to NAD(P)H: quinone oxidoreductase (NQOR). NADPH-dependent *p*NSP reduction by liver cytosol of ADH^+ animals is mostly dicumarol-sensitive which implicates NQOR as the major NADPH-dependent activity.

Although, extensive structural homology between horse and different isozymes of human ADH exist, significant differences occur within the active site, which account for great variability among substrate specificities, kinetic constants, and response to inhibitors. We have studied the metabolic activity of horse liver alcohol dehydrogenase (HLADH), purified class I $\alpha\alpha$, $\beta_1\beta_1$, and $\beta_2\beta_2$, class II π, class III χ and class IV σ human isozymes, and human liver cytosol (HLC) towards the C-nitroso substrate *p*NSP. Significant differences in the reaction rates towards *p*NSP were observed between HLADH and the human isozymes. The relative order of the rates of *p*NSP reduction by ADH was HLADH > $\alpha\alpha$ > π > σ > χ > $\beta_2\beta_2$ > $\beta_1\beta_1$. *p*NSP reduction catalyzed by HLADH, purified class I $\alpha\alpha$, $\beta_1\beta_1$, and $\beta_2\beta_2$, class III χ and class IV σ human isozymes show pH dependence with maxima greater than or equal to pH 6. This pH dependence seemingly reflects a protein moiety involved in the proton relay system.

Thiodiglycol (TDG) can undergo oxidation catalyzed by ADH. We have compared the catalytic activity of purified human liver class I $\alpha\alpha$, $\beta_1\beta_1$, $\beta_2\beta_2$ and $\gamma_1\gamma_1$ ADH, class II π ADH, class III χ ADH, and class IV σ ADH with respect to TDG oxidation. Specific activities with respect to TDG were 123, 79, 347, 647, and 12

nmol/min/mg for the $\alpha\alpha$, $\beta_1\beta_1$, $\beta_2\beta_2$, $\gamma_1\gamma_1$, and π ADH, respectively. Class III χ ADH did not exhibit activity with this substrate. The specific activity of class IV σ ADH was estimated at about 1632 nmol/min/mg. The activities of class IV σ and class I γ_1 ADH are of significant interest because of their prevalence in the eyes, lungs, stomach and skin, all potential target organs of sulfur mustard toxicity.

CHAPTER 1 INTRODUCTION

Alcohol dehydrogenase (ADH; EC 1.1.1.1) is the primary enzyme responsible for the oxidation of ethanol, with the production of acetaldehyde and NADH being the first step of ethanol elimination in humans (1). The reaction follows an ordered bi bi mechanism in which the binding of cofactor, NAD^+, near the enzyme active site precedes binding of substrate. This catalytically inactive binary complex then binds one molecule of ethanol to form the catalytically active ternary complex. Catalysis occurs instantly with hydride transfer from ethanol to the bound cofactor. Acetaldehyde is then released, followed by the release of NADH. This reaction is reversible, with the ADH catalyzed reduction of acetaldehyde resulting in the production of ethanol. Although its definitive functional activity is the oxidation of ethanol, alcohol dehydrogenase is a key enzyme in phase I xenobiotic metabolism, having a variety of substrates.

Alcohol dehydrogenases constitute a complex system of proteins derived from gene duplications at minimally four different levels. The system includes proteins of different type regarding family relationships and overall organization. It also includes different enzymes within each family, as well as different classes of the enzymes, and different isozymes within the classes, apart from allelic variants. The medium-chain alcohol dehydrogenases now constitute a well-established protein family with characterized relationships of general interest and include the classical alcohol dehydrogenases, the liver and yeast enzymes. In common, these enzymes typically contain a zinc ion at their active sites. The different enzymes within the family originated at an early stage of evolution and exhibit characteristic properties, distinguishable in quaternary structure, substrate specificity, and internal deletions/insertions (2, 3).

Mammalian zinc-containing ADH constitute an enzyme family of multiple isoforms. Of these Horse Liver Alcohol Dehydrogenase (HLADH) is the most widely studied. Being an 80 kDa dimer, HLADH is composed of two 40 kDa monomers, each containing 374 amino acids and two zinc ions, one having a structural function and the other a catalytic function.

1.1 Human ADH Isozymes

Humans produce more than 20 ADH isozymes composed of as many as nine different subunits (4). The horse enzyme shares between 87% and 60% sequence homology with the human isozymes. Having been differentiated into five classes based on their electrophoretic mobilities and inhibition by pyrazole and some of its 4-alkylated derivatives, the inter-class differences between the human isozymes are large and affect charge, enzyme activity, and inhibition patterns. The overall residue identity shows 60% homology between classes; many residues at the active site are substituted, especially in the substrate-binding pocket, which is large and hydrophobic in the traditional ethanol-active liver enzyme of class I, but different in the enzymes of the other classes.

Genes at three loci, ADH 1, ADH 2, and ADH 3, code for the class I isozymes α-, β-, and γ-ADHs, respectively, with allelic variants of β and γ (5, 6). These molecular forms are effectively inhibited by 4-methylpyrazole. Primary and secondary alcohols are almost equally good substrates for class I ADHs. Patterns of class I isozymes also vary because of allelic polymorphism within and among different racial groups. Variants involving the β subunit have been designated β_1 (Caucasian), β_2 (Oriental), and β_3 (African) (6). Class II and class III each consist solely of one

isozyme, π-ADH and χ-ADH, respectively, which are relatively insensitive to pyrazole inhibition. Class II ADH, translated by ADH 4, acts on primary aliphatic alcohols and aromatic aldehydes (7). All human isozymes catalyze the oxidation of ethanol; however, the K_M of class II ADH for ethanol oxidation is significantly higher than that of class I forms. Of the vertebrate ADHs that have been identified, only one form, class III ADH, has been conserved in all organisms (8). Class III has been implicated as the ancestral type, as supported by estimates of the divergence rate, and its presence in invertebrates and prokaroytes as well as animals (9). Class III ADH functions *in vitro* as a glutathione-dependent formaldehyde dehydrogenase, which suggests that this was the original function that drove the evolution of ADH (10). Class III is a product of the ADH 5 gene. The π and χ subunits share about 60% sequence homology with each other or the other isozymes and have not been observed to form heterodimers. Class IV is encoded by the ADH 7 locus, producing the σ-ADH. Found predominately in the stomach, the σ-ADH is considered to have a significant role in retinol metabolism and first-pass ethanol metabolism (11-13). As with HLADH, these medium chain dehydrogenases are dimeric 80kd NAD^+- and zinc-dependent ADHs, containing 4 mol of zinc per dimer (14, 15). These ADHs also illustrate separate genetic controls, with constituent forms (class III χ), inducible forms (class I γ), and genes differently expressed during ontogenesis, with fetal and adult forms (class I α, β, and γ) (16, 17). Classes I through IV have been investigated extensively by analyses of divergent natural variants and correlation of their replacements with the residues lining the substrate-binding pocket (Table 1.1), where a minimum of eleven positions are of major importance (18-20).

Table 1.1 Residues lining the substrate-binding cleft of HLADH and Human ADHs.

Class	Source	Amino acid at position										
		(inner)				(middle)				(outer)		
		48	93	140	141	57	116	294	318	110	306	309
I	Horse E	Ser	Phe	Phe	Leu	Leu	Leu	Val	Ile	Phe	Met	Leu
	Human α	Thr	Ala	Phe	Leu	Met	Val	Val	Ile	Tyr	Met	Leu
	Human β	Thr	Phe	Phe	Leu	Leu	Leu	Val	Val	Tyr	Met	Leu
	Human γ	Ser	Phe	Phe	Val	Leu	Leu	Val	Ile	Phe	Met	Leu
II	Human π	Thr	Tyr	Phe	Phe	Phe	Leu	Val	Phe	Leu	Glu	Ile
III	Human χ	Thr	Tyr	Tyr	Met	Asp	Val	Val	Ala	Leu	Phe	Val
IV	Human σ	Thr	Phe	Phe	Met	Met	Ile	Val	Val	Leu	Met	Phe

Table has been adapted from Eklund *et al.*, 1990 and Satre *et al.*, 1994.(13, 19)

1.2 Mechanism of Catalysis: The Role of Zinc in ADH Catalysis

A great deal of experimentation has been devoted to the role of the metal ion in catalysis, especially the mode of substrate binding and activation as well as the nature of metal-linked equilibria, including the role of metal-bound water. Although much work has been done to evaluate the kinetic mechanism of ADH catalyzed reactions, many questions remain concerning the coordination chemistry of the catalytic zinc and its role in substrate binding and hydride transfer. It is not clear whether all substrates are bound directly to the active site zinc or whether a second-sphere of coordination occurs. Many investigators support a protein-substrate structure with the carbonyl oxygen of an aldehyde substrate bound directly to the catalytic zinc in HLADH in a tetrahedral arrangement (21-24). On the other hand, some investigators have proposed that the metal ion remains coordinated to a water molecule and that the substrate is hydrogen bonded to this water molecule (25, 26). Necessary information to answer these questions is difficult to acquire because of the uninformative zinc ion in the active

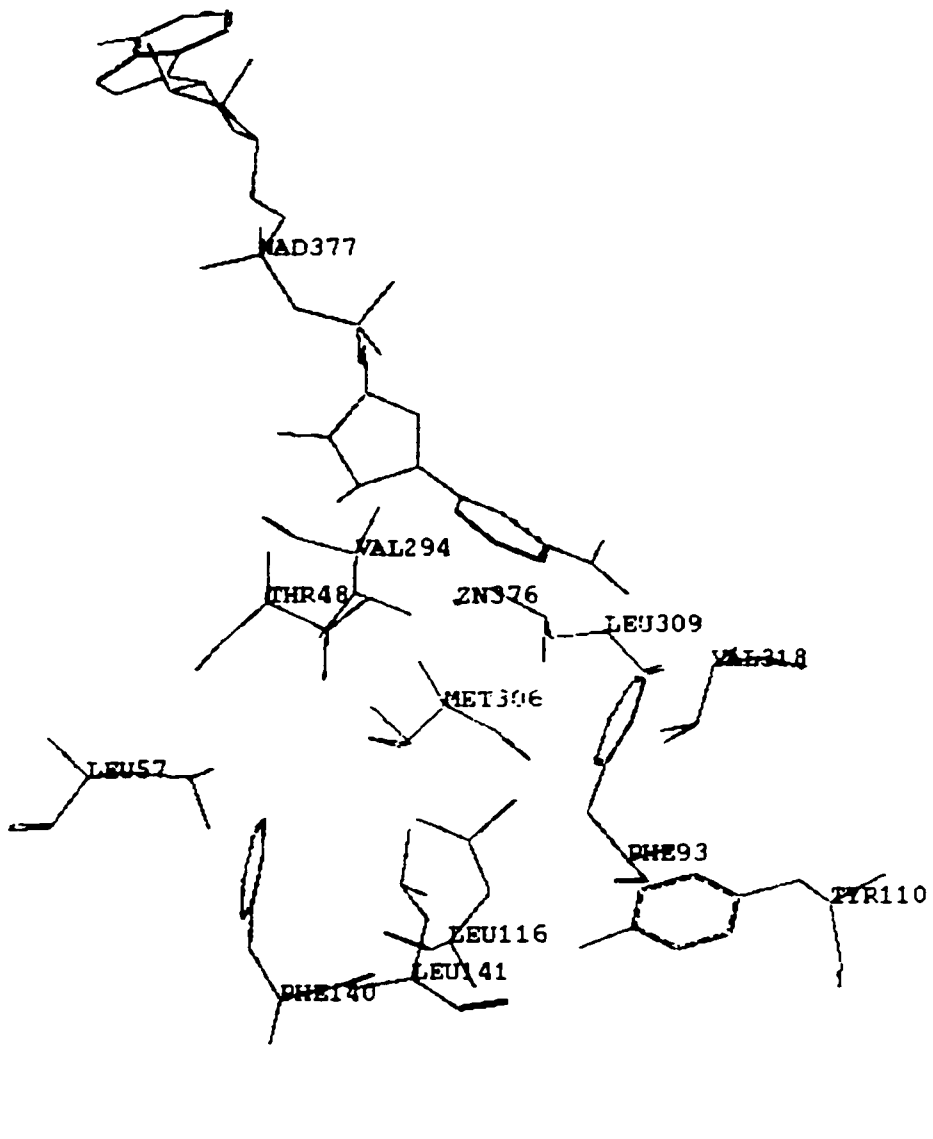

Fig. 1.1 Computer graphics model of the active site of β_1-ADH. This model indicates the positions of the active site residues, bound NAD^+, and the structural zinc ion relative to the catalytic zinc ion. This model was generated using the Sybyl (Tripos Associates, Inc.) molecular modeling software, version 6.4. The coordinates of the human β_1 isozyme (PDB code 3HUD) are those of Hurley *et al.* (27).

site of the enzyme. Because of its chemical nature, zinc does not lend itself to conventional methods of studying the active site metal ligands.

1.3 Physiological Substrates

1.3.1 Contribution to Phase I Metabolism

Aldehydes, ketones, and alcohols are frequent functional groups that appear in drugs and other xenobiotics. These functional groups are often metabolized *in vivo* by oxidation or reduction. Since these functional groups often impart pharmacological properties, the oxidation or reduction of these groups is a means of detoxification (28). However, in some cases more reactive species may be produced and can lead to toxicity. One of the most important enzymes for these reactions is ADH.

1.3.2 Activity in Ethanol Metabolism

Extrahepatic tissues contain isozymes of ADH with a much lower affinity for ethanol than the hepatic isozymes; as a consequence, at the levels of ethanol achieved in the blood, these extrahepatic enzymes are inactive and, therefore, extrahepatic metabolism of ethanol is negligible, with the exception of the stomach.

At least three different forms of ADH exist in the stomach, with either high or low K_M values for ethanol (11). Because of the extraordinarily high gastric ethanol concentration after alcohol ingestion, even the gastric ADH, with a high K_M for ethanol, becomes active and significant gastric ethanol metabolism ensues. This "first pass alcohol metabolism" decreases the bioavailability of ethanol and represents a barrier against its systemic effects, at least when ethanol is consumed in small amounts.

Although other enzymes such as catalase and those of the Microsomal Ethanol Oxidizing System may have significant roles in ethanol oxidation, especially at chronic levels, the main pathway for ethanol disposition involves hepatic ADH, an enzyme of

the cell cytosol. Ethanol ingestion results in numerous enzymatic and metabolic changes in the liver and other organs and tissues (29). These changes include an increased $NADH/NAD^+$ ratio, a decrease in the hepatic ratio of reduced versus oxidized glutathione, induction of cytosolic glutathione-S-transferases, and conversion of xanthine dehydrogenase to xanthine oxidase leading to an overall induction in the expression of xanthine oxidase activity in the liver (30). As a net result of ethanol oxidation, an excess of reducing equivalents in the liver, primarily as NADH, is obtained. The resulting enhanced $NADH/NAD^+$ ratio may produce a change in the ratio of those metabolites that depend on $NADH/NAD^+$ coupled reduction (31).

1.4 C-Nitroso Compounds as Substrates

1.4.1 Arylamines and Nitroarenes

Activation of nitroaromatic compounds to mutagens involves formation of partially reduced metabolites, such as C-nitroso- or hydroxylamino compounds (32). The mutagenicity of nitroarenes and arylamines is closely related to the steady-state concentrations of the nitroso and hydroxylamino intermediates produced during their respective reductive and oxidative metabolism. Therefore, formation and removal of the nitroso intermediates of arylamines and nitroaromatics is an important consideration in the mutagenic expression of these compounds. The potent mutagenic and carcinogenic potential of nitro- and nitrosoarenes is widely accepted to involve their facile reduction to N-hydroxyarylamines (Scheme 1). The nitroso moiety may undergo a two electron reduction via a nitroxyl radical to hydroxylamine, which has been reported as the proximal carcinogen. The hydroxylamine may either undergo direct conversion to the primary carcinogen, the nitrenium ion, or it may be acetylated and by

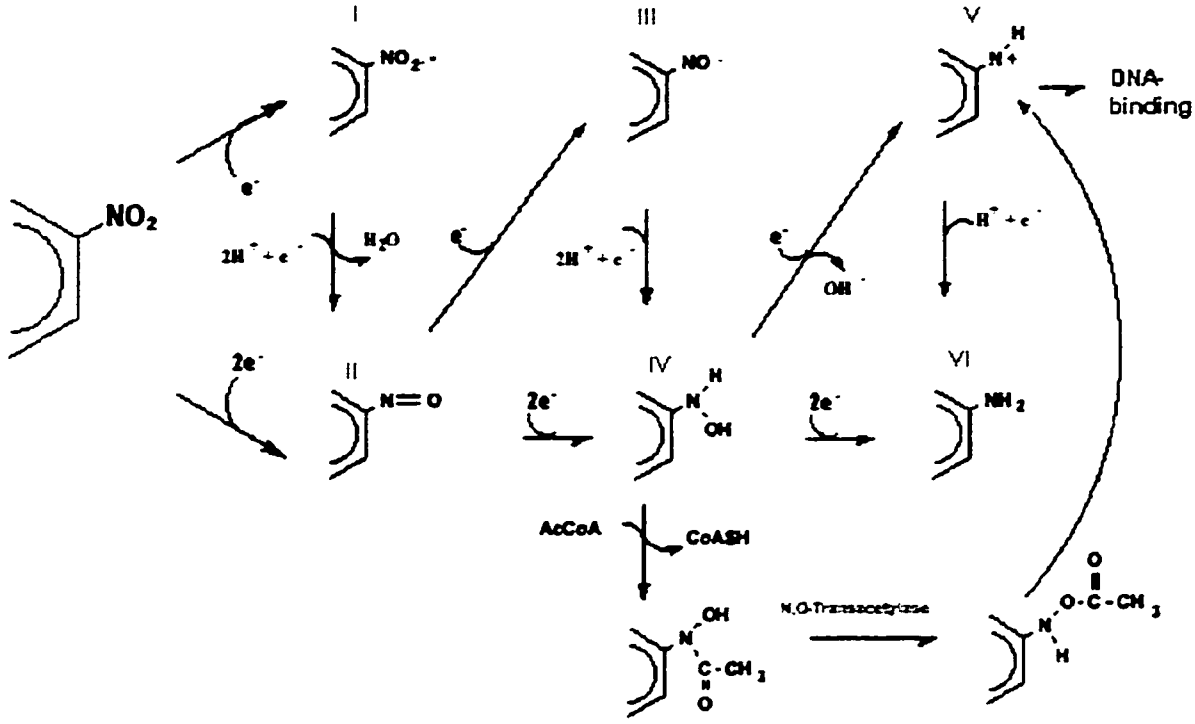

Scheme 1 Proposed 1- and 2-electron reduction pathways of nitroarenes. I. Nitroanion radical, II. Nitroso, III. Nitroxyl radical, IV. Hydroxyl amine, V. Nitrenium ion, VI. Amine

way of N,O-Transacetylase it is then converted to the DNA binding acetoxy hydroxylamine.

1.4.2 Nitroarene Reduction

Aromatic C-nitroso compounds are abundant in the environment (32). They are readily formed intermediates of reductive metabolism of nitroarenes and oxidative metabolism of arylamines. Microsomal and cytosolic enzymes are involved in the metabolism of mutagenic nitroarenes and arylamines (33-37). Arylamines are synthetic industrial compounds. Much research has been undertaken to understand the toxic sequelae of arylamines. Nitroarenes are ubiquitous, anthropogenically generated

contaminants formed predominantly by incomplete combustion (38). They have been detected in gasoline emissions, fly ash, cigarette smoke, grilled foods, incinerator emissions, residential home heaters and wood burning stoves (38, 39). Aromatic C-nitroso compounds have also been used in the vulcanization of some synthetic rubbers, as antioxidants in lubricating oils.

In 1971, Dunn and Bernhard reported the reduction of *p*-nitroso-N,N-dimethylaniline catalyzed by horse liver alcohol dehydrogenase. It was noted that the nitroso moiety is both isosteric and isoelectronic with aldehyde functionality. Purified horse liver ADH and yeast ADH catalyzed NADH-dependent reduction of *p*-nitroso-N,N-dimethylaniline to the corresponding amine (40-42). The cytosolic fraction of rat liver contains various NADH- or NADPH-linked enzymes which can reduce certain nitrosoarenes to the corresponding amines (43). Based on the sensitivity of the reaction to pyrazole, a role for alcohol dehydrogenase in NADH-dependent C-nitroso reductase activity of liver cytosol was indicated (44-48). ADH catalyzed the 4-electron reduction of *p*-nitrosophenol to *p*-aminophenol and showed a slightly acidic pH optimum. The C-nitroso reductase activity of porcine heart, which lacks ADH activity, co-eluted with menadione reductase activity upon partial purification and was supported by either NADH or NADPH (46, 47). Maskos and Winston have shown that ADH catalyzes both the reduction of 2-nitrosofluorene and the rearrangement of N-hydroxy-2-aminofluorene (36). Moreover, NADH-dependent C-nitroso reductase activity catalyzed by rat liver cytosol is inhibited more than 85% by pyrazole (48). Although ADH has been known to catalyze reduction of the C-nitroso functional group to its

corresponding hydroxylamine for nearly two decades, the toxicological ramifications of this reaction have not been fully explored.

1.5 Metabolism of 2,2'-Thiobis-ethanol

Sulfur mustard is a poisonous chemical warfare agent. It was used as recently by Iraq to attack its own Kurdish population in the Iranian-occupied village of Halbja in 1988 (49). Mustard gas is toxic as droplets, liquid, vapor, and, primarily, in the form of an aerosol. It is easily absorbed by many foodstuffs, porous materials, paint and varnish coatings, and rubber articles, all of which will remain contaminated for long intervals (50). Public concern has arisen from possible exposure and potential health hazards resulting from destruction of stockpiles of these chemical agents. Scientific data are being accumulated concerning potential adverse effects, including toxicology, carcinogenicity, mutagenicity, and teratogenicity. Sulfur mustard is a poisonous chemical agent that exerts a local action on the eyes, skin, and respiratory tissues, with subsequent systemic action on the nervous, cardiac, and digestive systems in humans and laboratory animals (51).

Soon after introduction into body tissues, hydrolysis of sulfur mustard occurs to form 2,2'-Thiobis-ethanol (thiodiglycol) and semimustard, which are relatively nontoxic. Recent research has shown that sulfur mustard inhibits serine and threonine phosphatases and that this inhibition was more closely related to the concentration of thiodiglycol (TDG) than the mustard itself (52). Subsequent observations have shown TDG to be a substrate for HLADH and ADH in human skin cytosol (53).

The objective of these studies was two fold: 1. To determine the role of ADH in the reductive metabolism of C-nitroso compounds in cytosol where other nitroso reducing enzymes are present simultaneously; 2. To further elucidate the mechanism

by which ADH catalyzes the reduction of C-nitroso substrates by comparing the activities of HLC, purified HLADH, and purified human ADH isozymes with respect to the model C-nitroso substrate *p*NSP; and 3. To characterize the activities of individual human ADH isozymes with respect to thiodiglycol. Evidence is presented to show distinctly different mechanisms and kinetics by these different systems.

CHAPTER 2 *P*-NITROSOPHENOL REDUCTION BY LIVER CYTOSOL FROM ADH-POSITIVE AND NEGATIVE DEERMICE (*PEROMYSCUS MANICULATUS*)[1]

2.1 Introduction

Aromatic C-nitroso compounds are abundant in the environment (32). They are readily formed intermediates of reductive metabolism of nitroarenes and oxidative metabolism of arylamines. The cytosolic fraction of rat liver contains various NADH- or NADPH-linked enzymes which can reduce certain nitrosoarenes to the corresponding amines (43). Based on the sensitivity of the reaction to pyrazole, a role for alcohol dehydrogenase (ADH; EC 1.1.1.1) in NADH-dependent C-nitroso reductase activity of liver cytosol was indicated (44-48). ADH catalyzed the 4-electron reduction of *p*-nitrosophenol to *p*-aminophenol and showed a slightly acidic pH optimum. Purified horse liver ADH and yeast ADH catalyzed NADH-dependent reduction of *p*-nitroso-N,N-dimethylaniline to the corresponding amine (40-42). NAD(P)H: quinone oxidoreductase (EC 1.6.99.2) has been shown to reduce a variety of nitroso aromatics including *p*-nitrosophenol, nitrosobenzene, nitrosonaphthol and 5-nitroso-8-quinolinol (47). The C-nitroso reductase activity of porcine heart, which lacks ADH activity, co-eluted with menadione reductase activity upon partial purification and was supported by either NADH or NADPH (46, 47)

Activation of nitroaromatic compounds to mutagens occurs via nitroreduction and involves formation of partially reduced metabolites such as C-nitroso or hydroxylamino compounds. Therefore formation and removal of the nitroso intermediates of arylamines and nitroaromatics is an important consideration in the mutagenic expression of these compounds. The mutagenic and carcinogenic potential

[1] Reprinted by Permission of Archives of Biochemistry and Biophysics.

of nitro and nitroso arenes is a function of their ability to be reduced to their corresponding N-hydroxylamine (54, 55). Although ADH has been known to catalyze reduction of the C-nitroso functional group to its corresponding hydroxylamine for nearly two decades, the toxicological significance of this reaction remains largely unexplored.

We have recently characterized NAD(P)H-dependent reduction of *p*-nitrosophenol by liver cytosol from male Sprague-Dawley rats that had been maintained for 30 days on either an alcohol-containing liquid diet or a control diet in which carbohydrate was substituted isocalorically for ethanol (48). Based on potent inhibition by dicumarol of cytosolic NADPH-dependent *p*-nitrosophenol reduction, our studies indicated that this activity was mainly attributable to NAD(P)H: quinone oxidoreductase in liver; this was true with cytosol from ethanol- or pair-fed rats. The total *p*-nitrosophenol reductase of cytosol from ethanol-fed rats was about 2-fold higher than that of controls and the apparent ethanol-inducible portion of the activity was completely inhibitable by dicumarol. Pyrazole only weakly inhibited NADPH-dependent cytosolic reduction of *p*-nitrosophenol by the ethanol- and pair-fed systems, respectively, which indicated a relatively minor contribution of ADH. By contrast, NADH-dependent *p*-nitrosophenol reduction by cytosol from ethanol-and pair-fed rats was effectively inhibited by pyrazole (~60 %). Dicumarol was a relatively weak inhibitor of NADH-dependent *p*-nitrosophenol reduction in both the ethanol and pair-fed systems. Thus, NADH-dependent C-nitroso reductase activity of rat liver appears to be predominantly ADH-catalyzed.

The development of an ADH-negative deermouse by Burnett and Felder (56) has contributed significantly to the understanding of the *in vivo* ramifications of ADH (57). The model was used to show the predominant role of microsomal cytochrome P450 in non-ADH-dependent ethanol oxidation *in vivo* (58). As sundry other liver enzymes, eg. NAD(P)H: quinone oxidoreductase, xanthine oxidase (EC 1.1.3.22) or aldehyde oxidase (EC 1.2.3.1) are capable of nitro, nitroso and hydroxylamino reduction in liver, the ADH-negative deermouse offers advantages in elucidating ADH and non-ADH metabolism of nitroso and hydroxylamines *in vitro* and *in vivo*. Herein evidence is presented to show that ADH is the major NADH-dependent C-nitroso reductase of the deermouse liver and that in ADH-negative deermouse liver, NAD(P)H: quinone oxidoreductase is the predominant NADH- and NADPH- dependent C-nitroso reductase. The total insensitivity of *p*-nitrosophenol reduction to allopurinol suggests the lack of a role for xanthine or aldehyde oxidase as a *p*-nitrosophenol reductase in liver cytosol of both ADH-positive and negative deermice.

2.2 Materials and Methods

2.2.1 Chemicals and Enzymes

Allopurinol, dicumarol, pyrazole, NADH, NADPH, HLADH, and potassium ferricyanide were form Sigma (St. Louis, MO). *p*-Aminophenol, *p*-nitrosophenol, and phenol were from Aldrich Chemical Co. (Milwaukee, WI). All other chemicals were of the highest grade commercially available.

2.2.2 Animals

ADH-positive (ADH^+) and ADH-negative (ADH^-) deermice were provided by Dr. Michael R. Felder, Department of Biology, University of South Carolina, Columbia,

SC. These animals were acclimated for one week in the LSU animal housing facility on a 12:12 hour light:dark cycle and fed standard laboratory chow and water *ad libitum*.

2.2.3 Preparation of Cytosolic Fractions

Cytosolic fractions (105,000 x g supernatants) were prepared by differential centrifugation of liver homogenates according to standard techniques in the literature (59). Fractions were aliquoted and stored at -80°C prior to use.

2.2.4 Enzyme Assays

Formation of *p*-aminophenol from *p*-nitrosophenol was determined by a modification of the procedure described by Horie *et al.* (44). Essentially, *p*-nitrosophenol (0.05-1mM) was incubated for 15 minutes in the presence of 200 μM NADH or NADPH and an appropriate amount of activating enzyme (approximately 0.05 mg/ml cytosolic protein or 0.025 mg/ml purified HLADH) in 50 mM potassium phosphate buffer, pH 7.4, in a final volume of 2 ml. The reaction was initiated by addition of NAD(P)H and terminated by addition of 300 μl of 1 M Na_2CO_3. *p*-Aminophenol was detected spectrophotometrically by subsequent addition of 300 μl of 5% (w/v) aqueous phenol and 200 μl of 0.2% (w/v) potassium ferricyanide. The color was allowed to develop for 15 min and the absorbance measured at 630 nm against a blank containing all reagents but the enzyme fraction. The concentration of *p*-aminophenol formed was calculated from a standard curve using commercially available *p*-aminophenol. Additional incubations contained 15 μM dicumarol, 5 mM pyrazole, or 20 μM allopurinol. At these inhibitor concentrations, the reduction of dichlorophenolindolephenol (DCPIP) or *p*-nitrosophenol by purified NAD(P)H: quinone oxidoreductase, ethanol oxidation and *p*-nitrosophenol reduction by purified ADH and urate formation from hypoxanthine by purified xanthine oxidase were

inhibited 80-90%. Higher concentrations were without further effect. Time course studies followed the basic procedure except that reactions were begun at individual time points so that all could be terminated simultaneously.

Anaerobic experiments were conducted as stated above except that the reactions were run in a nitrogen atmosphere. The reaction mixture and a solution of NADH were degassed with nitrogen for 15 min and sealed with a rubber septum. Reactions were initiated by injecting the degassed NADH directly through the septum of test tubes containing the nitrogen saturated reaction mixture.

Cytosolic NAD(P)H: quinone oxidoreductase activity of deermouse liver cytosol was measured by monitoring the change in absorbance of DCPIP essentially by the method of Ernster *et al* (60). Liver cytosolic ADH activities were measured by the method of Bonnichsen *et al* (61), which is based on spectrophotometric measurement of NADH formation from NAD^+ in the presence of ethanol.

The oxidation of NAD(P)H catalyzed by either purified enzymes or cytosol was measured by following the loss of absorbance of the reduced pyridine nucleotide at 330 nm. This wavelength was chosen instead of the traditional 340 nm to correct for interferences at 340 nm by *p*-nitrosophenol (48). Specific activities were quantified from the corrected millimolar extinction coefficient of 5.87 $mM^{-1} \cdot cm^{-1}$ for the reduced pyridine nucleotide at 330 nm.

2.3 Results

2.3.1 NAD(P)H: Quinone Oxidoreductase and Alcohol Dehydrogenase Activities of Deermouse Liver Cytosol

The specific activities for dicumarol-sensitive, NADH- and NADPH-dependent DCPIP reduction (NAD(P)H: quinone oxidoreductase activity) catalyzed by liver

cytosol from ADH⁻ deermice were essentially identical (25.4 ± 3.1 and 25.1 ± 1.7 nmol/min/mg cytosolic protein, respectively). With cytosol from ADH⁺ deermice the specific activities were 7.2 ± 1.2 and 11.1 ± 1.7 nmol/min/mg for NADH and NADPH, respectively. Thus NAD(P)H: quinone oxidoreductase activity is about 2-3 times greater in the ADH⁻ deermouse than in the ADH⁺. The specific activity of liver cytosolic ADH in the ADH⁺ and ADH⁻ animals, respectively were 4.9 ± 0.7 and 0.4 ± 0.2 nmol/min/mg protein.

2.3.2 *p*-Nitrosophenol Reduction by ADH⁺ and ADH⁻ Deermouse Cytosol

Cytosolic fractions from ADH⁺ and ADH⁻ deermice catalyze NAD(P)H-dependent reduction of *p*-nitrosophenol to *p*-aminophenol (Figs. 2.1A and 2.1B). With either cofactor the reaction appears to be first order with respect to cytosolic protein concentration up to approximately 50 μg/ml. Figure 2.1A also shows that NADH-dependent rates were about three times greater with ADH⁺ cytosol than with ADH⁻ cytosol, whereas NADPH-dependent rates of *p*-aminophenol formation catalyzed by cytosol from ADH⁺ and ADH⁻ deermice were essentially equivalent (Fig. 2.1B).

The time courses for the reduction reactions are shown in Figure 2.2, where it is seen that *p*-aminophenol formation catalyzed by cytosol from ADH⁺ deermice (panel A) is linear for up to 15 minutes with either of the cofactors. However, with NADH (filled triangles) the reaction clearly plateaus more abruptly than it does with NADPH (open triangles). The initial velocity of the NADH-dependent reaction, taken at ten minutes, is about two times greater than the NADPH-dependent reaction (44 ± 6 vs. 24 ± 4 nmol/min/mg, respectively). With cytosol from ADH⁻ deermice (panel B), *p*-aminophenol formation was linear up to 30 minutes and, reminiscent of DCPIP reduction, specific activities were essentially identical with either NADH or NADPH

(13.4 ± 0.4 vs. 13 ± 0.6 nmol/min/mg, respectively). The patterns of *p*-nitrosophenol reduction by ADH$^+$ deermouse cytosol are similar to those reported previously by our laboratory for cytosol from male Sprague-Dawley rats (48).

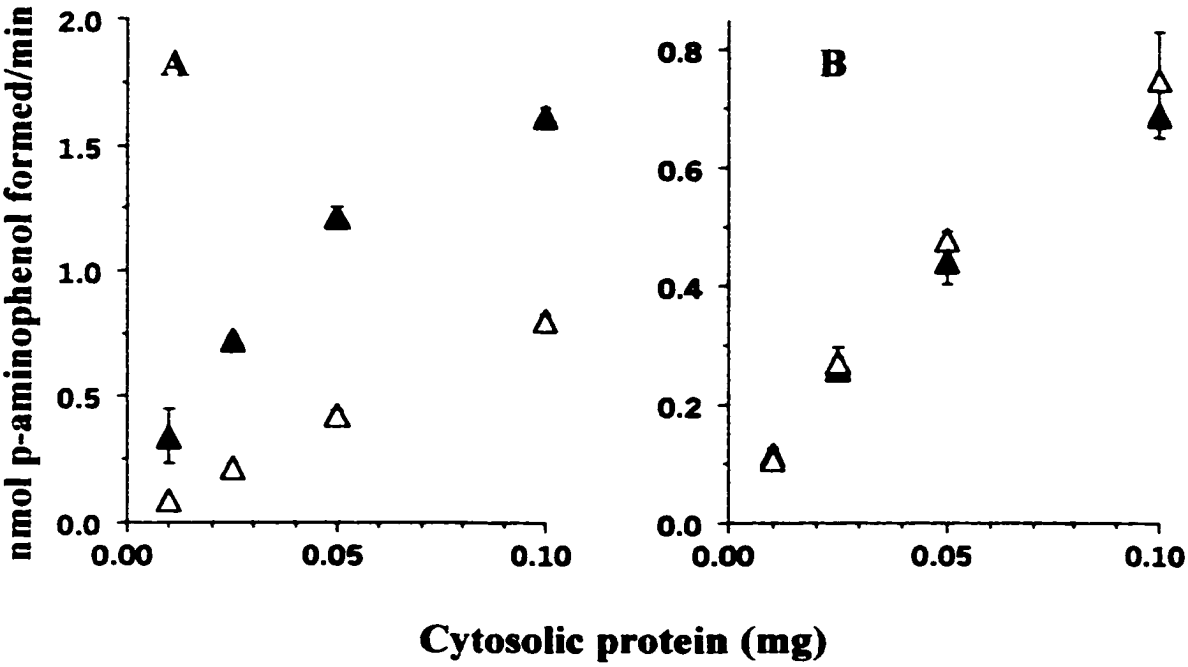

Fig. 2.1 Effect of varying the protein concentration on NADH- (A) and NADPH- (B) dependent formation of *p*-aminophenol from *p*-nitrosophenol by deermouse cytosolic fractions. Increasing concentrations of cytosol from ADH$^+$ (closed triangles) and ADH$^-$ (open triangles) were incubated in the presence of *p*-nitrosophenol as described under Materials and Methods. Each data point represents the mean ± SD of at least three experiments run in triplicate with cytosol pooled from 4 animals from each treatment group.

2.3.3 Effect of Inhibitors on *p*-Aminophenol Formation by ADH$^+$ Deermouse Cytosol

To evaluate the role of certain enzymes in the cytosolic fractions of the ADH$^+$ deermouse that might participate in the reduction of *p*-nitrosophenol to *p*-aminophenol, the effects of classical inhibitors of putative nitroso reductases present in liver cytosol

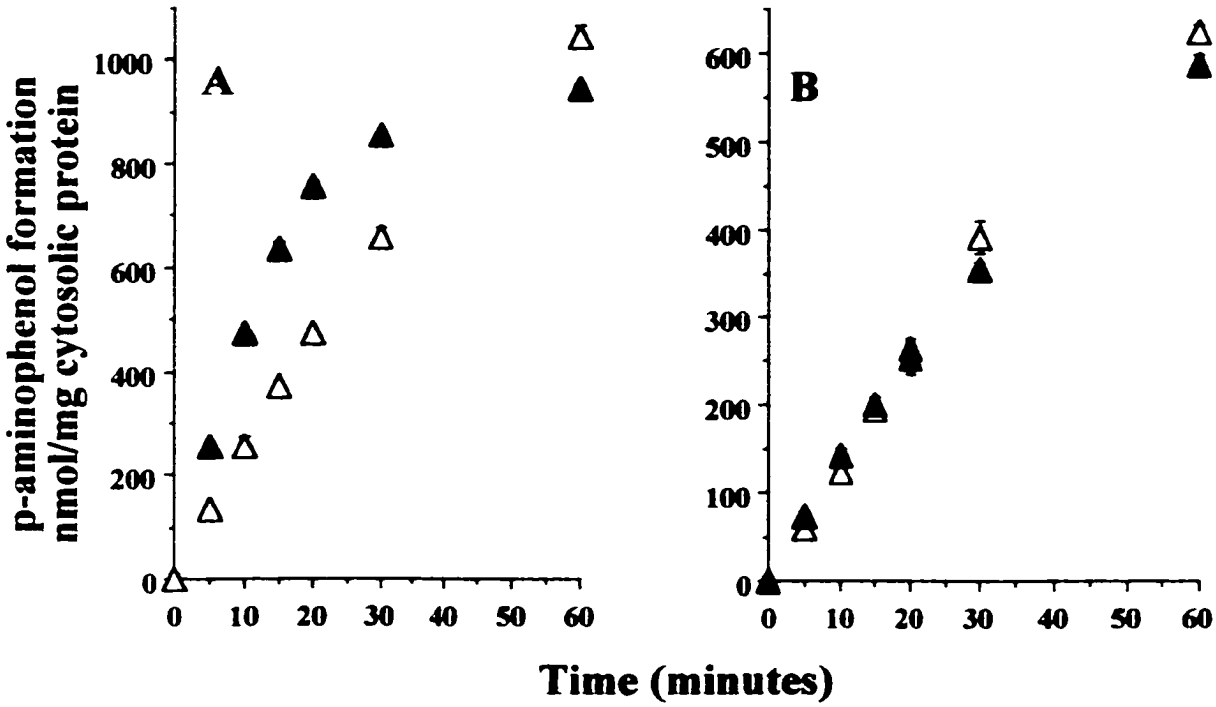

Fig. 2.2 Effect of NADH and NADPH on *p*-aminophenol formation from *p*-nitrosophenol by deermouse cytosolic fractions. Cytosol from ADH$^+$ (A) and ADH$^-$ (B) deermice was incubated in the presence of *p*-nitrosophenol for time periods ranging from 0-60 min as described under Materials and Methods. Rates for the NADH-dependent (closed triangles) and NADPH-dependent (open triangles) C-nitroso reductase activities are shown. Each data point represents the mean ± SD of at least three experiments run in triplicate with cytosol pooled from 4 animals from each treatment group.

were studied. The inhibitors employed were: allopurinol, which forms an irreversible complex with the molybdenum center of xanthine and aldehyde oxidase (62); dicumarol, a potent inhibitor of NAD(P)H: quinone oxidoreductase (60); and pyrazole, which forms a "dead-end" complex with ADH (63). Prior to using these inhibitors for our cytosolic studies preliminary experiments were conducted to establish their inhibitory effects on *p*-nitrosophenol reduction by purified NAD(P)H: quinone

oxidoreductase, ADH and xanthine oxidase. At the concentrations employed dicumarol inhibited *p*-nitrosophenol reduction by NAD(P)H: quinone oxidoreductase by greater than 80% and pyrazole inhibited purified horse liver and human $\beta_2\beta_2$-ADH (both class I ADH) by greater than 90%, (data not shown). Purified xanthine oxidase did not catalyze *p*-nitrosophenol reduction.

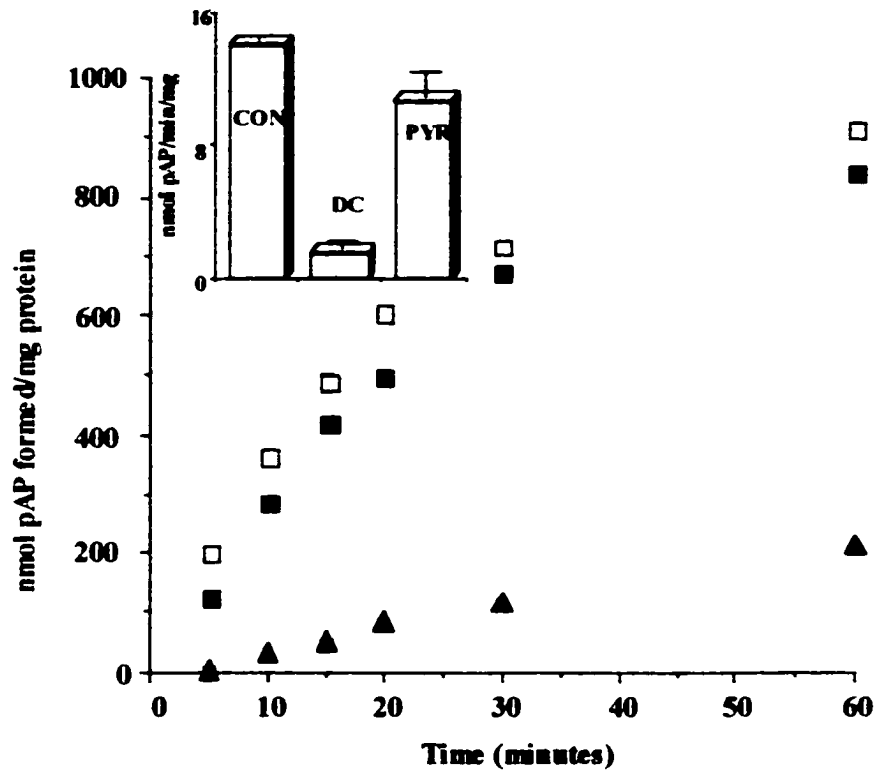

Fig. 2.3 Effect of pyrazole and dicumarol on NADH-dependent formation of *p*-aminophenol from *p*-nitrosophenol by cytosol from ADH$^+$ deermice. Cytosol from ADH$^+$ deermice was incubated in the presence of *p*-nitrosophenol for time periods ranging from 0-60 min as described under Materials and Methods. Final concentrations in 2 ml were: Pyrazole, 5 mM (closed triangles) and Dicumarol, 15 μM (closed squares). Control values are represented by the open squares. INSET: Effect of inhibitors on NADPH-dependent *p*-aminophenol formation from *p*-nitrosophenol by cytosol from ADH$^+$ deermice (data shown for a 15 min incubation period). CON, Control; DC, Dicumarol; PYR, Pyrazole. Each data point represents the mean ± SD of at least three experiments run in triplicate with cytosol pooled from 4 animals from each treatment group.

The effects of the inhibitors were significantly dependent upon the pyridine nucleotide cofactor employed in the reaction. Figure 2.3 shows pyrazole (5mM) to be an effective inhibitor (85-90%) of the NADH-dependent C-nitroso reductase activity of cytosol from ADH^+ deermice over the entire time course studied. Thus, this activity appears to be attributable to cytosolic ADH. With NADPH the inhibition by pyrazole was less than 20% and not statistically significant (Fig. 2.3 inset; shown for 15 min time point only). Dicumarol had little effect on the NADH-dependent reaction thus, NAD(P)H: quinone oxidoreductase does not appear to have a significant role in NADH-dependent reduction of p-nitrosophenol by these cytosolic preparations. In contrast to the nominal effect of dicumarol on NADH-dependent activity the NADPH-dependent reaction was inhibited by greater than 90% (Fig. 2.3 inset). Allopurinol, at concentrations (20-200 μM) that potently inhibit the formation of urate from hypoxanthine catalyzed by 0.15 units of purified xanthine oxidase, was without effect on NADH- or NADPH-dependent activities, which indicates that neither cytosolic xanthine oxidase nor aldehyde oxidase are likely to be involved in the cytosolic reduction of *p*-nitrosophenol (data not shown) under the conditions in which these experiments were conducted.

We considered the possibility that the insensitivity of *p*-nitrosophenol reduction by ADH^+ and ADH^- cytosol to allopurinol was due to failure to see an appropriate product contribution from xanthine oxidase activity under aerobic conditions. An identical experiment was conducted under nitrogen atmosphere to determine if the contribution of xanthine oxidase could be enhanced and therefore visualized under anaerobic conditions and, if so, whether the enhanced activity was allopurinol-sensitive.

The results showed that *p*-nitrosophenol reduction by ADH^+ cytosol was increased by 97% and by ADH^- cytosol by 60% under a nitrogen atmosphere. In both instances the increase in activity was insensitive to allopurinol. Thus, it appears that the increase in activity under nitrogen atmosphere is due to enzymes other than xanthine oxidase, which does not seem to have a role in *p*-nitrosophenol reduction by cytosol from either ADH^+ or ADH^- deermice whether oxygen is present or not.

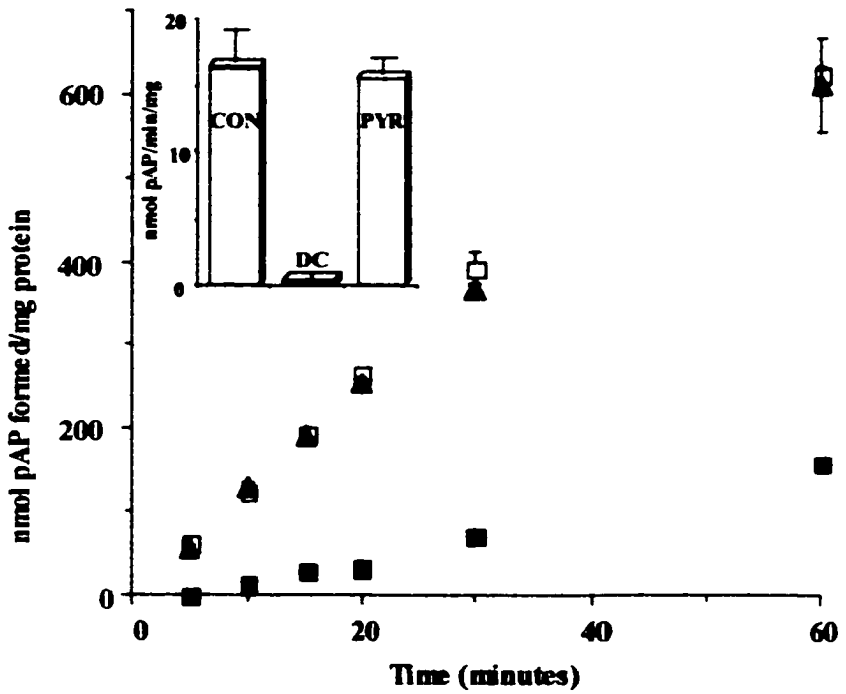

Fig. 2.4 Effect of pyrazole and dicumarol on NADPH-dependent formation of *p*-aminophenol from *p*-nitrosophenol by cytosol from ADH^- deermice. Cytosol from ADH^- deermice was incubated in the presence of *p*-nitrosophenol for time periods ranging from 0-60 min as described under Materials and Methods. Final concentrations in 2 ml were: Pyrazole, 5 mM (closed triangles) and Dicumarol, 15 μM (closed squares). Control values are represented by the open squares. INSET: Effect of inhibitors on NADH-dependent *p*-aminophenol formation from *p*-nitrosophenol by cytosol from ADH^- deermice (data shown for a 15 min incubation period). CON, Control; DC, Dicumarol; PYR, Pyrazole. Each data point represents the mean ± SD of at least three experiments run in triplicate with cytosol pooled from 4 animals from each treatment group.

2.3.4 Effect of Inhibitors on ADH⁻ Deermouse Cytosol

Whereas a significant cofactor preference was observed in the ADH⁺ deermouse model with respect to C-nitroso reductase activity, this was not the case with cytosolic fractions from ADH⁻ deermice; NADH- and NADPH-dependent activities were essentially equivalent (Fig. 2.4). Neither pyrazole nor allopurinol (not shown) significantly inhibited the rates of formation of *p*-aminophenol from *p*-nitrosophenol. However, with either of these cofactors, dicumarol potently inhibits reduction of *p*-nitrosophenol; the NADH-dependent reaction is shown for the 15 min time point only (Fig. 2.4 inset). Thus, the reduction of *p*-nitrosophenol by this ADH-deficient cytosolic fraction appears to be mainly catalyzed by NAD(P)H: quinone oxidoreductase. We note that at the concentrations of the inhibitors employed virtually no cross-reactivity was observed between these inhibitors and the enzymes probed in their respective purified forms. For example, 15 μM dicumarol was without effect on C-nitroso reduction by purified ADH from horse liver and xanthine oxidase from buttermilk, but did potently inhibit menadione and C-nitroso reduction by purified NAD(P)H: quinone oxidoreductase from rat liver (not shown).

2.3.5 NAD(P)H Oxidation by Deermouse Cytosol

ADH-dependent rates of NAD(P)H oxidation catalyzed by the two deermouse cytosolic fractions in the presence of the C-nitroso substrate were also determined to confirm the results obtained for the formation of *p*-aminophenol. These data are summarized in Table 2.1. Consistent with the data on *p*-aminophenol formation the rate of NADH oxidation in the presence of *p*-nitrosophenol was about twice that of NADPH oxidation with ADH⁺ cytosol (77 ± 6 vs. 36 ± 1 nmol/min/mg). With ADH⁻ cytosol the rates of NADH and NADPH oxidation were similar (71 ± 3 vs. 62 ± 5 nmol/min/mg).

Pyrazole inhibited NADH oxidation catalyzed by ADH^+ cytosol by about 70% (77 ± 6 to 22 ± 3 nmol/min/mg) and not that catalyzed by ADH^- cytosol (59 ± 4 vs. 62 ± 5 nmol/min/mg). Dicumarol inhibited the NADH-dependent ADH^+ and ADH^- cytosolic reactions by 51% and 85%, respectively. Results of the NADPH-dependent reaction were as expected, as the majority of NADPH oxidation catalyzed by ADH^+ and ADH^- cytosol was highly dicumarol-sensitive and nominally pyrazole-sensitive. NADPH oxidation by ADH^+ and ADH^- cytosol was inhibited by dicumarol by approximately 80%, (from 36 ± 1 to 7 ± 2 and 71 ± 3 to 13 ± 1 nmol/min/mg by ADH^+ and ADH^- cytosol, respectively).

Table 2.1 ADH-dependent NAD(P)H oxidation by deermouse cytosolic fractions.

	nmol NAD(P)H oxidized/min/mg cytosolic protein	
	ADH^+	ADH^-
NADH		
Control	77 ± 6[a]	62 ± 5
+Pyrazole	22 ± 3 [71%]	59 ± 4 [5%]
+Dicumarol	38 ± 2 [51%]	9 ± 1 [85%]
NADPH		
Control	36 ± 1	71 ± 3
+Pyrazole	28 ± 2 [22%]	70 ± 3 [1%]
+Dicumarol	7 ± 2 [81%]	13 ± 1 [82%]

Oxidation of NAD(P)H was monitored spectrophotometrically at 330 nm as described in Materials and Methods. [a]results represent means ± SD of triplicate determinations on cytosolic fractions pooled from four animals from each group. [b]Values in brackets represent percent inhibition relative to uninhibited controls. Pyrazole and dicumarol concentrations are 5 mM and 15 μM, respectively.

2.4 Discussion

The present study confirms in another mammalian species previous data from our laboratory that showed that cytosolic NADH-dependent *p*-nitrosophenol reduction is predominantly pyrazole-sensitive, which suggests that this C-nitroso reductase activity is associated with ADH in the liver (48). In fact, 5 mM pyrazole was significantly more effective as an inhibitor of *p*-nitrosophenol reduction by ADH^+ deermouse cytosol (85-90%) than that by rat liver cytosol (50-60%; see ref. (48)). Moreover, the present studies with the ADH-negative deermouse extend our earlier findings to show that non-ADH metabolism of a model C-nitroso substrate is apparently associated predominantly with liver cytosolic NAD(P)H: quinone oxidoreductase; this was true of both the NADH- and NADPH-dependent activities. In the ADH^- system NADH-dependent activity was as sensitive to dicumarol as was the NADPH-dependent activity, a result that is consistent with the equal affinity of NAD(P)H: quinone oxidoreductase for the two pyridine nucleotides. The higher specific activity of NAD(P)H: quinone oxidoreductase in the ADH^- animal renders the contribution of this enzyme approximately equivalent to that of the ADH^+ animal. Whether or not this is a compensatory action remains to be established. Nevertheless, ADH apparently was able to out compete the quinone oxidoreductase in the ADH^+ cytosol for *p*-nitrosophenol substrate when NADH was used as the cofactor.

Under the experimental conditions used herein, cytosolic C-nitroso reductase activity of neither the ADH^+ nor ADH^- animals was sensitive to allopurinol, even at concentrations that inhibited urate formation from hypoxanthine by purified commercial xanthine oxidase or cytosol by greater than 90% (not shown). Thus, under aerobic conditions liver cytosolic xanthine oxidase from ADH^+ or ADH^- deermice (and more

than likely aldehyde oxidase) does not catalyze reduction of *p*-nitrosophenol to the amine. One possibility which might explain the apparent lack of a role for xanthine oxidase as a cytosolic C-nitroso reductase in the rat (48), and presently the deermouse, is that in contrast to ADH and NAD(P)H: quinone oxidoreductase, xanthine oxidase involves univalent reduction of nitro and nitroso substrates to oxygen labile free radical intermediates (64). Thus, rapid loss of the free electron of the radical intermediate to molecular oxygen can be envisaged, which precludes formation of further reduced products (65). Under aerobic conditions in the presence of *p*-nitrosophenol and purified xanthine oxidase NADH oxidation was very slow and no faster than in the absence of *p*-nitrosophenol (not shown). This would indicate that *p*-nitrosophenol is not a suitable acceptor of electrons from xanthine oxidase. If a redox cycle was being mediated via a free radical intermediate of *p*-nitrosophenol in the manner described above, a stimulation in the rate of NADH oxidation relative to the rate catalyzed by the xanthine oxidase in the absence of *p*-nitrosophenol should have resulted. Furthermore, even in a nitrogen atmosphere, which did enhance *p*-aminophenol formation from *p*-nitrosophenol, allopurinol was without effect.

Both microsomal and cytosolic enzymes are involved in the metabolism of nitro and nitroso arenes (33, 65, 66). The equilibrium between the nitroso and hydroxylamine intermediates is an important consideration in the mutagenic expression of arylamines and nitroarenes (38) because the hydroxylamine is the precursor of the highly electrophilic arylnitrenium ion, which reacts strongly with nucleophilic centers of DNA. The results of kinetic studies indicated the transient formation of an enzyme-

bound intermediate of *p*-nitrosophenol by 2-electron transfer from one molecule of NADH (45).

Cytosolic NAD(P)H: quinone oxidoreductase is a major inducible nitro and nitroso reductase (67); it is induced by polychlorinated biphenyls (PCB, (67)), polynuclear aromatic hydrocarbons (68) and ethanol (48). ADH is not induced by exposure to these xenobiotics, therefore the contribution of NAD(P)H: quinone oxidoreductase to cytosolic C-nitroso reduction would be expected to be enhanced when it is induced. Under these experimental conditions, the induction of liver cytosolic NAD(P)H: quinone oxidoreductase upon pretreatment of rats with the PCB mixture Aroclor-1254® was nearly 20-fold over non-treated controls (67). When the effects of pyrazole and dicumarol on NADH-dependent cytosolic *p*-nitrosophenol reduction was compared in control and PCB-induced rats the inhibition pattern in the controls were similar to that reported herein for ADH^+ deermice and in PCB-induced rats pyrazole inhibition was only about 10-15% and dicumarol inhibition about 85-90% (unpublished results).

The reduction of a nitro group to the amine involves transfer of six electrons. Thus, aside from possible conjugated products, e.g. acetylated, etc. there are five potential intermediates of nitroarene reductive metabolism. These include, the nitroso and hydroxylamine intermediates and three free radical species, the nitro anion, the nitroxyl and the aminoxyl radicals. The radical intermediates could either bind to nucleophilic centers of tissue macromolecules or lose the free electron to molecular oxygen thereby producing various oxygen radicals via a redox cycle. We have noted that neither NAD(P)H: quinone oxidoreductase purified from rat liver nor ADH purified

from horse liver enhance the rates of oxygen consumption or NAD(P)H oxidation in the presence of nitronapthalene or 4-nitroquinoline N-oxide (69), whereas these parameters are markedly increased by purified cytochrome P450 reductase and xanthine oxidase. Thus, it does not appear that the reduction of C-nitroso substrates catalyzed by ADH or NAD(P)H: quinone oxidoreductase results in significant production of radical intermediates.

The results of this study, in conjunction with those of others cited herein, suggest a complex interplay of cytosolic enzymes in the metabolism of nitro and nitrosoarenes. This complexity is in part related to the content of the enzyme in the liver and availability and redox status of pyridine nucleotide cofactors in the cytosolic fraction, both of which are subjected to alteration by xenobiotic exposure. Further, it is likely that intermediates of a primary or secondary reaction can shift loci, for example, a nitroaromatic might first be reduced by NAD(P)H: quinone oxidoreductase or xanthine oxidase and the resulting nitroso product might preferentially be further reduced by ADH. Certainly a great deal more investigation is required before the metabolic sequelae of biotransformation of nitro or nitroso arenes to DNA adduct formation is elucidated with precision.

CHAPTER 3 REDUCTION OF *P*-NITROSOPHENOL BY ALCOHOL DEHYDROGENASE: COMPARISON OF HUMAN AND HORSE LIVER ISOZYMES

3.1 Introduction

Alcohol dehydrogenase (ADH, EC 1.1.1.1) is the primary enzyme responsible for the oxidation of ethanol, with the production of acetaldehyde and NADH being the first step of ethanol elimination (1). The reaction follows an ordered bi bi mechanism in which the binding of the cofactor NAD^+ near the enzyme active site precedes binding of substrate. This binary complex then binds one molecule of ethanol to form the catalytically active ternary complex. Catalysis occurs by hydride transfer from ethanol to the bound cofactor followed by the ordered release of acetaldehyde and NADH. This reaction is reversible with the ADH-catalyzed reduction of acetaldehyde resulting in the production of ethanol.

Mammalian zinc-containing ADH constitute an enzyme family of multiple isoforms. Horse liver alcohol dehydrogenase (HLADH) is the most widely studied. HLADH is composed of two 40 kDa monomers, each containing 374 amino acids and two zinc ions, one having a structural function and the other a catalytic function (70, 71).

Humans express more than 20 ADH isozymes composed of as many as nine different subunits (4). The horse enzyme shares between 60% and 87% sequence identity with the human isozymes. Having been differentiated into five classes based on their genotypes, electrophoretic mobilities and inhibition by pyrazole and some of its 4-alkylated derivatives, the inter-class differences between the human isozymes are large and affect charge, enzyme activity, and inhibition patterns. The overall residue identity shows 60% homology between classes; many residues at the active site differ especially

in the substrate-binding pocket, which is large and hydrophobic in the traditional ethanol-active liver enzyme of class I, but different in the enzymes of the other classes.

Genes at three loci, ADH 1, ADH 2, and ADH 3, code for the class I isozymes α-, β-, and γ-ADHs, respectively, with allelic variants of β and γ (5, 6). These molecular forms are effectively inhibited by 4-methylpyrazole. Primary and secondary alcohols are almost equally good substrates for class I ADHs. Patterns of class I isozymes also vary because of allelic polymorphism within and among different racial groups. Variants involving the β subunit have been designated β_1 (Caucasian), β_2 (Oriental), and β_3 (African) (6). Class II and class III each consist solely of one isozyme, π-ADH and χ-ADH, respectively, which are relatively insensitive to pyrazole inhibition. Class II ADH, translated by ADH 4, acts on primary aliphatic alcohols and aromatic aldehydes (7). All human isozymes catalyze the oxidation of ethanol; however, the K_M of class II ADH for ethanol is significantly higher than that of class I forms. Of the vertebrate ADHs that have been identified, only one form, class III ADH, has been conserved in all organisms (8). Class III ADH functions *in vitro* as a glutathione-dependent formaldehyde dehydrogenase, which suggests that this was the original function that drove the evolution of ADH (10). Class III is produced from the ADH 5 gene. The π and χ subunits share about 60% sequence identity with each other or the other isozymes and have not been observed to form heterodimers. Class IV is encoded by the ADH 7 locus that expresses the σ-ADH. Found predominately in the stomach, σ-ADH is considered to have a significant role in retinol metabolism and first-pass ethanol metabolism (11-13). As with HLADH, these medium chain

dehydrogenases are dimeric 80kd NAD^+- and zinc-dependent ADHs, containing 4 zinc atoms per dimer (14, 15).

Microsomal and cytosolic enzymes are involved in the metabolism of mutagenic nitroarenes and arylamines (33, 34). Arylamines are synthetic industrial compounds. Much research has been undertaken to understand the toxic sequelae of arylamines (66, 72). Previous studies have shown that the mutagenic activation of 2-aminofluorene, a benchmark mutagenic arylamine, is lowered by liver microsomal fractions from ethanol-fed rats, but increased by the corresponding cytosolic fraction, when compared to pair-fed controls (66). Nitroarenes are ubiquitous, anthropogenically-generated contaminants formed predominantly by incomplete combustion (38). They have been detected in gasoline emissions, fly ash, cigarette smoke, grilled foods, incinerator emissions, residential home heaters and wood burning stoves (38, 39).

Dunn and Bernhard (1971) reported the reduction of *p*-nitroso-N,N-dimethylaniline by horse liver ADH (40). It was noted that the nitroso moiety is both isosteric and isoelectronic with aldehyde functionality. Activation of nitroaromatic compounds to mutagens involves formation of partially reduced metabolites, such as C-nitroso- or hydroxylamino compounds (67). The mutagenicity of nitroarenes and arylamines is closely related to the steady-state concentrations of the nitroso and hydroxylamino intermediates produced during their respective reductive and oxidative metabolism (54, 55). The potent mutagenic and carcinogenic potential of nitro- and nitrosoarenes is widely accepted to involve their facile reduction to N-hydroxyarylamines.

ADH catalyzes both the reduction of 2-nitrosofluorene and the rearrangement of N-hydroxy-2-aminofluorene, which provides cogent evidence for the production of the electrophilic intermediate arylnitrenium ion (36). Moreover, NADH-dependent C-nitroso reductase activity catalyzed by both ADH-positive deermouse cytosol and rat liver cytosol is inhibited more than 85% by pyrazole, thereby implicating ADH as an important catalyst in these cytosolic fractions. (48, 73). Leskovac *et al.* have reported the metabolism of *p*-nitroso-N,N-dimethylaniline by yeast ADH and the HLADH catalyzed reduction of *p*NSP (74, 75). Although ADH has been known to catalyze the reduction of the C-nitroso functional group to its corresponding hydroxylamine for nearly two decades, the toxicological ramifications of this reaction had not been fully explored until recently (36, 37, 48, 73). To implicate a role for the various human ADH in the toxicity of C-nitroso compounds we compared the activities of purified human ADH isozymes with respect to the model C-nitroso substrate *p*NSP. The results were compared with those of purified HLADH, a benchmark ADH in biochemical studies. Evidence is presented to show distinctly different mechanisms and kinetics of *p*NSP reduction by these different ADH isozymes.

3.2 Materials and Methods

3.2.1 Chemicals and Enzymes

Pyrazole, NADH, NADPH, benzaldehyde and potassium ferricyanide were obtained from Sigma (St. Louis, MO). *p*AP, *p*NSP, and phenol were obtained from Aldrich Chemical Co. (Milwaukee, WI). Crystalline HLADH was obtained from Boehringer-Mannheim (Indianapolis, IN). All other chemicals were of the highest grade commercially available. Purified human liver ADH isozymes were generously

provided for these studies by Dr. W. F. Bosron, Department of Biochemistry and Molecular Biology, Indiana University School of Medicine.

3.2.2 Preparation of Cytosolic Fractions

Human liver obtained from a normal caucasian female human liver autopsy sample was generously provided by Dr. Sanda Clejan (Department of Pathology, Tulane University Medical Center, New Orleans, Louisiana). The cytosolic fraction (105,000 x g supernatant) of this human liver sample was prepared by differential centrifugation of liver homogenates according to standard techniques in the literature (59). Fractions were aliquoted and stored at -80°C prior to use.

3.2.3 Enzyme Assays

Formation of *p*AP from *p*NSP was determined essentially by the method of Horie *et al.* (44) with modifications (48). *p*NSP (0.05-1mM) was incubated for 15 minutes in the presence of 200 μM NADH or NADPH and approximately 0.05 mg/ml cytosolic protein or 1 μg/ml purified HLADH or 0.7-1 μg/ml purified human ADH in 50 mM potassium phosphate buffer or 0.1 M MES, 51 mM NEA, 51 mM DEA, pH 7.4, in a final volume of 2 ml. The reaction was initiated by addition of cofactor and terminated by addition of 300 μl of 1 M Na_2CO_3. *p*AP formation was detected spectrophotometrically by subsequent addition of 300 ml of 5% (w/v) aqueous phenol and 200 ml of 0.2% (w/v) potassium ferricyanide. The color was allowed to develop for at least 15 min and the absorbance was read at 630 nm against a reagent blank. The concentration of *p*AP formed was calculated from a standard curve using commercially available *p*AP. Additional reactions contained 15 mM dicumarol, 5 mM pyrazole, or 20 mM allopurinol. The extent of *p*NSP reduction was determined spectrophotometrically by tracing the loss of absorbance at 400 nm. The enzyme-catalyzed reaction was

quantified using the extinction coefficient of *p*NSP, ε_{400}= 21.92 $mM^{-1}cm^{-1}$. Spectral transition studies were determined in tandem cuvettes. The two chambers of the sample cuvette contained: 1) 50 mM potassium phosphate buffer, pH 7.4, and 2) 120 μM *p*NSP, 200 μM NADH, 50 mM potassium phosphate buffer, pH 7.4, and purified ADH in a final volume of 1 ml. Those of the reference cuvette contained: 1) 200 μM NADH, 50 mM potassium phosphate buffer, pH 7.4,and purified ADH, and 2) 120 μM *p*NSP and 50 mM potassium phosphate buffer, pH 7.4, in a final volume of 1 ml. The reactions were initiated with addition of the enzyme. Reactions were followed spectrophotometrically at 1-1.5 min intervals for 15 min time periods. ADH activities were measured by the method of Bonnichsen *et al.* (61), which is based on spectrophotometric measurement of NADH formation from NAD^+ in the presence of ethanol. All spectrophotometric measurements were performed with a Hitachi U-3110 UV-visible spectrophotometer at 25°C.

Quinone reductase activity by ADH was determined by a modification of the procedure described by Ernster *et al.* (76) for NAD(P)H: quinone oxidoreductase (DT-diaphorase). 1,4-Benzoquinoneimine (BQI) was synthesized by Dr. Zofia Maskos in our laboratory by oxidation of *p*AP in CH_3CN in the presence of Ag_2O at room temperature as described by Novak and Martin (77). The reaction mixture contained 0.05 M phosphate buffer, pH 7.4, 0.2 mM NAD(P)H and 32 mM BQI. The reaction was followed by recording the reduction of BQI at 262 nm (ε_{262}= 28.2 mM^{-1} cm^{-1}) and the oxidation of NADH at 340 nm (ε_{340}= 6.22 mM^{-1} cm^{-1}).

3.3 Results

3.3.1 Effect of Inhibitors on NADH-Dependent *p*-Aminophenol Formation by Human Liver Cytosol

As a first approach to evaluating a role for the various NADH-linked enzymes in the cytosolic fractions of human liver that might participate in the reduction of *p*NSP to *p*-aminophenol (*p*AP), the effects of classical inhibitors of putative nitroso reductases present in liver cytosol were studied (Fig. 3.1). The inhibitors employed were allopurinol, which forms an irreversible complex with the molybdenum center of xanthine (EC 1.1.3.22) and aldehyde (EC 1.2.3.1) oxidase (62); dicumarol, a potent inhibitor of NAD(P)H:quinone oxidoreductase (60); and pyrazole, which forms a "dead-end" complex with some ADH isozymes and NAD^+ (63).

Cytosol prepared from a normal female human liver autopsy sample catalyzed NAD(P)H-dependent reduction of *p*NSP (Fig. 3.1). As was reported for this activity catalyzed by cytosol from rat liver and ADH-positive deermouse liver (48, 73), NADH-dependent *p*NSP reduction catalyzed by human liver cytosol was sensitive to inhibition by pyrazole. These experiments showed that 5 mM pyrazole potently inhibited (> 90%) the NADH-dependent formation of *p*AP from *p*NSP; this inhibition was actually greater than that caused by pyrazole on the cytosolic reduction of *p*NSP by the rodent liver cytosols, which were 75% and 85%, respectively (48, 73). Thus, this activity appears to be attributable to cytosolic ADH. Dicumarol inhibited the NADH-dependent reaction by only 7%; thus, NAD(P)H:quinone oxidoreductase does not appear to have a significant role in NADH-dependent reduction of *p*NSP. NADPH-dependent activity was potently inhibited by dicumarol in rodent and human liver cytosol. Unexpectedly, and in direct contrast to rodent liver cytosol, pyrazole inhibited the NADPH-dependent

reduction of *p*NSP by human liver to about 80%. In agreement with our studies of deermouse and rat liver cytosols, allopurinol inhibited neither NADH- nor NADPH-dependent *p*AP formation by human liver cytosol. Pyrazole also inhibited the NADH-dependent activity of purified horse liver by greater than 90% and the NADPH-dependent activity by about 30% (Figure 3.2).

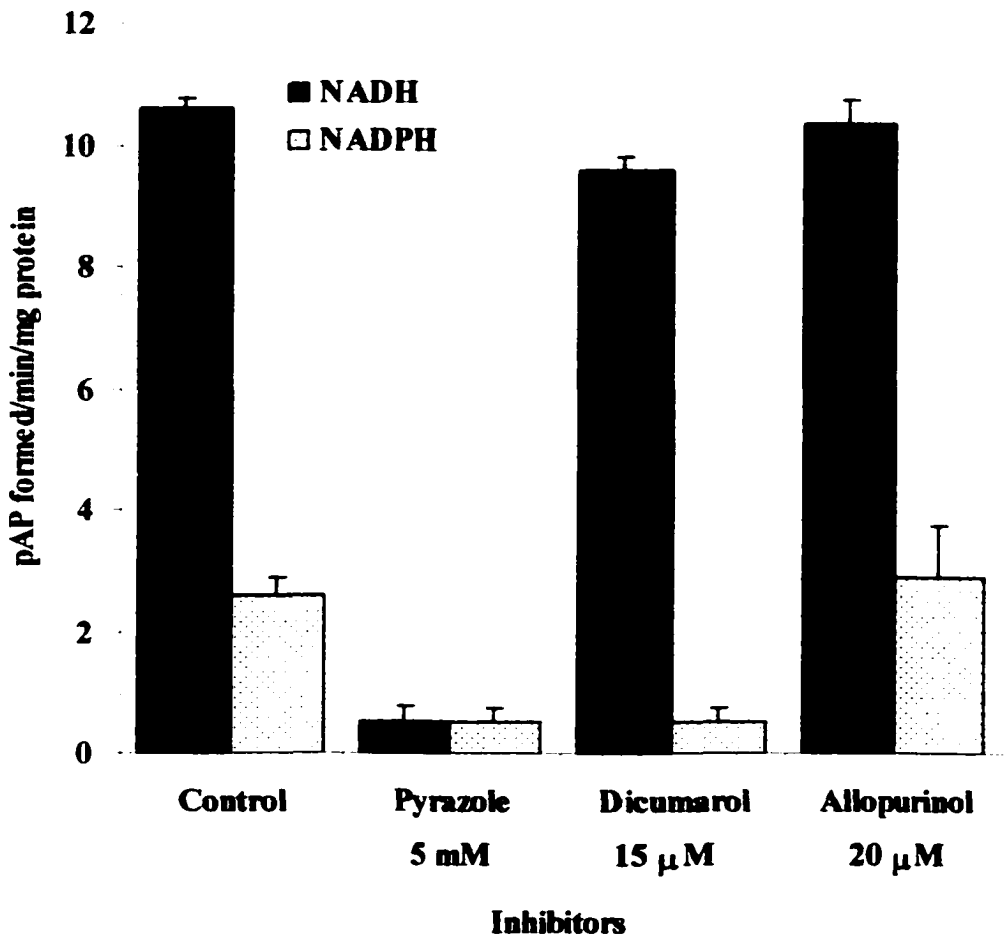

Fig. 3.1 Effect of Inhibitors on NADH-dependent *p*AP formation by HLC. Reaction conditions are: 50 mM phosphate buffer, pH 7.4; 0.2 mM NADH; 120 μM *p*NSP; and 0.05 mg/ml cytosolic protein. Data shown for 15 min time point and is the result of triplicate determinations.

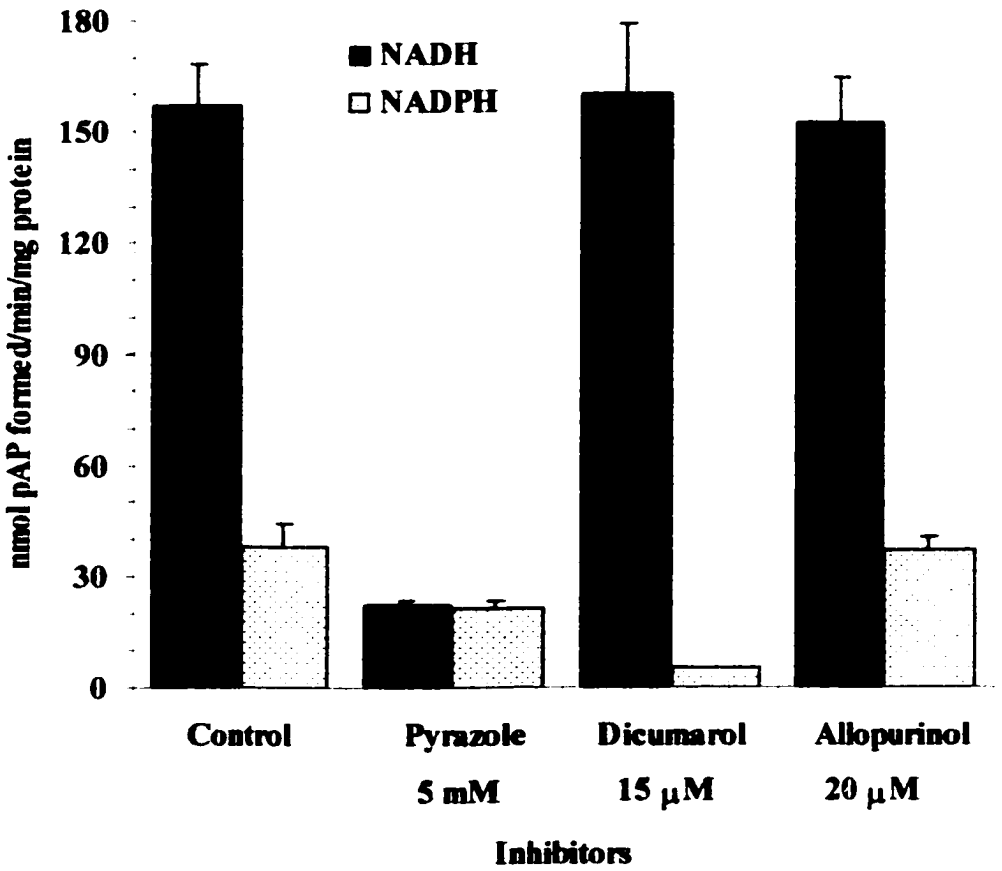

Fig. 3.2 Effect of Inhibitors on NAD(P)H-dependent *p*AP formation by HLADH. Reaction conditions are: 50 mM Potassium phosphate, pH 7.4; 0.2 mM NADH; 120 μM *p*NSP; and 2.5 μg/ml HLADH. Data shown for 15 min time point and is the result of triplicate determinations.

3.3.2 NADH-Dependent *p*NSP Reduction by HLADH and Purified Human ADH Isozymes: Effect of Pyrazole

Because NADH is the preferred cofactor for ADH-catalyzed C-nitroso reduction further studies were done only with respect to NADH-dependent activity. Figure 3.3 A & B shows the time courses of NADH-dependent C-nitrosoreductase activity of purified human ADH representatives of classes I - IV and HLADH. The graphs illustrate the formation of *p*AP over a period of 60 min, except in the case of the human

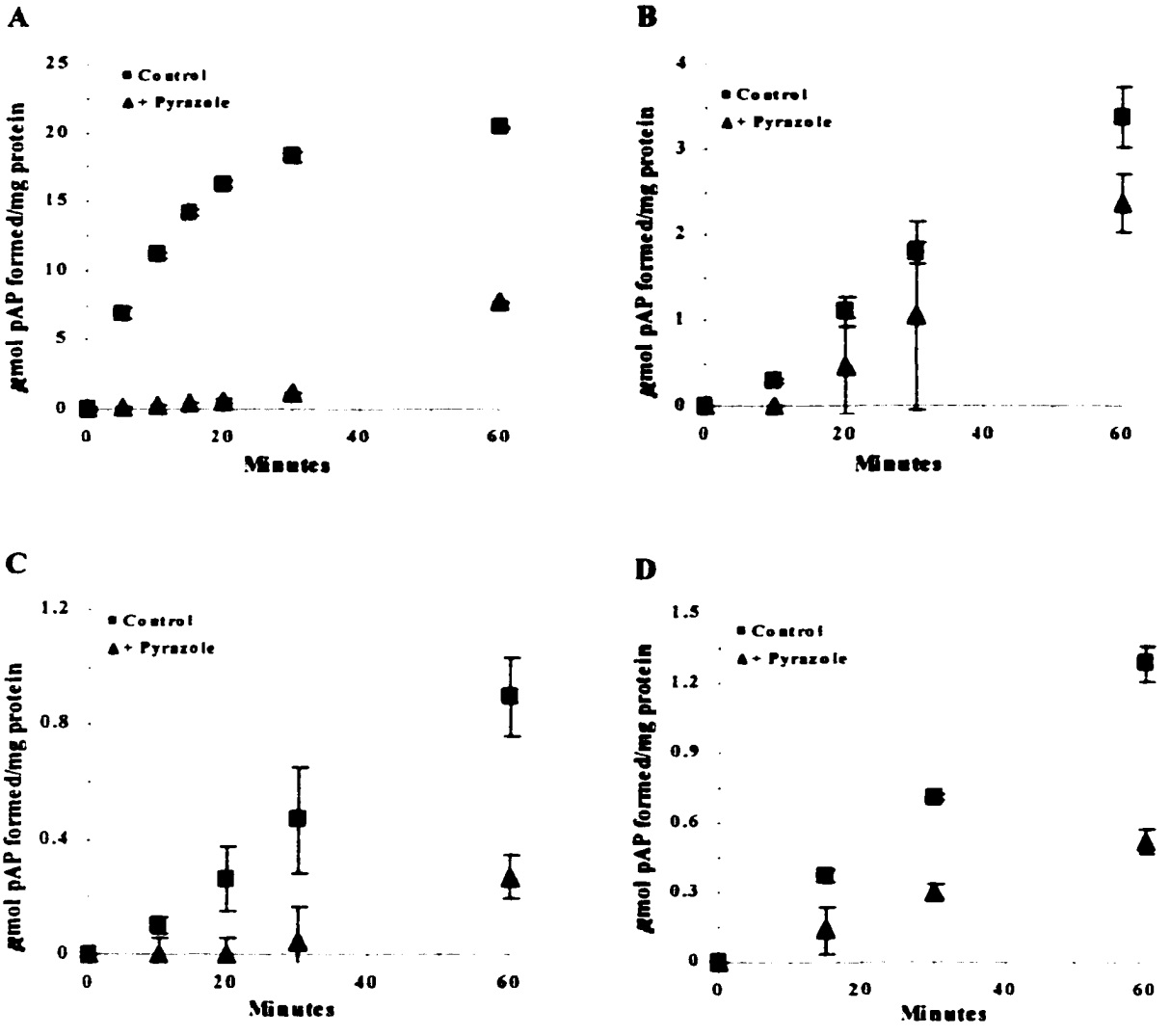

Fig. 3.3A NADH-dependent pNSP reduction by HLADH and purified human isozymes: Effect of pyrazole. Reaction Conditions: In 2 ml, 50 mM Potassium phosphate, pH 7.4; 0.2 mM NADH; 5 mM pyrazole. (A) 1 μg/ml HLADH; 120 μM *p*NSP. (B) 0.75 μg/ml αα-ADH; 300 μM *p*NSP. (C) 0.75 μg/ml $\beta_1\beta_1$-ADH; 300 μM *p*NSP. (D) 1 μg/ml $\beta_2\beta_2$-ADH; 300 μM *p*NSP. (E) 0.41 μg/ml χ-ADH; 300μM *p*NSP. (F) 0.7 μg/ml π-ADH; 120 μM *p*NSP. (G) 0.8 μg/ml σ-ADH; 300 μM *p*NSP.

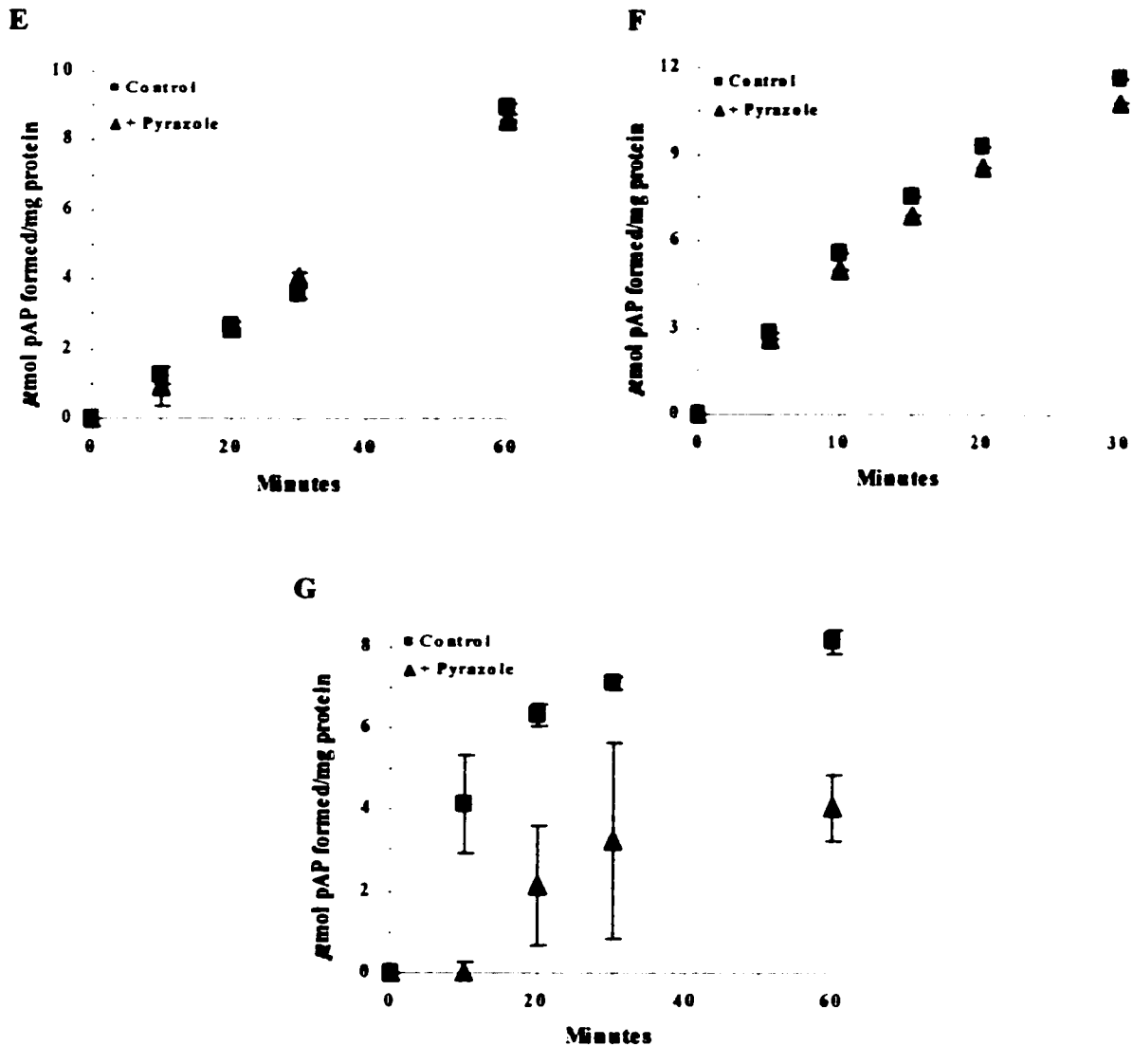

Fig. 3.3B NADH-dependent pNSP reduction by HLADH and purified human isozymes: Effect of pyrazole. Reaction Conditions: In 2 ml, 50 mM Potassium phosphate, pH 7.4; 0.2 mM NADH; 5 mM pyrazole. (A) 1 μg/ml HLADH; 120 μM *p*NSP. (B) 0.75 μg/ml αα-ADH; 300 μM *p*NSP. (C) 0.75 μg/ml $\beta_1\beta_1$-ADH; 300 μM *p*NSP. (D) 1 μg/ml $\beta_2\beta_2$-ADH; 300 μM *p*NSP. (E) 0.41 μg/ml χ-ADH; 300μM *p*NSP. (F) 0.7 μg/ml π-ADH; 120 μM *p*NSP. (G) 0.8 μg/ml σ-ADH; 300 μM *p*NSP.

class II π-ADH, where only a 30 min time course is presented. The data illustrate the marked differences in the metabolism of *p*NSP by the various purified human ADHs and HLADH. Initial experiments were performed at a concentration of *p*NSP (120 μM) comparable to that used in our previous studies (48, 73). However, at this concentration of *p*NSP, the class I, III, and IV ADH isozymes did not catalyze the formation of *p*AP at levels high enough to achieve quantifiable data at all of the time points studied; therefore, time courses with these isozymes were determined using 300 μM *p*NSP. Class II π-ADH showed greater preference for the C-nitroso substrate than the class I αα-, $\beta_1\beta_1$-, and $\beta_2\beta_2$-, class III χ-, and class IV σ-ADHs. Pyrazole, which is a potent inhibitor of ethanol oxidation by class I ADH and a weak inhibitor of that by class II π-ADH, potently inhibited *p*NSP reduction by class I $\beta_1\beta_1$-ADH and HLADH but not that by class I αα- and $\beta_2\beta_2$-ADH, class II, class III and class IV ADH. NADH-dependent pNSP reduction by class I αα-ADH was linear for the entire time course studied and 5 mM pyrazole inhibited this activity by 40% (Fig. 3.3A). The activities of the human beta isozyme homodimers, $\beta_1\beta_1$ and $\beta_2\beta_2$, were linear for up to 60 min, however, they show varying degrees of inhibition by pyrazole. *p*NSP reduction by the $\beta_1\beta_1$-ADH isozyme was inhibited 90% by 5 mM pyrazole whereas the $\beta_2\beta_2$-ADH-catalyzed activity was inhibited by about 60%. As was seen for ethanol oxidation, pyrazole inhibition of the Class II π and Class III χ isozymes was negligible (< 5%). At 300 μM *p*NSP class IV σ-ADH-catalyzed formation of *p*AP was linear for up to 20 min. Thereafter, product formation began to plateau, indicating that the concentration of *p*NSP had become limiting in the reaction. In this regard the *p*NSP concentrations are

presumed to be below saturating in the reaction. The reaction catalyzed by class IV σ-ADH was inhibited 50% by pyrazole.

3.3.3 Determination of Steady-State Kinetic Constants for Acetaldehyde and *p*NSP Reduction via HLADH

Figure 3.4A shows a Lineweaver-Burk plot for *p*NSP reduction by HLADH where *p*NSP concentrations were varied over a range of 0.03-1.2 mM in the presence of a constant concentration of 50 nM HLADH and 0.9 mM NADH. A similar plot was obtained for acetaldehyde (1.2-14.2 mM) reduction via 10 nM HLADH and 0.3 mM NADH (Fig. 3.4B). Calculated K_M and V_{max} values for each were determined using a statistical program described by Cleland (78) and are compared in Table 3.1. The catalytic efficiency (k_{cat}/K_M) of HLADH toward *p*NSP reduction was similar to its efficiency toward acetaldehyde reduction (2017 mM^{-1} min^{-1} vs. 2332 mM^{-1} min^{-1}, respectively). However, the K_M and V_{max} values for acetaldehyde reduction were at least three times greater than those obtained for *p*NSP reduction. The kinetic constants for the human ADH-catalyzed reduction of *p*NSP were determined for the class I αα-, $\beta_1\beta_1$-, and $\beta_2\beta_2$-, and the class II π-ADH isozymes. Each human isozyme appeared to be at least one order of magnitude less efficient in catalyzing *p*NSP reduction than HLADH. The lower efficiencies are attributable to higher K_M and lower V_{max} values associated with *p*NSP reduction.

3.3.4 Spectral Transitions During the Reduction of *p*NSP by ADH Isozymes

As reported by Maskos and Winston (37) a unique feature of HLADH-catalyzed reduction of *p*NSP (Fig. 3.5) was the formation of a spectral intermediate between 252 and 261 nm, which arises concomitantly with loss of absorbance associated with the nitroso compound at 400 nm. This intermediate then decayed slowly, giving rise to an

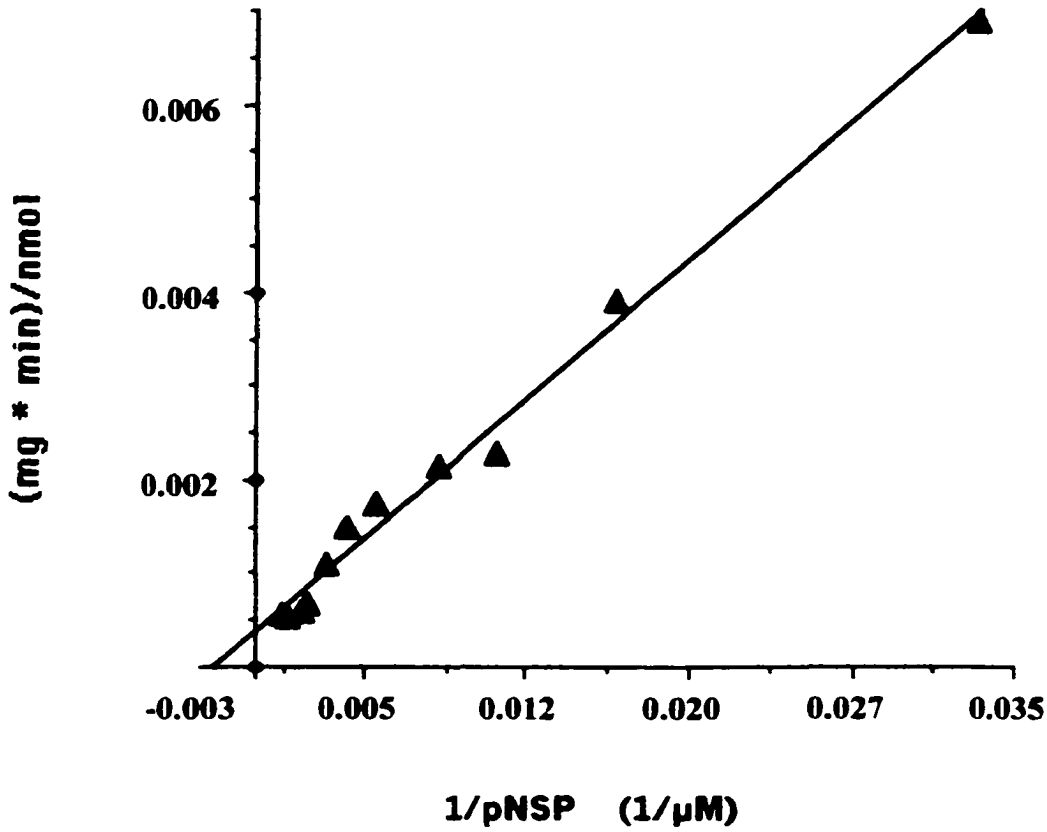

Fig. 3.4A Determination of Kinetic Constants for pNSP and Acetaldehyde Reduction by HLADH. Reaction with 0.9 mM NADH in 50 mM phosphate buffer at pH 7.4. HLADH was present at 50 nM. Each data point represents the mean of at least three experiments run in triplicate.

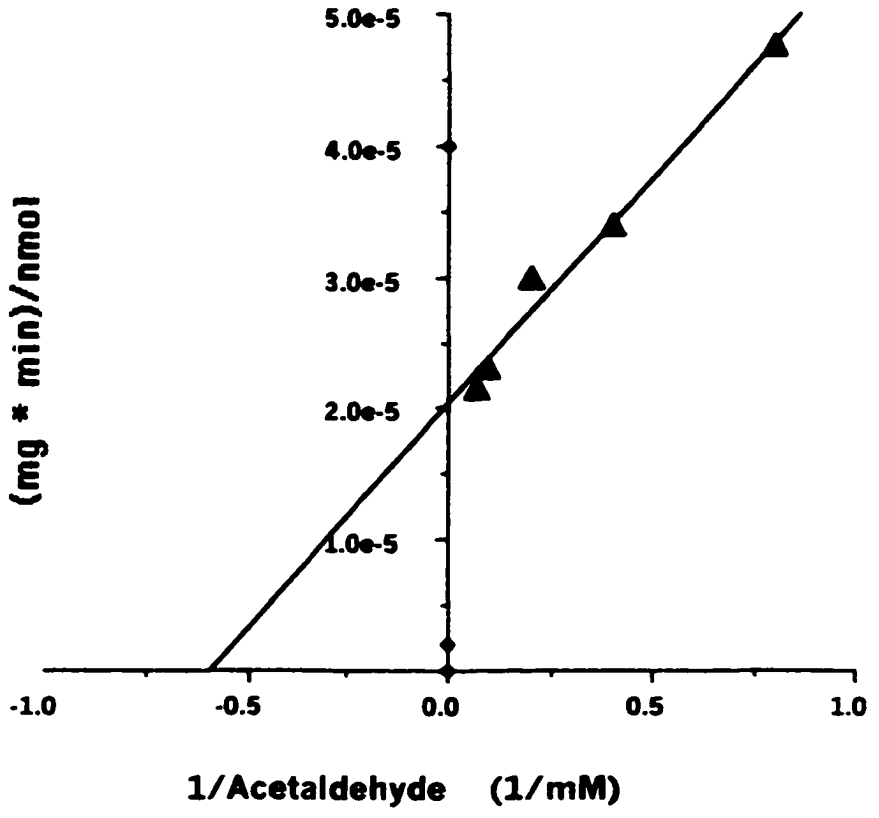

Fig. 3.4B Determination of Kinetic Constants for pNSP and Acetaldehyde Reduction by HLADH. Reaction with 0.3 mM NADH in 50 mM phosphate buffer at pH 7.4. HLADH was present at 10 nM. Each data point represents the mean of at least three experiments run in triplicate.

Table 3.1 Kinetic constants for Horse Liver ADH towards *p*NSP and acetaldehyde at pH 7.4.

	K_M (mM)	V_{max} (μmol/min/mg)	k_{cat}/K_M mM^{-1} min^{-1}
*p*NSP	0.52	13.11	2017
Acetaldehyde	1.68	48.98	2332

Kinetic constants for *p*NSP reduction via Human ADH isozymes at pH 7.4

	K_M (mM)	V_{max} (μmol/min/mg)	k_{cat}/K_M mM^{-1} min^{-1}
αα-ADH	4.19	2.55	49
$\beta_1\beta_1$-ADH	1.10	1.66	121
$\beta_2\beta_2$-ADH	2.02	1.49	59
π-ADH	2.19	4.84	177
χ-ADH	0.70	1.46	168
σ-ADH	1.30	6.95	428

Reaction conditions were as follows: 50 mM Potassium phosphate buffer; 30-1270 μM *p*NSP; 1.25–15 mM Acetaldehyde; 2 mM NADH; 0.8-4 μg/ml HLADH; 2.3 μg/ml αα-ADH; 2.5 μg/ml $\beta_1\beta_1$-ADH; 3.3 μg/ml $\beta_2\beta_2$-ADH; 1.9 μg/ml π-ADH. Assays with χ- and σ-ADH were performed in 0.1 M MES, 51 mM NEA, 51 mM DEA, pH 7.4; 3.8 μg/ml χ-ADH; 1.2 μg/ml σ-ADH.

absorbance due to *p*AP formation (232 nm). Neither HLC nor any of the human ADH isozymes tested appeared to catalyze the formation of this intermediate. The reaction catalyzed by human ADH indicated that the decay of *p*NSP at 400 nm and NADH at 340 nm is associated with the formation of *p*AP with an absorbance maximum at 232 nm (Fig. 3.5). The maxima associated with the intermediate at 252 and 261 nm in the HLADH catalyzed reaction are characteristic of the observed spectrum of 1,4-benzoquinoneimine (BQI) (77). Maskos and Winston (37) have proposed two distinct

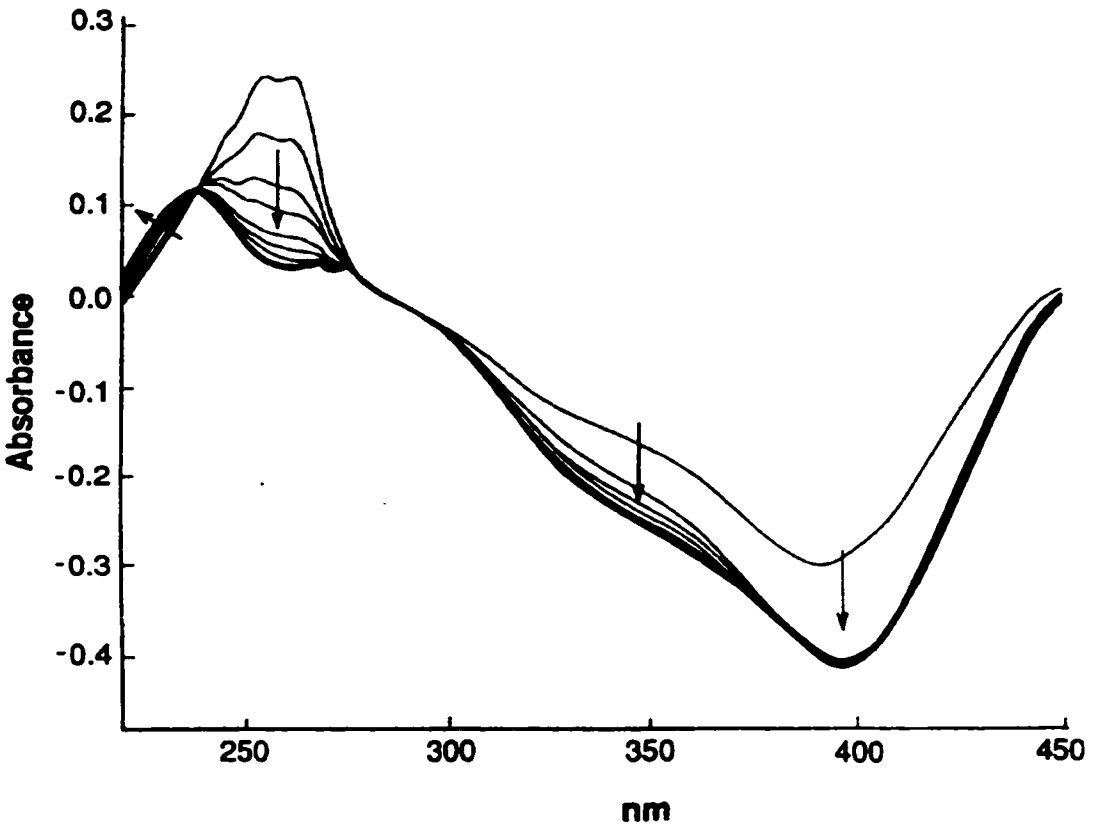

Fig. 3.5A Changes in absorption spectra during the reduction of *p*NSP by HLADH. Time interval between scans is 1 min. Reaction Conditions: 50 mM Potassium phosphate, pH 7.4 in 1ml; 0.1 mM *p*NSP, 0.1mM NADH. Enzyme concentration: 20 µg/ml HLADH. Graph was reprinted from Maskos and Winston, 1994 (37).

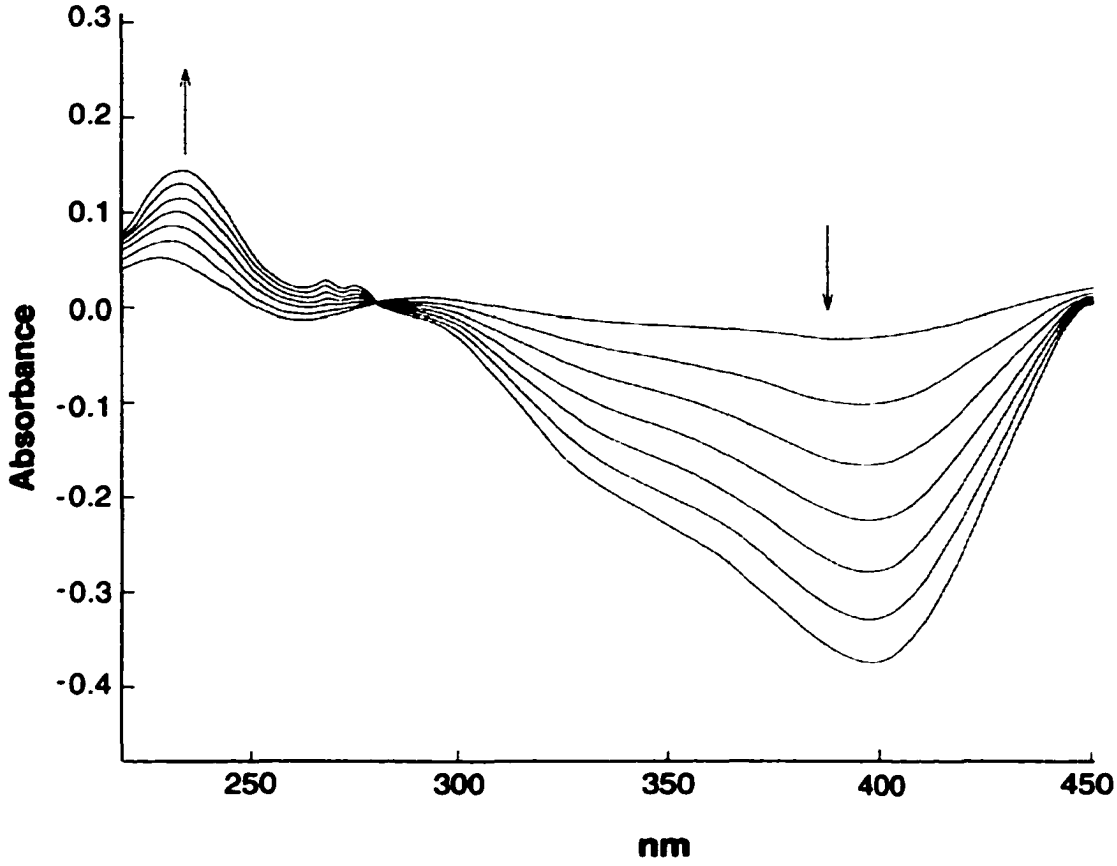

Fig. 3.5B Changes in absorption spectra during the reduction of *p*NSP by π-ADH. Time interval between scans is 1.5 min. Reaction Conditions: 50 mM Potassium phosphate, pH 7.4 in 1ml; 0.1 mM *p*NSP, 0.1mM NADH. Enzyme concentration: 25 μg/ml π-ADH. Graph was reprinted from Maskos and Winston, 1994 (37).

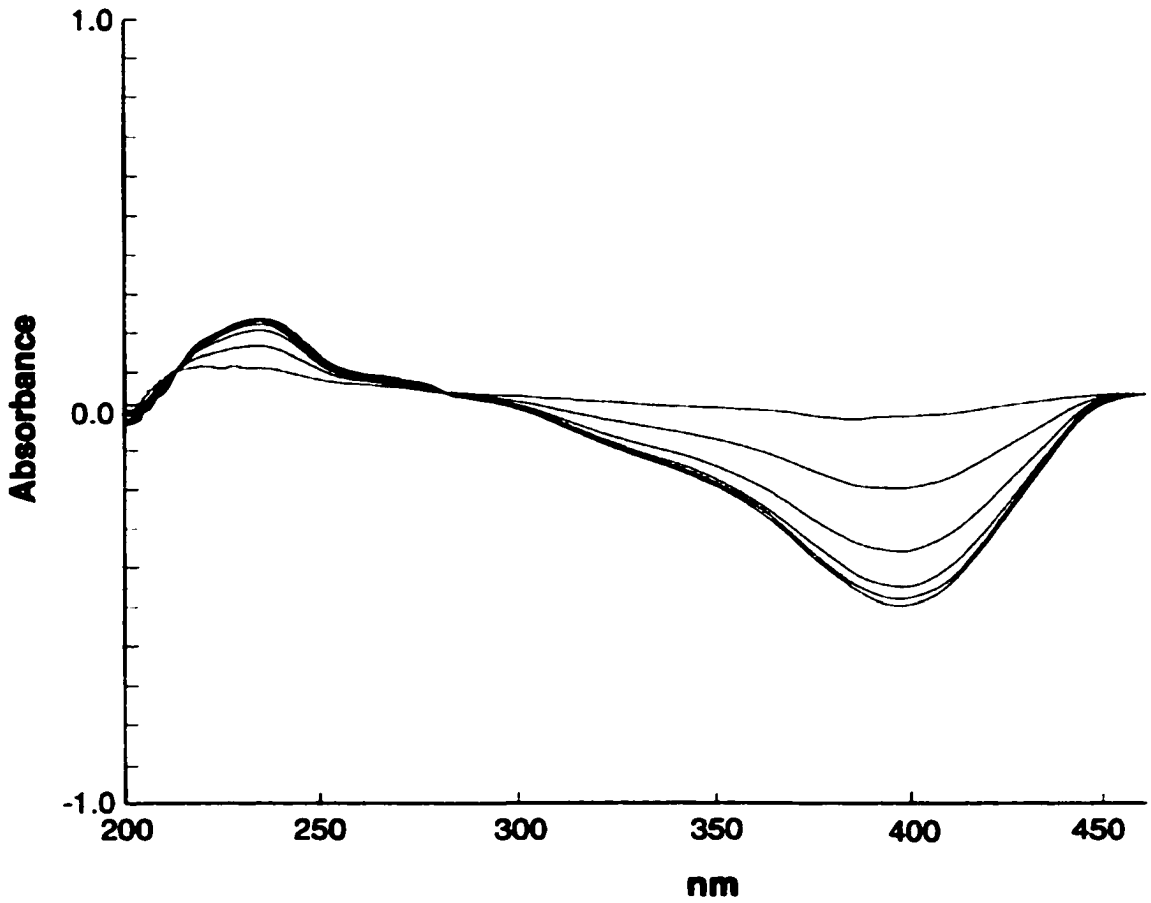

Fig. 3.5C Changes in absorption spectra during the reduction of *p*NSP by αα-ADH. Time interval between scans is 1.5 min. Reaction Conditions: 50 mM Potassium phosphate, pH 7.4 in 1ml; 0.1 mM *p*NSP, 0.1mM NADH. Enzyme concentration: 15 μg/ml αα-ADH.

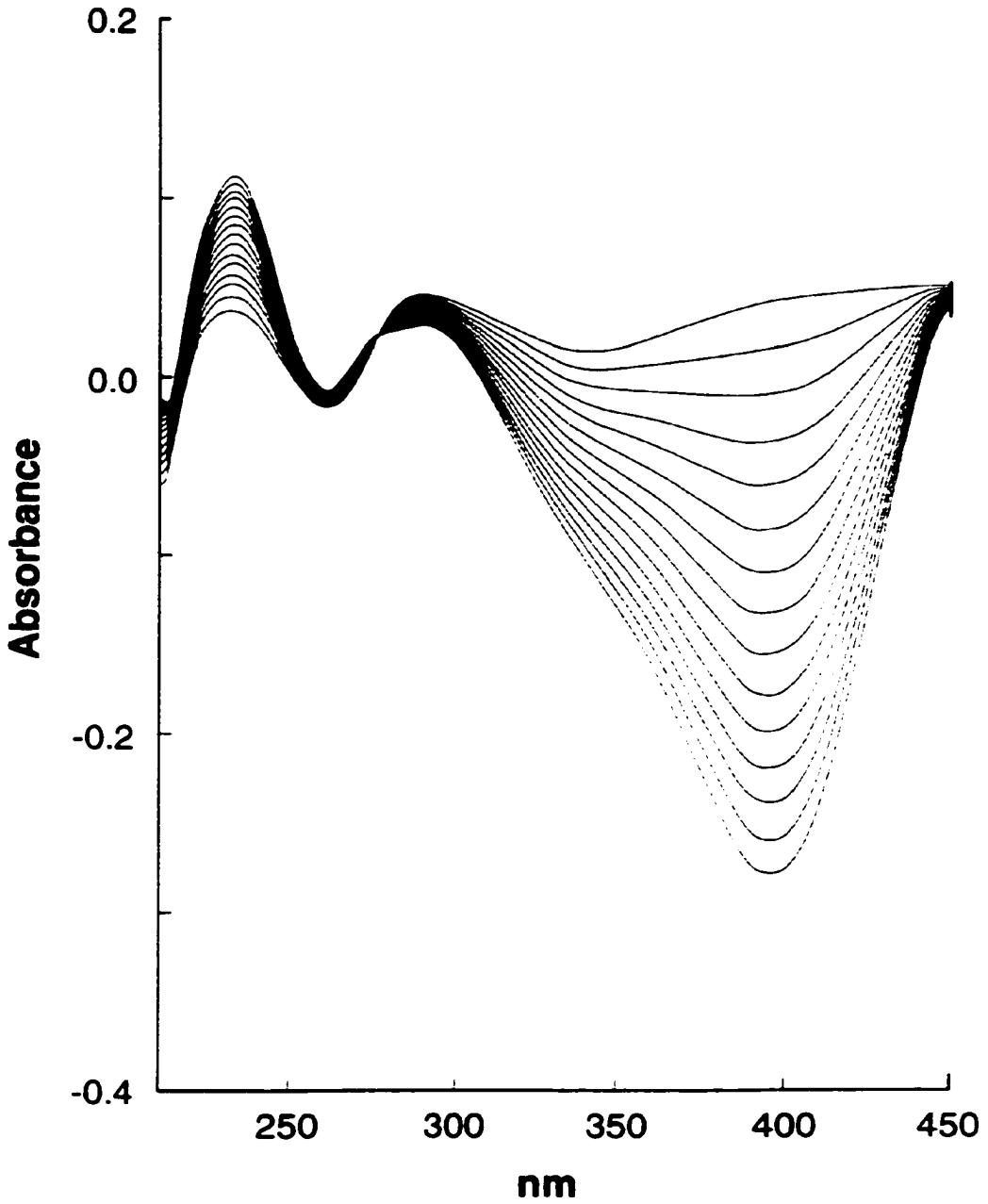

Fig. 3.5D Changes in absorption spectra during the reduction of *p*NSP by $\beta_1\beta_1$-ADH. Time interval between scans is 1.5 min. Reaction Conditions: 50 mM Potassium phosphate, pH 7.4 in 1ml; 0.1 mM *p*NSP, 0.1mM NADH. Enzyme concentration: 39 μg/ml $\beta_1\beta_1$-ADH.

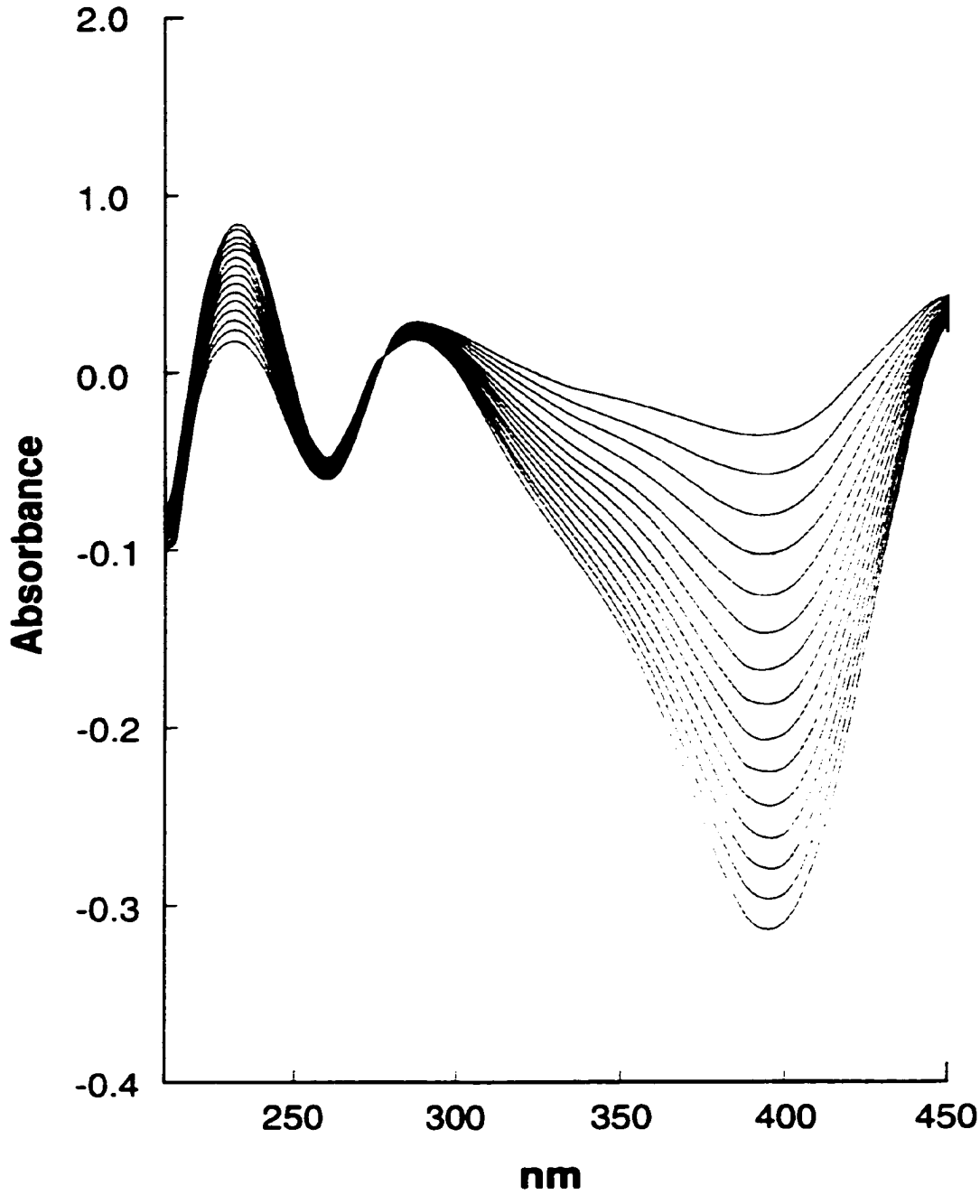

Fig. 3.5E Changes in absorption spectra during the reduction of *p*NSP by $\beta_2\beta_2$-ADH. Time interval between scans is 1.5 min. Reaction Conditions: 50 mM Potassium phosphate, pH 7.4 in 1ml; 0.1 mM *p*NSP, 0.1mM NADH. Enzyme concentration: 24 μg/ml $\beta_2\beta_2$-ADH.

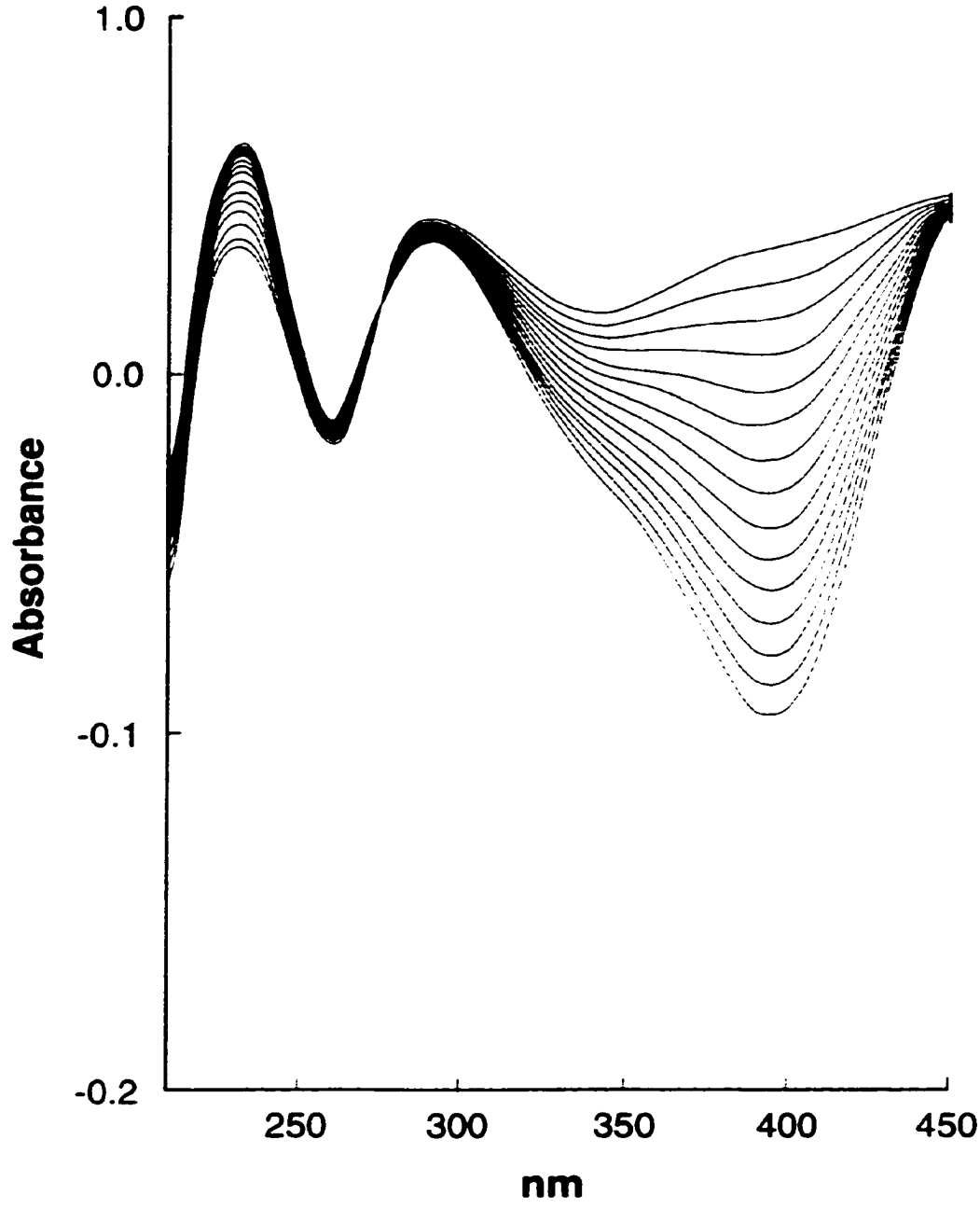

Fig. 3.5F Changes in absorption spectra during the reduction of *p*NSP by χ-ADH. Time interval between scans is 2 min. Reaction Conditions: 50 mM Potassium phosphate, pH 7.4 in 1ml; 0.1 mM *p*NSP, 0.1mM NADH. Enzyme concentration: 24 μg/ml χ-ADH.

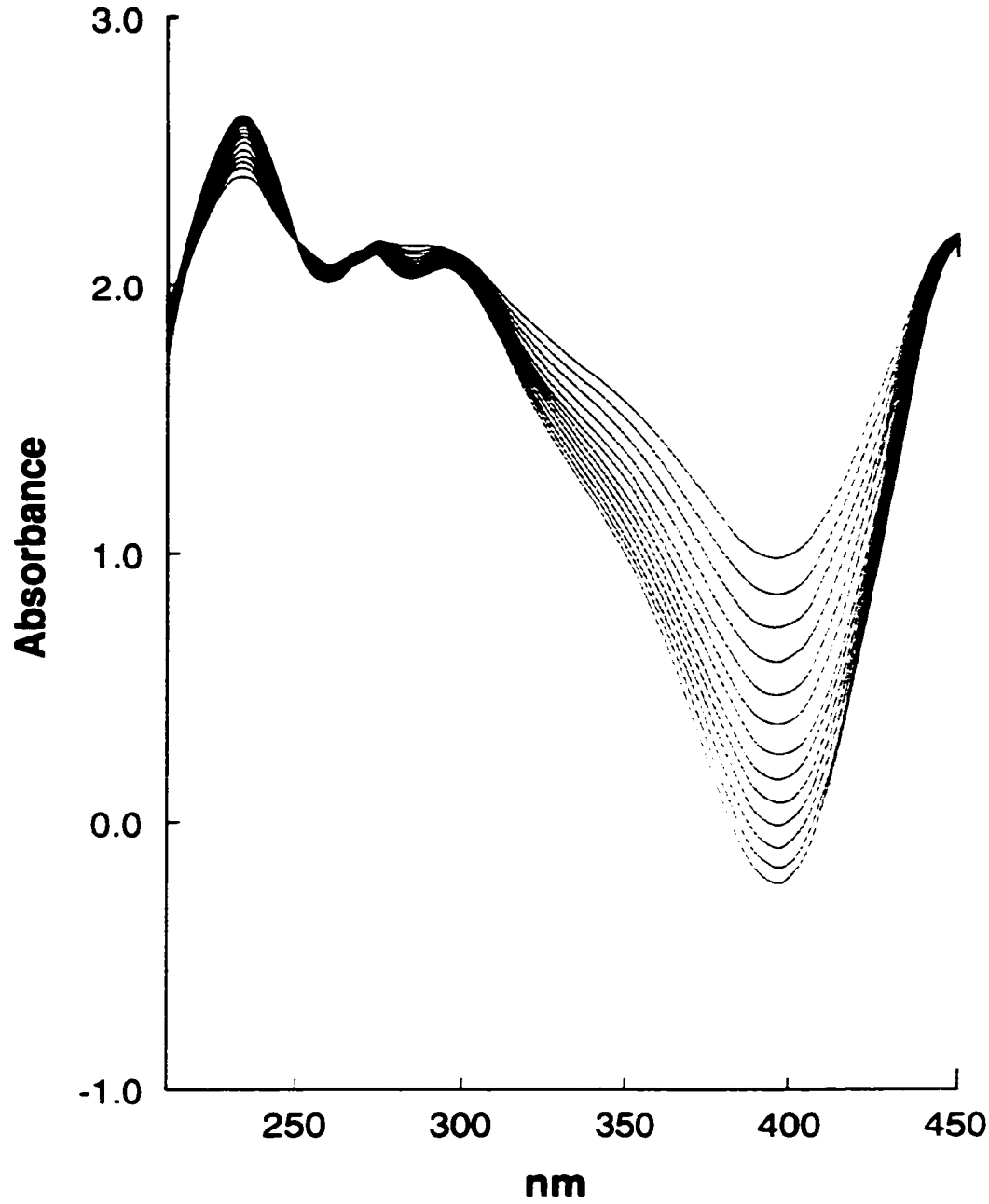

Fig. 3.5G Changes in absorption spectra during the reduction of *p*NSP by σ-ADH. Time interval between scans is 1 min. Reaction Conditions: 50 mM Potassium phosphate, pH 7.4 in 1ml; 0.1 mM *p*NSP, 0.1mM NADH. Enzyme concentration: 8 μg/ml σ-ADH.

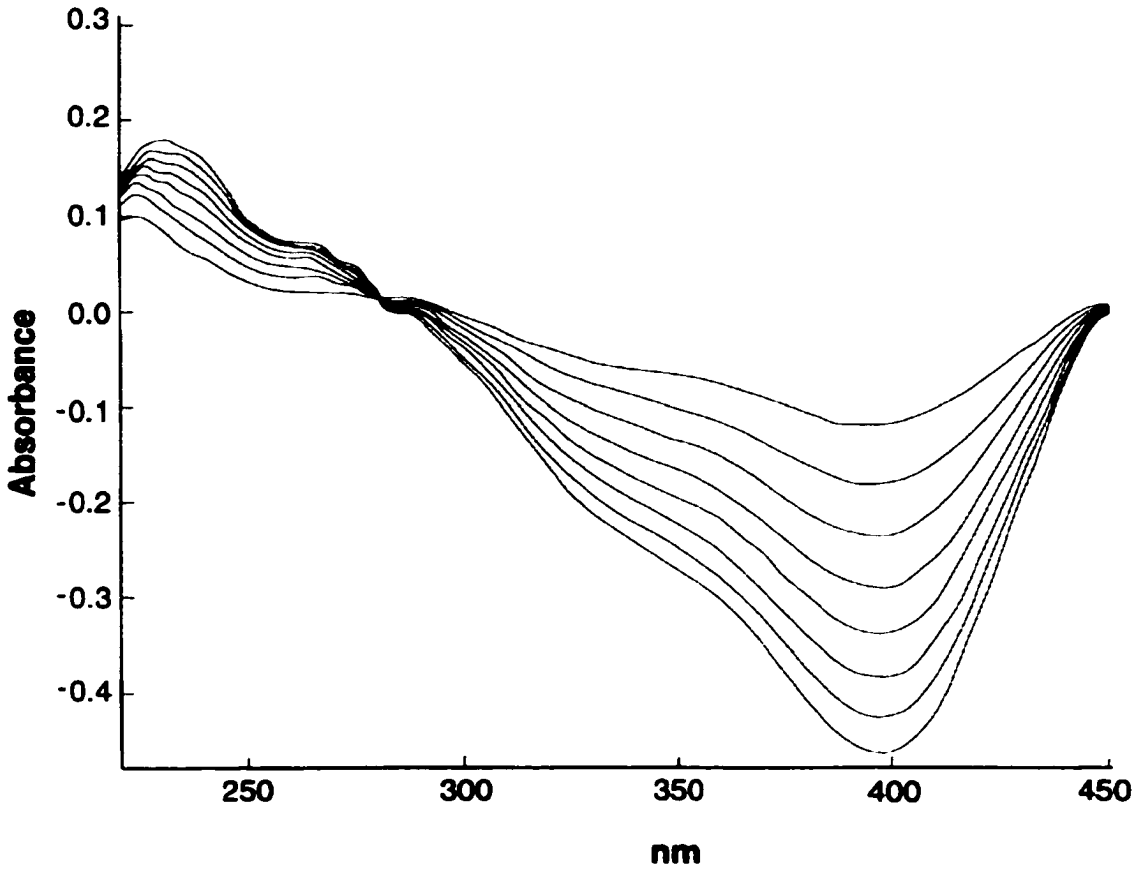

Fig. 3.5H Changes in absorption spectra during the reduction of *p*NSP by HLC. Time interval between scans is 1.5 min. Reaction Conditions: 50 mM Potassium phosphate, pH 7.4 in 1ml; 0.1 mM *p*NSP, 0.1mM NADH. Enzyme concentration: 0.38 mg/ml HLC.

mechanisms for the metabolism of *p*NSP by ADH isozymes dependent on the ability of the individual enzymes to efficiently metabolize BQI.

Pursuant to the study of Maskos and Winston, we show the comparative activities of HLADH and various human ADH isozymes with respect to nitroso and benzoquinoneimine reduction and ethanol oxidation (Table 3.2). The rates for reduction of *p*NSP and appearance of *p*AP were calculated based on the change in absorbance at 400 and 232 nm, respectively, as seen in the spectral profiles. HLADH was considerably more active than the human isozymes as a *p*NSP reductase. The specific activity for reduction of *p*NSP by HLADH was 1.53 μmol/min/mg, which was two times greater than that of the most active human ADH. However, HLADH, which exhibits relatively poor activity as a benzoquinoneimine reductase (0.001 μmol/min/mg), had a specific activity of 0.218 μmol/min/mg for *p*AP formation.

Table 3.2 Activity of HLADH and Human ADH isozymes as ethanol oxidases, nitroso- and benzoquinoneimine reductases.

	Ethanol Oxidation	*p*NSP reduction	1,4-Benzoquinoneimine reduction	*p*AP formation
	μmol/min/mg		μmol/min/mg	
HLADH	1.1	1.53	0.001	0.218
Human αα-ADH	1.43	0.707	0.369	0.635
Human $\beta_1\beta_1$-ADH	0.12	0.027	0.012	0.025
Human $\beta_2\beta_2$-ADH	0.6	0.090	0.200	0.082
Human χ-ADH	4.69	0.145	ND[a]	0.140
Human π-ADH	0.08	0.530	6.650	0.541
Human σ-ADH	40.0	0.189	No Activity	0.180

Reaction conditions were as follows: 50 mM phosphate buffer; 10 mM EtOH (6mM Cinnamyl Alcohol with χ-ADH); 120 μM *p*NSP; 32 μM BQI; 0.1-0.2 mM NADH; 25-50 μg/ml HLADH; 0.75-15 μg/ml αα-ADH; 22-93 μg/ml $\beta_1\beta_1$-ADH; 4.2-42 μg/ml $\beta_2\beta_2$-ADH; 1.9-48 μg/ml π-ADH; 0.45-2.7 μg/ml χ-ADH; 8-22 μg/ml σ-ADH. Results represent mean of triplicate determinations.

[a]Activity not determined.

The specific activity of class I αα-ADH for the reduction of *p*NSP was 0.707 μmol/min/mg, which was higher than all other human isozymes tested. The relative order of specific activities for *p*NSP reduction by these ADH isozymes was HLADH > αα > π > σ >χ > $\beta_2\beta_2$ > $\beta_1\beta_1$. The specific activity of class I $\beta_2\beta_2$-ADH for ethanol oxidation was about 8 times higher than that of class II π-ADH (0.6 μmol/min/mg vs. 0.08 μmol/min/mg, respectively). Class II π-ADH is known to have a much lower ethanol oxidase activity than $\beta_2\beta_2$-ADH (79). In contrast to ethanol oxidation, the specific activity of class II π-ADH for reduction of *p*NSP was 6 times higher than that of class I $\beta_2\beta_2$-ADH (0.53 μmol/min/mg vs. 0.09 μmol/min/mg, respectively). Class I αα-ADH catalyzed ethanol oxidation with activity similar to HLADH, i.e. 1.4 μmol/min/mg vs. 1.1 μmol/min/mg, respectively. In the reactions catalyzed by human ADH, the rate of *p*AP formation was almost identical to the rate of *p*NSP disappearance (0.6 vs. 0.7 μmol/min/mg, respectively, for αα-ADH). Thus, the second step of the reaction, the reduction of benzoquinoneimine, does not appear to be rate limiting for the overall reaction. The rate of BQI reduction catalyzed by class II π-ADH was at least an order of magnitude higher than all other ADH isoenzymes tested, which may indicate a role for π-ADH as a biological quinone reductase (37). Each of the human ADH isozymes showing BQI reductase activity catalyzed the reduction of BQI at least 2 orders of magnitude faster than the corresponding rate for HLADH-catalyzed BQI reduction. At first hand, a comparison of the rates of *p*NSP reduction versus the rates of BQI reduction (Table 3.2) would indicate that the activities of class I αα- and $\beta_1\beta_1$-ADH toward BQI were slightly lower than their corresponding activities toward *p*NSP. The concentration of *p*NSP used in these reactions was 120 μM. Since the lowest K_M

value obtained for *p*NSP with any of the human ADH isozymes was approximately 700 μM, *p*NSP is subsaturating. At 32 μM the concentration of BQI used in these reactions was also most likely not saturating; therefore, an increase in BQI concentration to levels used for *p*NSP would likely increase the rates of its reduction. Thus, the rate of BQI reduction, the second reductive step, potentially could exceed that of *p*NSP reduction, the first reductive step of the reaction. In contrast, HLADH-catalyzed reduction of BQI was 3 orders of magnitude lower than *p*NSP reduction, 0.001 μmol/min/mg vs. 1.53 μmol/min/mg, respectively. Reduction of BQI (32 μM) with class IV σ-ADH was not observed.

3.4 Discussion

Both microsomal and cytosolic enzyme activities are involved in the metabolism of nitroaromatics and arylamines. Activation of nitroaromatic compounds to mutagens involves formation of partially reduced metabolites, such as C-nitroso or hydroxylamino compounds, via nitroreduction (54, 55). Formation and removal of the nitroso intermediates of arylamines and nitroaromatics is of the utmost importance in their mutagenic expression.

The objective of our previous studies was to determine the role of ADH in the reductive metabolism of C-nitroso compounds in cytosol where other C-nitroso group reducing enzymes are present simultaneously. In these studies *p*NSP was used as an aldehyde-substrate analog to compare the C-nitroso reductase activities of several ADH isozyme representatives of the four major classes of ADH expressed in human liver and other tissues. In our previous studies with deermouse cytosol it was suggested that the metabolism of *p*NSP involves a complex interplay of cytosolic enzymes. Therefore, our

approach to the study of cytosolic C-nitroso reduction was to use assay specific enzyme inhibitors of different putative C-nitrosoreductases, i.e. pyrazole, allopurinol, and dicumarol. The rate of NADPH-dependent C-nitroso reduction by cytosolic fractions was about 50% lower than the NADH-dependent rate; indicating that a substantial amount of the C-nitroso reduction is due to NADH-dependent enzymes. Pyrazole inhibited NADH-dependent *p*NSP reduction by ADH-positive deermouse cytosol by > 85%. Thus, ADH appears to contribute substantially to NADH-dependent C-nitroso reduction. The NAD(P)H: quinone oxidoreductase inhibitor, dicumarol, inhibited NADH-dependent *p*AP formation from *p*NSP by about 25%; however, dicumarol potently inhibited the NADPH-dependent formation (90-95%). Similar results were also reported by Hajos and Winston for the rat cytosolic system (48).

Our experiments with human liver cytosol showed that pyrazole potently inhibited the NADH-dependent formation of *p*AP from *p*NSP. This inhibition was more profound than that seen with rat liver cytosol. NADPH-dependent activity was potently inhibited by dicumarol and not inhibited by pyrazole. In agreement with our previous studies with deermouse and rat liver cytosols, allopurinol did not inhibit either NADH- or NADPH-*p*AP formation by human liver cytosol. The data indicate NADH-dependent C-nitrosoreductase activity in human liver cytosol, as in rat and deermouse liver, as being associated mainly with alcohol dehydrogenase. Thus, NADH-dependent reduction of *p*NSP by human liver cytosol behaves essentially identical to that observed in the rat and deermouse liver cytosols. Although NADPH-dependent *p*NSP reductase activity of human liver cytosol was only about 15% of NADH-dependent activity, it was strongly inhibited by both dicumarol and pyrazole. NADPH can be used as a

cofactor by certain ADH isozymes, albeit less efficiently than NADH (70, 80). Our data suggest the presence of an ADH in human liver cytosol with preference for NADPH that is not present in the rodent cytosols studied, or the presence of ADH that can use NADPH with similar efficiency as NADH. Supporting evidence of significant NADH-dependent C-nitroso reduction due to ADH is the fact that purified HLADH presented the same general trends as those seen with the cytosolic preparations. HLADH catalyzed NADH-dependent reduction of *p*NSP and was potently inhibited (90%) by 5 mM pyrazole.

ADH isozymes display wide variation in both substrate and inhibitor specificity (81). There are both inter- and intraclass differences in their substrate specificities (14, 82, 83). Methanol, digitoxigenins, the glycol intermediates in norepinephrine metabolism, and the intermediary alcohols and aldehydes of dopamine metabolism are substrates of class I ADH (14, 82-84), while class II preferentially catalyzes benzyl alcohol/benzaldehyde oxidoreduction (14). Thus far, only long-chain aliphatic alcohols have been found to be good substrates of class III ADH (83). Purified class IV ADH exhibits the highest catalytic efficiency with long chain alcohols. It also exhibits activity with more complex alcohols such as all-*trans*-retinol. Therefore, it was not surprising that human ADH exhibited marked differences in the metabolism of *p*NSP. Class II π-ADH, which has a much lower preference for ethanol than the class I isozymes (79, 85), showed significantly greater efficiency in the reduction of the C-nitroso substrate than the class I ADH. *p*NSP reduction by class I αα- and $\beta_2\beta_2$-ADH and class II π-ADH inferred a lower affinity with these isozymes for the nitroso substrate as compared to HLADH, $\beta_1\beta_1$-, χ- and σ-ADH.

Pyrazole, a potent inhibitor of ethanol oxidation by class I ADH and a weak inhibitor of that by classes II and III, potently inhibited *p*NSP reduction by $\beta_1\beta_1$-ADH but not that by π-ADH and χ-ADH. The activity of human π- and χ-ADHs appeared to be relatively insensitive to inhibition by 5 mM pyrazole. Whereas, the activity of $\alpha\alpha$-, $\beta_2\beta_2$- and σ-ADH were inhibited by about 50%, $\beta_1\beta_1$-ADH is inhibited by about 90%. As the $\beta_1\beta_1$-ADH isoform is the predominate ADH found in the liver of caucasians, it is significant to note the similarities in the nitrosoreductase capabilities of this enzyme and HLC. Inhibition by pyrazole was similar between HLC and $\beta_1\beta_1$-ADH; both were inhibited by more than 90%. These results lend credence to the interpretation that the predominance of C-nitrosoreductase activity in the cytosol is due to ADH.

The differences in the activities between ADH isozymes may be attributed to their distinctively different active site geometries. The inner part of the substrate-binding pocket is formed by the zinc atom, its ligands, the nicotinamide ring of NADH, and residues 48 and 93 (18). The class I $\alpha\alpha$-ADH isozyme has the greatest overall structural identity with class I β-ADH. However, their substrate binding pockets differ dramatically (86). For instance, the active site of $\beta_1\beta_1$-ADH is narrow and restrictive near the catalytic zinc atom and can bind small substrates in relatively few conformations, thus increasing opportunities for productive bonds between the substrate and amino acid side chains of the active site. The active site of the $\alpha\alpha$-ADH isozyme cannot restrict the binding of small substrates and more non-productive bonds may be formed. The $\alpha\alpha$-ADH, having an Ala-93 substitution for the Phe-93 that is present in other class I, II, and IV ADH, exhibits a more spacious active site near the catalytic zinc atom and narrows as the distance from the zinc increases. In contrast to small substrates

such as ethanol, the increased volume of the active site near the catalytic zinc atom of αα-ADH may accommodate the phenol ring of *p*NSP in a more productive orientation than can be accomplished with $\beta_1\beta_1$-ADH. Eklund *et al.* have reported that the active site of $\beta_1\beta_1$-ADH limits access to the catalytic zinc ion for bulky compounds such as benzyl alcohol and cyclohexanol (18), which are of similar size and geometry as *p*NSP.

The preference of class III χ-ADH for larger substrates, as seen in its preference for cinnamyl alcohol over ethanol explains its ability to catalyze *p*NSP reduction at a rate more than twice that of the β isoforms, the predominate liver ethanol dehydrogenases. Cinnamyl alcohol has a phenyl ring bound to a propenol moiety. This preference may be due to a unique substrate binding site that encloses twice the volume of the $\beta_1\beta_1$ substrate binding site (86). While the inner portion of the active site in these isozymes is similar, the larger outer portion of the χ-ADH active site may allow the phenol ring of *p*NSP greater degrees of movement and thus allow this substrate to achieve an orientation more conducive to catalysis.

The substrate-binding site of class IV σ-ADH is enlarged near the catalytic zinc ion and the middle region of the substrate-binding pocket is narrow. In general, σ-ADH catalyzed oxidation of primary aliphatic alcohols presents increasing catalytic efficiencies as the chain length increases (4, 11). However, σ-ADH shows different kinetic properties with more complex alcohols, such as steroid alcohols and secondary alcohols. Class IV σ-ADH is unable to oxidize bulky secondary alcohols efficiently. Likewise, while σ-ADH exhibits considerably greater activity as an ethanol oxidase, its activity is comparatively much lower than HLADH and π-ADH with respect to *p*NSP reduction. However, it has been shown that the σ-ADH generally exhibits greater

efficiency catalyzing the reduction of aldehydes (nitroso analogs) than corresponding alcohols at pH 7.5, having both lower K_M and higher V_{max} values (11). Aromatic compounds have also been shown to be good substrates for class IV σ-ADH. The best substrate found so far for σ-ADH is *m*-nitrobenzaldehyde, having a K_M and k_{cat}/K_M of 41 μM and 135,000 mM^{-1} min^{-1}, respectively (11). Benzaldehyde was also a good substrate with K_M and k_{cat}/K_M values of 430 μM and 6,900 mM^{-1} min^{-1}, respectively. Given the structural similarity between these two aldehydes and *p*NSP, it is surprising that the σ-ADH does not exhibit activities and efficiencies with the nitroso substrate (k_{cat}/K_M = 428 mM^{-1} min^{-1}) more comparable to the benzaldehyde substrate. This comparatively lower activity may indicate inhibitory secondary interactions of the *p*NSP hydroxyl moiety with active site residues.

As in alcohol oxidation, the overall *p*NSP reduction rate is likely dependent on coenzyme-binding residues since the rate-limiting step in alcohol oxidation has been shown to be the dissociation of NADH. The clearest example of this is the difference in *p*NSP reduction rates between $\beta_1\beta_1$-ADH and $\beta_2\beta_2$-ADH. These two class I β-ADH variants differ by only one residue in their substrate- and coenzyme-binding sites; Arg 47 in β_1 has been replaced by a His residue in β_2 (6). Yet, $\beta_2\beta_2$-ADH catalyzed *p*NSP reduction at a rate 4 times higher than that of $\beta_1\beta_1$-ADH.

As the nitroso moiety is both isosteric and isoelectronic with aldehyde functionality, it was informative to compare the ADH catalyzed reductions of *p*NSP and acetaldehyde. HLADH shows a three-fold higher K_M and V_{max} for acetaldehyde than for *p*NSP. In comparison, Leskovac *et al.* (75) showed similar results in that the V_{max} values for *p*NSP and acetaldehyde were of the same order of magnitude. It is of more

significance that the catalytic efficiency of the HLADH-catalyzed reduction of *p*NSP is virtually identical to that of the reduction of acetaldehyde, the classical substrate of the enzyme, which indicates that *p*NSP is an excellent substrate for the liver enzyme. Moreover, the higher K_M for acetaldehyde may indicate a greater affinity of the enzyme for the larger *p*NSP substrate.

In a study that compared HLADH with class II π-ADH, Maskos and Winston (37) observed a spectral intermediate in the reaction of HLADH-dependent reduction of *pNSP* that was not present in the reaction catalyzed by π-ADH. This intermediate was identified base on its spectral characteristics as BQI. Assuming that the initial stages of the *p*NSP reductase reaction are identical for both ADH isozymes, it was suggested that the human π-ADH removed BQI more efficiently than HLADH removed it. This led Maskos and Winston (37, 87) to propose a dual mechanism for the reduction of *p*NSP by ADH. The first mechanism, attributed to π-ADH, invisages a homogeneous chemical reaction that is coupled between two successive electron transfer reactions. During ADH-dependent reduction of *p*NSP, coordination of the nitroso oxygen to the active site zinc activates the substrate for nucleophilic attack by NADH, which yields *p*-hydroxyaminophenol and NAD^+ at the active site. The *p*-hydroxyaminophenol may then undergo rapid dehydration to *p*-benzoquinoneimine, which is subsequently reduced in an ADH-dependent manner to *p*AP. In the other mechanism, BQI is released from the ADH active site and undergoes a non-enzymatic reaction to form an arylnitrenium ion. This nitrenium ion may undergo subsequent hydrolysis to benzoquinone or nonenzymatic NADH-dependent reduction to *p*AP. This latter mechanism was suggested for HLADH. The present data indicates that all of the human class I and

class II ADH studied are capable of catalyzing the 2-electron reduction of 1,4-benzoquinoneimine to *p*AP. Class II π-ADH was particularly efficient (k_{cat}/K_M = 30 μM^{-1} min^{-1}). Uniquely, the class IV σ-ADH enzyme is not indicated to catalyze benzoquinoneimine reduction. The apparent inability of σ-ADH to reduce BQI suggested a mechanism for *p*NSP reduction analogous to that for HLADH. However, the fact that a spectral intermediate in the σ-ADH-catalyzed reaction was not detected precludes this assumption. The fact that the rate of *p*NSP disappearance (0.189 μmol/min/mg) is similar to the rate of *p*AP appearance (0.180 μmol/min/mg) indicates that any intermediate formed in the σ-ADH catalyzed reaction is efficiently removed. As stated previously, the initial step of *p*NSP reduction involves ADH-dependent formation of *p*-hydroxyaminophenol, which is then dehydrated to BQI. One possible explanation for the absence of an intermediate in the σ-ADH profile is that this isozyme may stabilize the hydroxyaminophenol, preventing dehydration, and may efficiently catalyze the direct reduction of the hydroxyaminophenol to *p*AP. It is also possible that the σ-ADH does indeed catalyze BQI reduction; however, at 32 μM the concentration of BQI is insufficient to overcome diffusion and initiate catalysis. It is well known that class IV σ-ADH exhibits a substantially higher K_M for ethanol oxidation as compared to the other human enzymes. However, because reduction of *p*NSP leads to formation of BQI at the active site of σ-ADH, the obstacle imposed by diffusion into the active site is eliminated, thereby allowing immediate BQI reduction.

The present data show significant differences in the metabolism of *p*NSP by purified human ADH and HLADH isozymes and in the sensitivities of these ADH to inhibition by pyrazole. These results may prove important in the understanding of the

mutagenic activation of C-nitroso intermediates in the metabolism of arylamines and nitroarenes. Detailed characterization of the steady state kinetic parameters of the C-nitroso reductase activity of these enzymes is presented in Chapter 4.

CHAPTER 4 EFFECT OF pH ON ALCOHOL DEHYDROGENASE DEPENDENT REDUCTION OF *P*-NITROSOPHENOL: COMPARISON OF HORSE LIVER AND HUMAN ISOZYMES

4.1 Introduction

The ADH-dependent oxidation of alcohols and reduction of aldehydes is critically dependent on one or more proton transfer steps. These proton transfers would be expected to involve ionizing groups at the active center of the enzyme. A proton relay system has been proposed for HLADH catalyzed alcohol oxidation in which a proton is transferred from the alcohol to form an alcoholate anion that is bound to the active site zinc atom (88). In the relay, the proton is transferred through a hydrogen-bonded network from the alcohol to Ser 48, to the 2′-hydroxyl of the nicotinamide ribose, and finally to the His 51 imidazole, which acts as the terminal general base catalyst that transfers the proton to solvent. Structural analysis of human $\beta_1\beta_1$-ADH shows that this hydrogen bond network is also present in this isozyme, in which threonine substitutes for serine at position 48 (27).

Evidence for the mechanistic importance of ionizing groups at the active center of HLADH has been obtained by examination of the pH dependence of individual reaction steps in the catalytic mechanism (70). Such studies, however, have led to different conclusions concerning the effect of pH on the hydride transfer process. Brooks *et al.* reported base catalysis by a dissociating group with a pK_a of 6.5 for hydride transfer from ethanol to NAD^+ (89). McFarland *et al.* (90) concluded that ternary-complex inter-conversion cannot be subject to acid-base catalysis by a protonic acid with a pK_a between 6 and 10. These authors found that the rate of hydride transfer from NADH to aromatic aldehydes is nearly independent of pH within the range of 6 – 10.

The present investigation was undertaken in order to establish the pH-dependence of the ADH-catalyzed reduction of *p*NSP, a model C-nitroso compound. Herein, we compare the C-nitrosoreductase activities of HLADH, human class I αα-, $\beta_1\beta_1$-, and $\beta_2\beta_2$-ADH, class III χ-ADH, and class IV σ-ADH with respect to pH.

4.2 Materials and Methods

4.2.1 Chemicals and Enzymes

Pyrazole, NADH, NADPH, HLADH, benzaldehyde and potassium ferricyanide were obtained from Sigma (St. Louis, MO). *p*AP, *p*NSP, and phenol were obtained from Aldrich Chemical Co. (Milwaukee, WI). All other chemicals were of the highest grade commercially available.

4.2.2 Expression of Human ADH Isozymes

E.coli JM105 cells containing the cDNA of individual human ADH isozymes subcloned into the EcoRI site of the procaryotic expression vector pKK223-3 (Pharmacia Biotech) were a generous gift of Dr. Tom Hurley (Department of Biochemistry and Molecular biology, Indiana University School of Medicine, Indianapolis, IN 46202). The cells were grown at 37°C to $OD_{595} \geq 0.6$ in 4 L of modified TB media (12 g/liter peptone, 12 g/liter yeast extract, 4 ml/liter glycerol, 17 mM KH_2PO_4, 72 mM K_2HPO_4) containing 50 μg/ml of ampicillin and 50 μl/L of antifoam A. Then $ZnSO_4$ and isopropyl-β-thiogalactopyranoside was added to a final concentration of 7 μM and 0.2 mM, respectively, to induce the expression of the alcohol dehydrogenase gene. The cultures were then placed in a 16°C shaking water bath and incubated for 24 hrs. The cells were centrifuged at 5,000 x g and lysed in isozyme specific buffer (αα: 10 mM Tris, 1 mM benzamidine, 10 μM $ZnSO_4$, 2 mM DTT, pH 8;

$\beta_1\beta_1$ and $\beta_2\beta_2$: 10 mM Tris, 10 μM $ZnSO_4$, 1 mM EDTA, 1 mM benzamidine, 1 mM DTT, pH 8; σ: 50 mM Tris, 1 mM benzamidine, 2 mM DTT, pH 8.8; χ: 10 mM Tris, 10 μM $ZnSO_4$, 1 mM EDTA, 1 mM benzamidine, 2 mM DTT, pH 7.5) using ultrasonication (output control to 4.5 with a pulse of 1 second and a duty cycle of 50%) (91). The lysate was centrifuged at 35,000 x g for 35 min.

4.2.3 Purification of Enzymes

Purification procedures were modified from previous reported methods (83, 86, 92). All of the recombinant enzymes were initially purified from the lysate-supernatant by batch chromatography over DEAE-cellulose (DE52, Whatman International, LTD.) equilibrated in the appropriate lysis buffer at 4°C. Alcohol dehydrogenase does not stick to the resin and was eluted in the column flow-through and concentrated.

The activity pools of the ADH isozymes $\beta_1\beta_1$ and $\beta_2\beta_2$ were then buffer exchanged into 7 mM HEPES, 10 μM $ZnSO_4$, 1 mM EDTA, 1 mM benzamidine, 1 mM DTT, pH 7.7. The enzyme was then applied to an S-Sepharose column (Sigma Biochemicals, 100 ml resin). The bound enzyme was washed and then eluted with a 0-100% gradient of 200 mM NaCl. The active fractions were pooled and dialyzed into 50 mM Tris, 10 μM $ZnSO_4$, 1 mM DTT, pH 7.5. The dialyzed sample was applied to an Affi-Gel Blue (BioRad Laboratories, 30 ml resin) equilibrated with the dialysis buffer. The bound enzyme was washed and then removed by bump stripping the column with 800 mM NaCl in equilibration buffer. The eluted sample was then dialyzed into 10 mM Tris, 10 μM $ZnSO_4$, 0.5 mM DTT, pH 7.5 and, when not used immediately, stored in 50% glycerol.

The recombinant human αα-ADH isozyme was purified using modifications of the procedure for purification of the human ββ isoenzymes. Briefly following batch chromatography over DEAE in lysis buffer, the enzyme was dialyzed into 7 mM HEPES, 10 μM $ZnSO_4$, 1 mM benzamidine, 2 mM DTT, pH 7.2. The enzyme was then applied to an S-Sepharose column. The bound enzyme was washed and then eluted with a 0-100% gradient of 250 mM NaCl. The active fractions were pooled and dialyzed into 50 mM Tris, 10 μM $ZnSO_4$, 0.5 mM DTT, pH 7.5. The dialyzed sample was applied to an Affi-Gel Blue equilibrated with the dialysis buffer. The bound enzyme was washed and then removed by bump stripping the column with 800 mM NaCl in equilibration buffer. The eluted sample was then dialyzed into 10 mM ACES, 0.5 mM DTT, pH 6.8.

The recombinant σ isozyme was purified using the following procedure. Following DEAE chromatography, the flow through was buffer exchanged into 7 mM Sodium Phosphate, 1 mM benzamidine, 1 mM DTT, pH 6.4 by dialysis. The enzyme was then applied to a 100 ml resin S-Sepharose column equilibrated with dialysis buffer. The bound enzyme was washed and then eluted with a linear gradient of sodium phosphate from 7 to 65 mM. The active fractions were pooled and then dialyzed into 20 mM Sodium Phosphate, 0.5 mM DTT, pH 8.

As with the previous isozymes, the supernatant containing the human class III χ-ADH isozyme was first subjected to DEAE chromatography. The elutant was then dialyzed against 10 mM Tris, 10 μM Zinc Sulfate, 1 mM DTT, pH 8 and then applied to a 100 ml Q-Sepharose (Sigma Biochemicals) column equilibrated with dialysis buffer.

Class III χ-ADH was then eluted from the resin with a 0-100% 200 mM NaCl gradient. Active fractions were pooled and dialyzed into 10 mM Tris, 0.5 mM DTT, pH 7.5.

Enzyme was detected after each purification step by protein determination and activity assays of each fraction. Pooled fractions were concentrated using the Centricon (Amicon) system at individual purification steps as needed.

4.2.4 Western Blot Analysis

To determine the extent of purification and confirm the presence of purified ADH isozymes SDS-PAGE and Western blot analyses were performed. SDS-PAGE and Western blots were done by standard techniques described by Laemmli (93) and Towbin *et al.* (94), respectively. For western blots, the primary antibody used to probe the blots was rabbit-anti-HLADH. The secondary antibody was an anti-rabbit containing biotinylated conjugate. The blot was then treated with alkaline phosphatase conjugated ExtraAvidin (Sigma) followed by staining with nitroblue tetrazolium and 5-bromo-6-chloro-3-indolyl-phosophate in 100 mM sodium bicarbonate (pH 9.8) containing 1 mM $MgCl_2$. A representative gel and western blot are presented in figures 4.1 and 4.2, respectively. A purification chart has been provided in Table 4.1. Total protein concentrations were determined by the method of Bradford (95) using the Bio-Rad protein kit. Where minor bands were present, the concentrations of the purified ADH isozymes were confirmed by taking densitometric scans of SDS-PAGE gels and comparing those densities to a standard curve compiled using densities of known concentrations of HLADH.

Table 4.1 Purification chart for human alcohol dehydrogenase.

Sample	Total vol. (ml)	Protein (mg/ml)	Total Protein (mg)	Total Activity (μmols/min)	Specific Activity (μmol/min/mg)	% Yield	FP
Sigma							
35K	50	2.33	116.5	11.30	96.97	100	1.00
DEAE (conc)	20	1.44	28.8	8.72	121.10	77	1.25
S-Seph	30	0.04	1.2	3.75	1872.99	33	19.32
Beta II							
35K	65	2.91	189.2	7.42	51.01	100	1.00
DEAE (conc)	30	1.43	42.9	6.05	84.55	81	1.66
S-Seph	40	0.24	9.6	2.60	217.04	35	4.25
Affi Blue	30	0.10	3.0	2.31	461.41	31	9.05
Beta I							
35K	80	1.99	159.2	48.63	488.73	100	1.00
DEAE (conc)	35	1.66	58.1	39.73	478.65	82	0.98
S-Seph	45	0.16	7.2	11.57	1446.38	24	2.96
Affi Blue	30	0.09	2.8	12.35	2684.37	25	5.49
Alpha							
35K	74	0.70	51.8	8.39	239.63	100	1.00
DEAE (conc)	28	1.43	40.0	6.17	86.32	74	0.36
S-Seph	35	0.36	12.6	3.58	198.65	43	0.83
Affi Blue	30	0.14	4.2	2.90	413.80	35	1.73
Chi							
35K	86	2.56	220.2	24.03	187.75	100	1.00
DEAE (conc)	20	2.36	47.2	23.33	197.69	97	1.05
Q-Seph	30	0.30	9.0	13.01	867.04	54	4.62

Q-Seph and S-Seph denote the respective sepharose columns; FP, fold purification; conc, concentrated.

Fig. 4.1 SDS-PAGE for class I αα-ADH purification steps. Gel was loaded with 5-10 μg protein /lane and stained with coomasie blue dye reagent. Lanes represent: 1, αα-ADH 35K-supernatant; 2, αα-ADH DEAE pool; 3, αα-ADH S-sepharose pool; 4, αα-ADH Affi-Gel blue pool; 5, Standards.

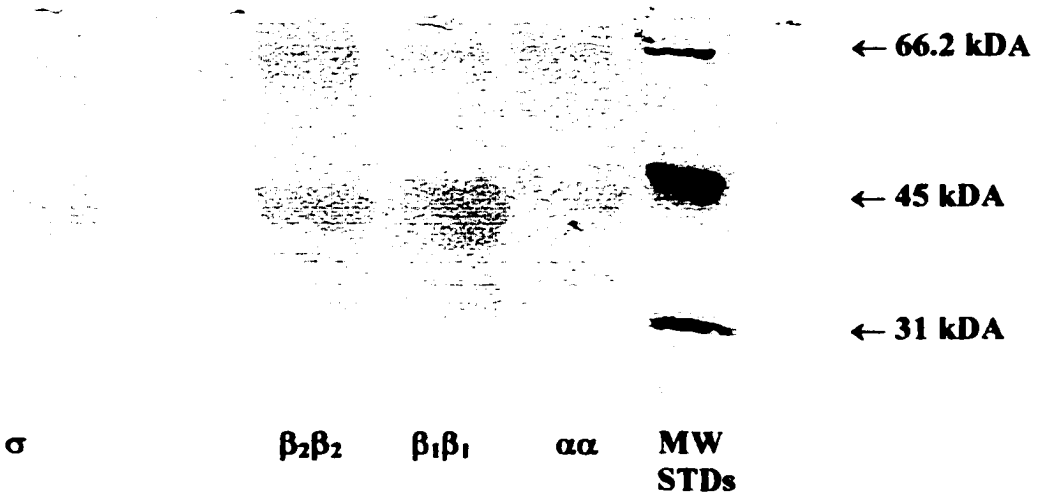

Fig. 4.2 Western blot of purified human ADH. 3-5 μg protein was loaded per lane. Blot was probed with rabbit-anti-HLADH antibody.

4.2.5 Enzyme Assays

Formation of *p*AP from *p*NSP was determined essentially by the method of Horie *et al.* (44) with modifications (48). *p*NSP (0.12-1mM) was incubated for 15 minutes in the presence of 1 mM NADH and an appropriate concentration of purified HLADH or purified human ADH in a 100 mM MES, 51 mM NEA, 51 mM DEA three component buffer in a final volume of 200 µl. The reaction was initiated by addition of cofactor and terminated by addition of 30 µl of 1 M Na_2CO_3. *p*AP formation was detected spectrophotometrically by subsequent addition of 30 ml of 5% (w/v) aqueous phenol and 20 ml of 0.2% (w/v) potassium ferricyanide. The color was allowed to develop for at least 15 min and the absorbance was read at 630 nm on a Biotek P750 Microplate reader. The concentration of *p*AP formed was calculated from a standard curve of commercially available *p*AP. Additional reactions contained 4.75 mM acetaldehyde.

4.2.6 Kinetic Analysis

ADH activities were measured by the method of Bonnichsen *et al.* (61), which is based on spectrophotometric measurement of NADH formation from NAD^+ in the presence of ethanol. Activity was monitored at 340 nm in a Hatachi spectrophotometer using a molar extinction coefficient of 6.22 mM^{-1} cm^{-1} for NADH. To determine the recovery of enzyme during purification and the stability of the purified alcohol dehydrogenases, the activity was measured with 2.5 mM NAD^+ and 33 mM ethanol (100 mM for σ-ADH) as substrates in 0.1 M glycine, pH 10.0 (for αα, $\beta_1\beta_1$, and σ) or in 0.1 M sodium phosphate, pH 8.5 ($\beta_2\beta_2$). Activity measurements for the class III χ-

ADH were performed using 2.5 mM NAD^+ and 5 mM cinnamyl alcohol in 0.1 M glycine, pH 10.0.

4.2.7 Data Processing

Data were fitted to the appropriate rate equations using the statistical software *Enzymes Kinetics* (version 1.2) described by Cleland (96). The variation of the kinetic parameters with pH was determined by examining the rates at each pH value, with NADH present at a saturating concentration and the concentration of *p*NSP varied. The V_{max}/K_M values obtained from a fit to Eq. 1 at low pNSP concentrations for each pH, where v is the observed velocity, V_{max} is the maximum velocity, K_M is the Michaelis constant, and S is the concentration of *p*NSP, were plotted against pH in a log-log plot (97). These pH profile curves were fitted to Eq. 2 to obtain pK values (96), where y is V_{max}/K_M and C is the pH-independent maximum value of that parameter. K_b is the dissociation for groups on the enzyme or substrate. Equation 2 was used to fit a single ionization on the pH profile. The competitive inhibition constants were determined by fitting the data at each pH to Eq. 3. The value I represents the concentration of inhibitor and K_i is the inhibition constant.

Equation 1 $$v = V_{max}S/(K_M + S)$$

Equation 2 $$\log y = \log [C/(1 + K_b/[H^+])]$$

Equation 3 $$v = V_{max}S/[K_M(1 + I/K_i) + S]$$

4.3 Results

The C-nitrosoreductase activities of natural variants of the human ADH enzyme and HLADH have been compared and contrasted. The individual human isozymes

were expressed in *E. coli* and, following purification, were analyzed for their ability to catalyze NADH-dependent reduction of *p*NSP to *p*AP in the direct reaction and in the NAD^+-dependent coupled reaction in which NADH is generated from metabolic conversion of NAD^+ by ADH-dependent oxidation of ethanol. The effects of varying the pH on these reactions were also studied.

4.3.1 Determination of Kinetic Constants for C-Nitrosoreduction and Dependence on pH

The C-nitrosoreductase activity of each ADH isozyme was determined by measuring the production of pAP as a function of the concentration of pNSP and pH. The reactions were run for 15 min at which time the amount of pAP formed was determined colorimetrically at 630 nm as described previously (48, 73). The basis of this assay is the conversion of *p*AP to benzoquinonimine (BQI) by potassium ferricyanide with subsequent color development by aqueous phenol (44). HLADH catalyzes the reduction of *p*NSP by a mechanism that is different from that of human isozymes (Chapter 3) (37, 87). Reduction of *p*NSP involves the formation of BQI, the dehydration product of *p*N-OHAP, as a reaction intermediate. Unlike with the human isozymes, the conversion of this intermediate to *p*AP is not efficiently catalyzed by HLADH (37). *p*NSP reduction and *p*AP formation rates catalyzed by human ADH isozymes are essentially identical (Table 3.2). The colorimetric assay, which detects the ultimate reduced product of *p*NSP reduction, *p*AP, and any remaining BQI, is a reliable method for measuring *p*NSP reduction catalyzed by ADH. As noted in Chapter 3, ADH-catalyzed formation of pAP from 300 μM *p*NSP was linear for at least 20 min with each of the isozymes studied. In these studies, the concentration of *p*NSP did not exceed 1 mM as higher concentrations resulted in spectral interference of the assay due

to the strong absorbance of *p*NSP. The v vs. S plots shown in figure 4.3 show that each of the ADH enzymes approximated Michealis-Menten kinetics. Accurate quantitative measurement of V_{max} for these reactions at higher pH was problematic because of spectral interferences at the higher concentrations of *p*NSP alluded to above. However, reasonable approximations of K_M and V_{max} for ADH-catalyzed reduction of pNSP were possible from the substrate concentration range studied.

The human ADH variants exhibited distinct pH profiles. The concentration of hydrogen ion ($[H^+]$) was shown to be a noncompetitive mixed type activator/inhibitor of the ADH catalyzed reduction of *p*NSP. The double reciprocal plots in figure 4.4 for the various human ADH show the dependence of both K_M and V_{max} on the pH of the reaction. Varying the pH of the enzyme-catalyzed reaction results in double reciprocal plots that intersect either below or above the x-axis for all of the ADH studied, except in the case of the class I αα-ADH, which shows a pattern more reminiscent of competitive interactions. In the pH range studied, the HLADH and class IV σ-ADH-catalyzed C-nitrosoreductase activity decreased with increasing pH, i.e. decreasing $[H^+]$, throughout. For the remaining human ADH isozymes C-nitrosoreductase activity reached a maximum or plateaued at lower pH values indicating an inhibitory effect of $[H^+]$ (Fig. 4.3 and 4.4). *p*NSP reduction by HLADH and σ-ADH were maximal at pH values of 6 or greater, while reductions catalyzed by αα- and χ-ADH were maximal at 6.8 and 6.4, respectively.

In the pH range studied, pH 6 – 8, *p*NSP can exist in two tautomeric forms, the predominate quinone monoxime and the nitroso form. Equilibrium between these two forms involves a mesomeric common ion. In aqueous solution at pH > 6, *p*NSP exists

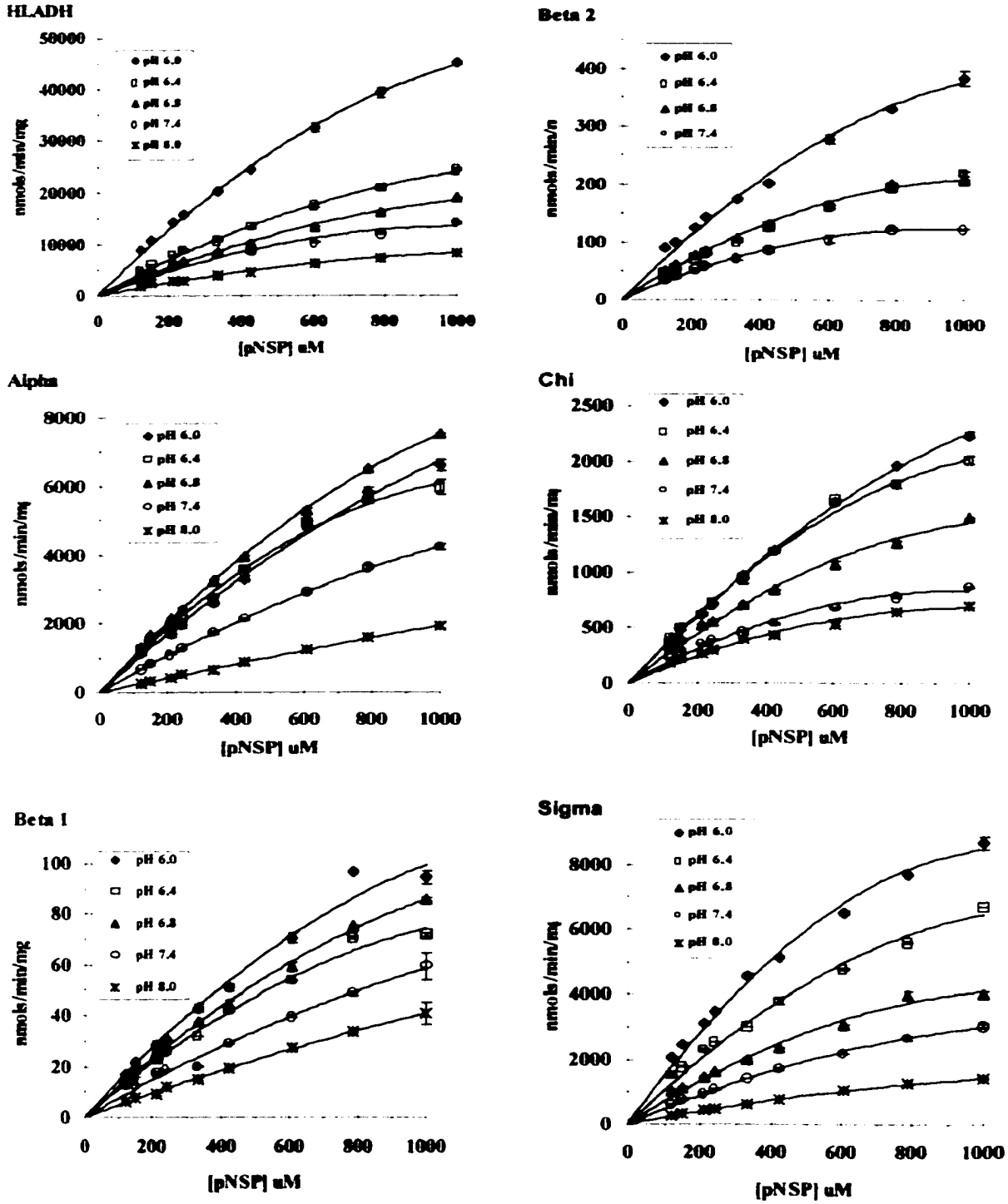

Fig. 4.3 Effect of pH on the reduction of *p*-Nitrosophenol. Reactions were conducted in a 0.1 M MES, 0.051 M NEA, 0.051 M DEA three component buffer system, 1mM NADH, 0.12 – 1 mM *p*NSP, 4.8 mM Acetaldehyde. Enzyme concentrations: HLADH 0.25 μg/ml, αα–ADH 0.8 μg/ml, $\beta_1\beta_1$-ADH 54.5 μg/ml, $\beta_2\beta_2$-ADH 22.5 μg/ml, χ-ADH 3.75 μg/ml, σ-ADH 1.228 μg/ml. Individual data points are the means of at least 4 determinations.

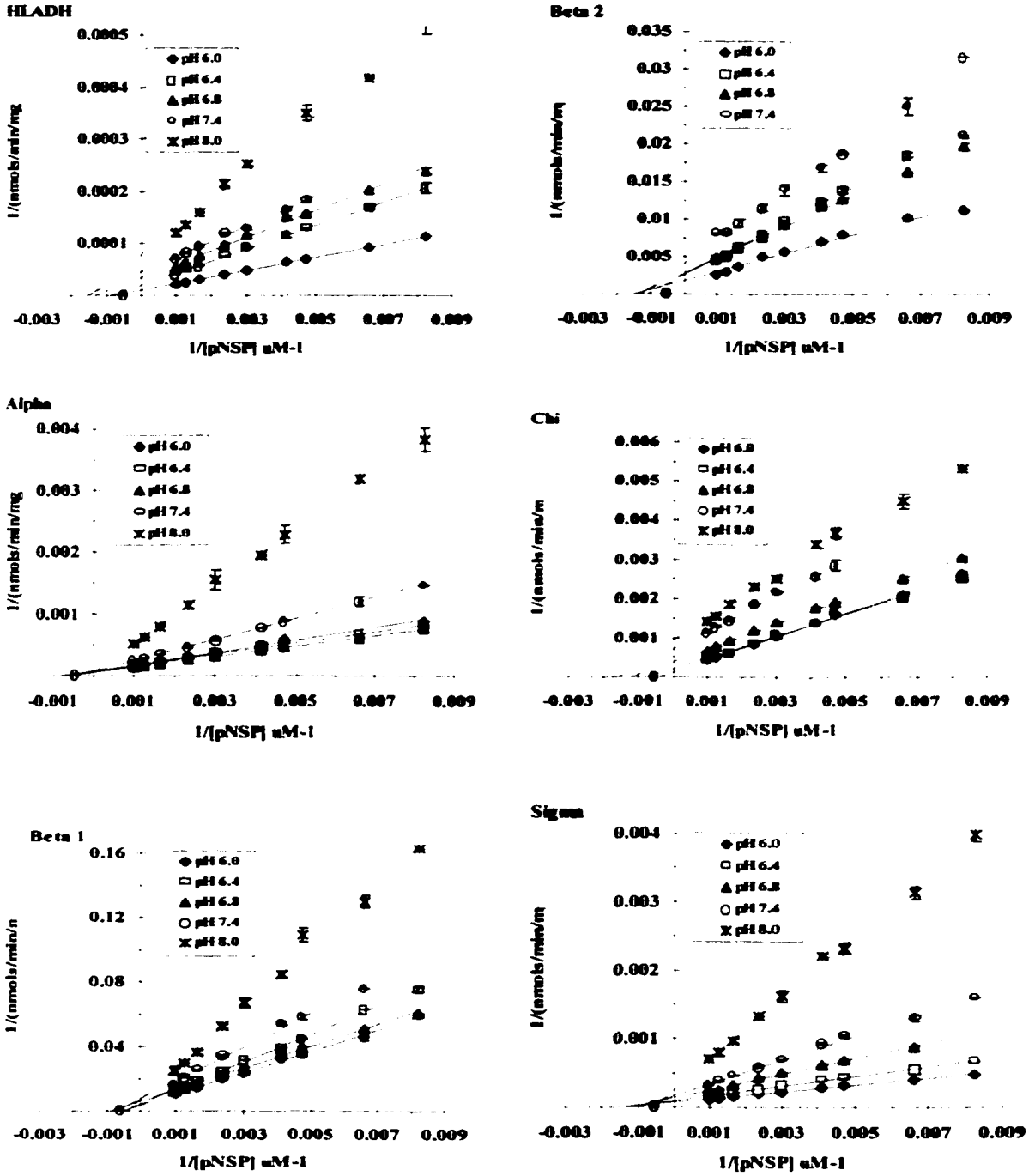

Fig. 4.4 Effect of pH on the reduction of *p*-Nitrosophenol: 1/v vs. 1/S. Reactions were conducted in a 0.1 M MES, 0.051 M NEA, 0.051 M DEA three component buffer system, 1mM NADH, 0.12 – 1 mM *p*NSP, 4.8 mM Acetaldehyde. Enzyme concentrations: HLADH 0.25 μg/ml, αα–ADH 0.8 μg/ml, $\beta_1\beta_1$-ADH 54.5 μg/ml, $\beta_2\beta_2$-ADH 22.5 μg/ml, χ-ADH 3.75 μg/ml, σ-ADH 1.228 μg/ml. Individual data points are the means of at least 4 determinations.

primarily in the ion form with a wavelength maximum at 400 nm (98, 99). Maskos and Winston have determined that the pK value for the ionization of free *p*NSP is 6.20 ± 0.05 (100). While the ionization of *p*NSP appears to lower the binding affinity of *p*NSP to the active site of horse liver ADH, it does not totally prevent it. Thus, a significant decrease in activity between pH 6 and 6.4 may be attributable to the ionization of free *p*NSP. However, as seen in figures 4.3 and 4.4, *p*AP formation catalyzed by individual ADH isozymes is not significantly altered in this pH range.

The apparent K_M and V_{max} for HLADH- and human ADH-catalyzed *p*NSP reduction are presented in Table 4.2. Kinetic constants were determined using the kinetics programs of Cleland (96) and from Hanes-Woolf plots (97). Each ADH isozyme catalyzed *p*NSP reduction with maximum activities at acidic pH. V_{max} values for *p*NSP reduction decrease with increasing pH. As seen in our previous studies (chapter 3), HLADH catalyzed the reduction of *p*NSP at a rate significantly greater than the most active human isozyme tested, i.e., α-ADH (96 vs. 24 μmol/min/mg at pH 6, respectively). The relative orders of activity were HLADH > α > σ > χ > β_2 > β_1. The ADH isozymes exhibited slight variations in K_M as the pH was varied. Michaelis constants for the class IV σ-ADH remained fairly stable between pH 6 and 7.4, then increased as the pH of the reaction was increased to pH 8 (0.72 mM to 1.73 mM), indicating a decrease in the enzymes affinity for the nitroso substrate at alkaline pH. In contrast, K_M values for HLADH, $\beta_2\beta_2$ -, and χ-ADH decreased with increasing pH. K_M values for *p*NSP reduction by αα- and $\beta_1\beta_1$-ADH showed minima between pH 6.4 – 6.8, and maxima at pH 8. Of the ADH isozymes studied, class I αα-ADH presented the highest K_M value for *p*NSP, with a maximum of 9.2 mM at pH 8.

Table 4.2 pH dependence of the apparent kinetic parameters for the reduction of *p*-nitrosophenol by ADH isozymes.

Class	Isozyme		pH 6	6.4	6.8	7.4	8
I	HLADH	K_M	1.40	1.12	0.75	0.64	0.84
		V_{max}	95.5	49.3	29.3	22.0	14.8
	αα-ADH	K_M	2.53	1.48	1.92	2.81	9.18
		V_{max}	23.8	15.7	22.1	16.3	20.1
	$\beta_1\beta_1$-ADH	K_M	1.82	2.08	1.18	1.42	2.78
		V_{max}	0.27	0.24	0.17	0.13	0.14
	$\beta_2\beta_2$-ADH	K_M	1.25	1.20	0.95	0.63	ND
		V_{max}	0.86	0.49	0.43	0.21	ND
III	χ-ADH	K_M	2.00	1.32	0.81	0.63	0.56
		V_{max}	6.72	4.71	2.50	1.38	1.04
IV	σ-ADH	K_M	0.72	0.74	0.86	0.98	1.73
		V_{max}	14.4	10.5	7.42	5.64	3.87

Units for kinetic constants: K_M, mM; V_{max}, μmol/min/mg. Reactions were conducted in a 0.1 M MES, 0.051 M NEA, 0.051 M DEA three component buffer system, 1mM NADH, 0.12 – 1 mM *p*NSP. Enzyme concentrations: HLADH 0.25 μg/ml, αα–ADH 0.8 μg/ml, $\beta_1\beta_1$-ADH 54.5 μg/ml, $\beta_2\beta_2$-ADH 22.5 μg/ml, χ-ADH 3.75 μg/ml, σ-ADH 1.228 μg/ml. ND, Not Determined.

4.3.2 Determination of Ionization Constants for *p*NSP Reduction Catalyzed by HLADH and Human ADH

Table 4.3 shows the ionization constants for the free enzymes and the enzyme-substrate complexes. The constants were determined from secondary plots (example in Fig. 4.6) of the slopes and intercepts of the double reciprocal plots (Fig. 4.4) versus the inverse of the concentration of hydrogen ion or from plotting log V_{max}/K_M vs. pH (Fig. 4.5). For all of the ADH isozymes the efficiencies for *p*NSP reduction decreased with increasing pH. Therefore, ionization constants were determined using a statistics program which determined the constants according to equation 2. With both methods

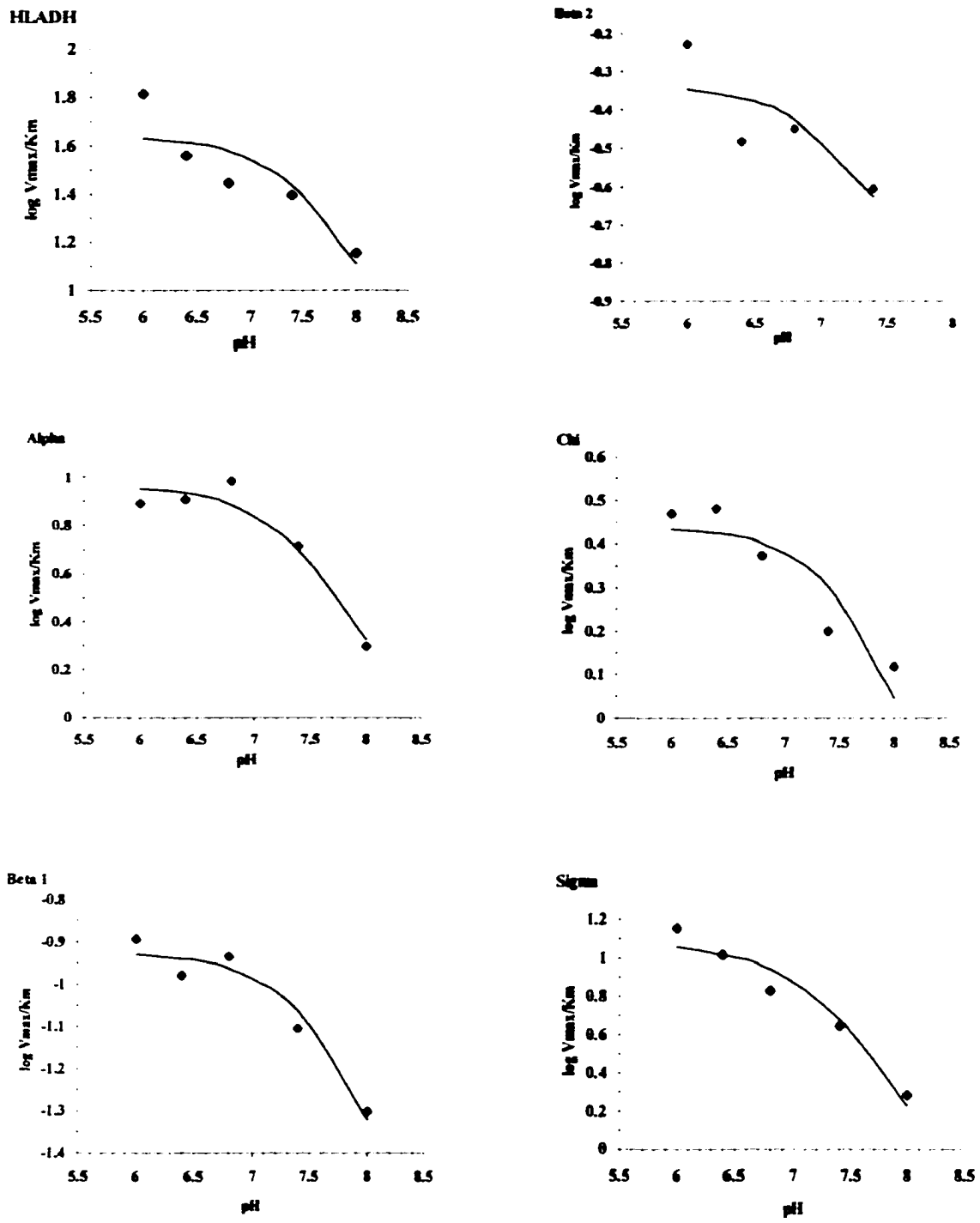

Fig. 4.5 pH-dependence of the catalytic efficiency (log V_{max}/K_M) for HLADH and human ADH-dependent reduction of *p*NSP. The curve drawn through the experimental data points was obtained by fitting the data to equation 2.

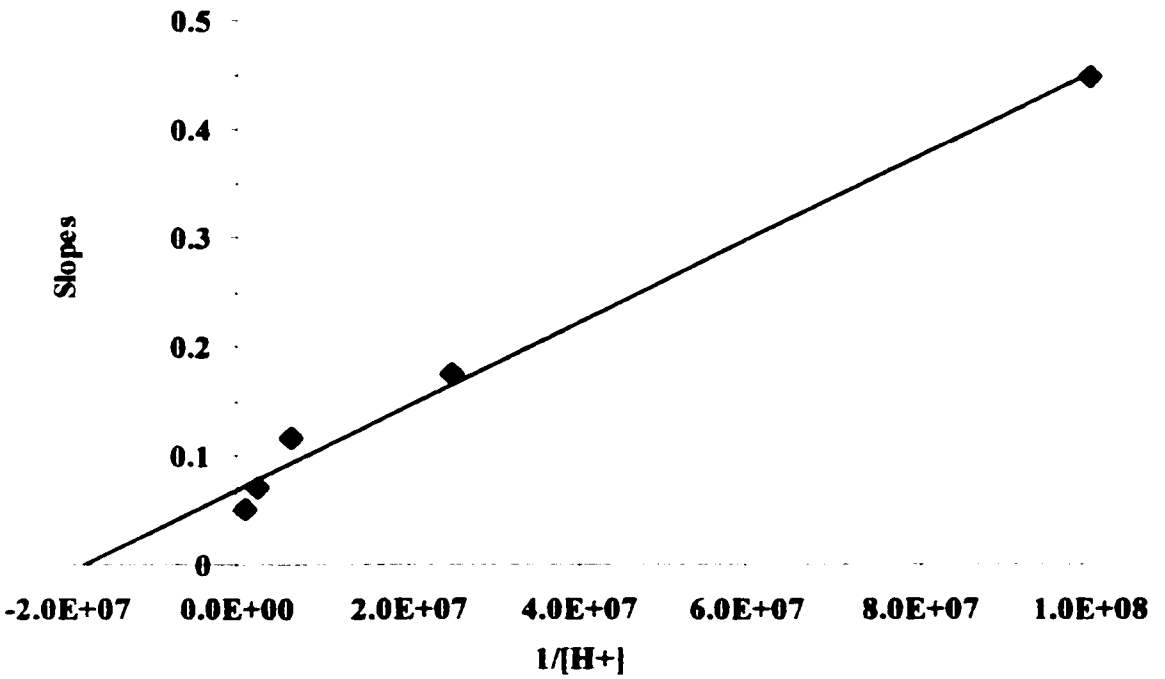

Fig. 4.6 Secondary Plot of the slopes determined from pH-dependent double reciprocal plots versus $1/[H^+]$. Reaction conditions: 120 – 1000 μM *p*NSP; 3.75 mM NAD^+; and 0.1 M MES, 0.051 M NEA, 0.051 M DEA, pH 7.4. Enzyme concentration: 1.228 μg/ml σ-ADH.

the ionizations effecting the reduction of *p*NSP by the enzymes were equivalent despite the method of determination. Each ADH isozyme showed a pK_b^E (pK of the free enzyme) of 7.3 –7.7. Only for the class I αα- and $\beta_1\beta_1$-ADH were the ionization constants for the enzyme-substrate complex significantly different from those of the free enzyme (8.8 vs. 7.2 for αα-ADH, respectively). Standard errors for each determination were ± 0.1 or less.

Table 4.3 Comparison of the pK_b^E and pK_b^{ES} values determined from secondary plots and plots of log V_{max}/K_M against pH.

		Secondary Plots		log V_{max}/K_M	
Class	**Isozyme**	pK_b^E	pK_b^{ES}	pK_b^E	C
I	HLADH	7.8	7.5	7.6	4.4
	αα-ADH	7.2	8.8	7.5	1.1
	$\beta_1\beta_1$-ADH	7.8	8.4	7.8	1.2
	$\beta_2\beta_2$-ADH	7.4	7.6	7.4	4.7
III	χ-ADH	7.6	7.0	7.8	2.8
IV	σ-ADH	7.3	7.8	7.2	1.2

The values of pK_b^E and pK_b^{ES} represent the pK of the free enzyme and enzyme-substrate complex, respectively.

4.3.3 Inhibition Kinetics

The effect of acetaldehyde on the kinetic parameters for reduction of *p*NSP was examined as a function of pH. Because the C-nitroso moiety is isosteric and isoelectronic with the aldehyde functional group (40) it was anticipated that acetaldehyde would competitively inhibit *p*NSP reduction by the various ADH. Inhibition by acetaldehyde was indeed competitive with respect to *p*NSP for all of the ADH isozymes in the pH range studied. To illustrate this point, Fig. 4.7 shows a Hanes-Woolf plot (S vs. S/v) for σ-ADH catalyzed *p*NSP reduction at pH 7.4 in the absence and presence of 4.75 mM acetaldehyde where parallel lines indicate changes in K_M without concurrent changes in V_{max}. Apparent K_is for acetaldehyde are presented in Table 4.4. Inhibition constants range from 3.7 – 51 mM for all of the ADH at all pH values studied. The class I αα-ADH isozyme was only inhibited by 4.75 mM

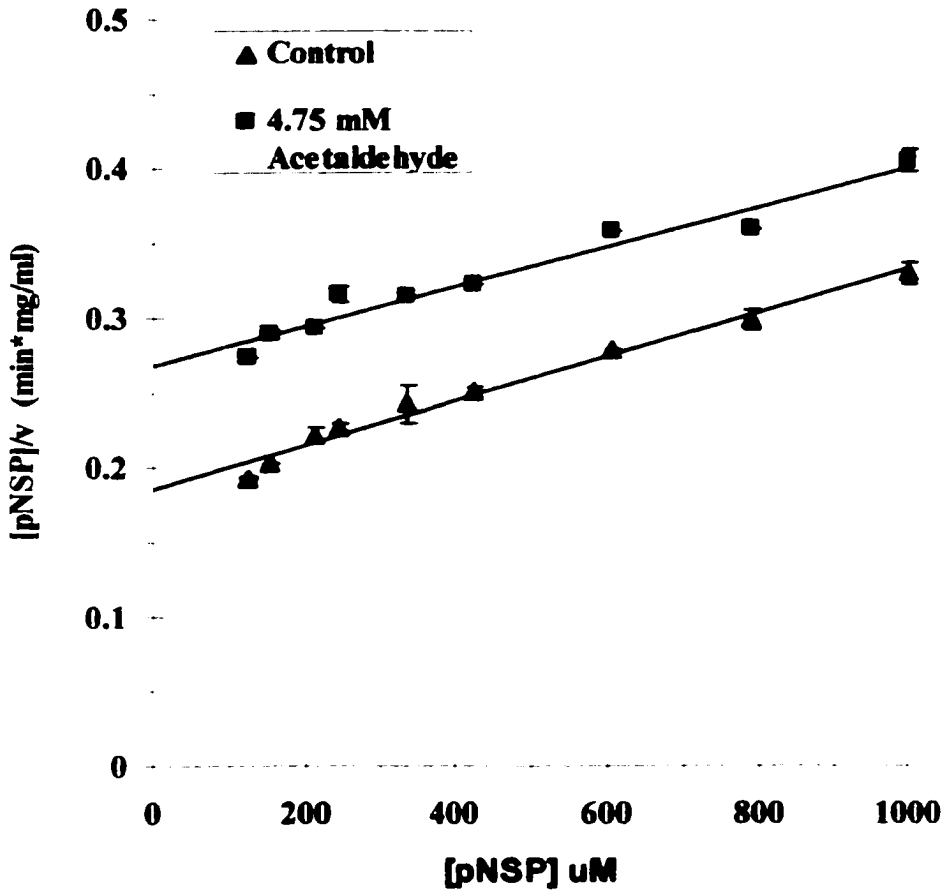

Fig. 4.7 Competitive inhibition of σ-ADH catalyzed C-nitrosoreduction by 4.75 mM acetaldehyde. Reaction conditions: 120 – 1000 μM *p*NSP; 3.75 mM NAD^+; and 0.1 M MES, 0.051 M NEA, 0.051 M DEA, pH 7.4. Enzyme concentration: 1.228 μg/ml σ-ADH.

acetaldehyde in the pH range of 6.8 – 7.4. At pH values of 6, 6.4, and 8, αα-ADH-catalyzed *p*NSP reduction was either not inhibited or showed increases in activity.

Table 4.4 Apparent K_i values for the inhibition of ADH-catalyzed *p*NSP reduction by acetaldehyde.

		pH				
Class	Isozyme	6	6.4	6.8	7.4	8
I	HLADH	5.6	24.3	32.1	17.2	27.3
	αα-ADH	NI	NI	50.1	3.7	NI
	$\beta_1\beta_1$-ADH	51.3	27.9	31.7	20.4	40.0
	$\beta_2\beta_2$-ADH	10.6	28.1	11.3	9.4	ND
III	χ-ADH	41.7	14.3	9.7	15.0	18.4
IV	σ-ADH	20.7	24.2	29.4	15.8	10.8

Units for kinetic constants: K_i, mM. Reactions were conducted in a 0.1 M MES, 0.051 M NEA, 0.051 M DEA three component buffer system, 1mM NADH, 0.12 – 1 mM *p*NSP, 4.8 mM Acetaldehyde. Enzyme concentrations: HLADH 0.25 μg/ml, αα–ADH 0.8 μg/ml, $\beta_1\beta_1$-ADH 54.5 μg/ml, $\beta_2\beta_2$-ADH 22.5 μg/ml, χ-ADH 3.75 μg/ml, σ-ADH 1.228 μg/ml. NI, No Inhibition. ND, Not Determined.

4.4 Discussion

The effects of varying the hydrogen ion concentration [H^+] on the activity of enzymes have close similarities to the effects of activators and inhibitors (101). Treatment of the effects of the [H^+] may be viewed in the same way as other effectors and can yield valuable information on the nature of the kinetic mechanism obeyed by the enzyme. In addition, the characteristic ionization constants of amino acid side-chain groups may help to identify specific groups as playing a role in the reaction. Here, we have considered the effects of the [H^+] on ADH-dependent C-nitrosoreductase activity, both in terms of kinetic analysis with the [H^+] as the variable and in terms of the use of the effects of pH to identify specific ionizing groups.

Kinetic and structural comparisons have illustrated that homologous enzymes can differ markedly in substrate specificity. Increasing the size of the active site enhances the reactivity of alcohol dehydrogenase with large substrates such as

benzaldehyde but decreases the reactivity of small substrates such as ethanol (86). Although ADH isozymes have broad specificity, variations in amino acid residues in the substrate-binding pocket produce different activities, which may be of physiological significance.

The ADH isozymes studied catalyze the reduction of *p*NSP at significantly different rates and exhibit different affinities for the nitroso substrate. The relative orders of ADH dependent *p*NSP reduction were HLADH > αα- > σ- > χ- > $\beta_2\beta_2$- > $\beta_1\beta_1$-ADH. Seemingly in opposition to its high rate of catalysis with the nitroso substrate, the class I αα-ADH exhibits the lowest affinity for *p*NSP as inferred from its comparatively high K_M at each pH studied. While K_M values for *p*NSP showed marginal differences over the pH range studied, V_{max} values for each ADH isozyme showed significant variations with pH. However, the pH dependent variation in enzyme-catalyzed *p*NSP reduction is essentially the same for all of the ADH isozymes studied. The data shows that as pH is increased there is a concurrent decrease in *p*AP formation, i.e. C-nitrosoreduction. Therefore, there is a significant dependence of ADH-catalyzed C-nitrosoreduction on the $[H^+]$. As seen in Fig. 4.3, at comparatively low $[H^+]$, pH 6.8 – 8, C-nitrosoreduction by each ADH isozyme is directly proportional to the increase in pH. When the pH is more acidic, formation of *p*NSP is not directly proportional to decreases in pH, indicating a change in ionization of either the enzyme or the enzyme–substrate complex. Ionizations associated with free substrate are important in various enzyme catalyzed reactions, however, as stated above, the pK_a of *p*NSP is 6.2, and thus, is not a consideration here.

In these studies, acetaldehyde was employed as an alternate substrate in the ADH-catalyzed reactions. In this role, acetaldehyde would be expected to compete with *p*NSP and inhibit the formation of the productive ADH-NADH-*p*NSP ternary complex. As expected, the competitive inhibitor acetaldehyde decreased the efficiency of the ADH isozymes in the reduction of *p*NSP. Furthermore, plots of log V_{max}/K_M vs. pH for acetaldehyde inhibited reactions indicate the same ionizations as the uninhibited reactions (Fig. 4.8).

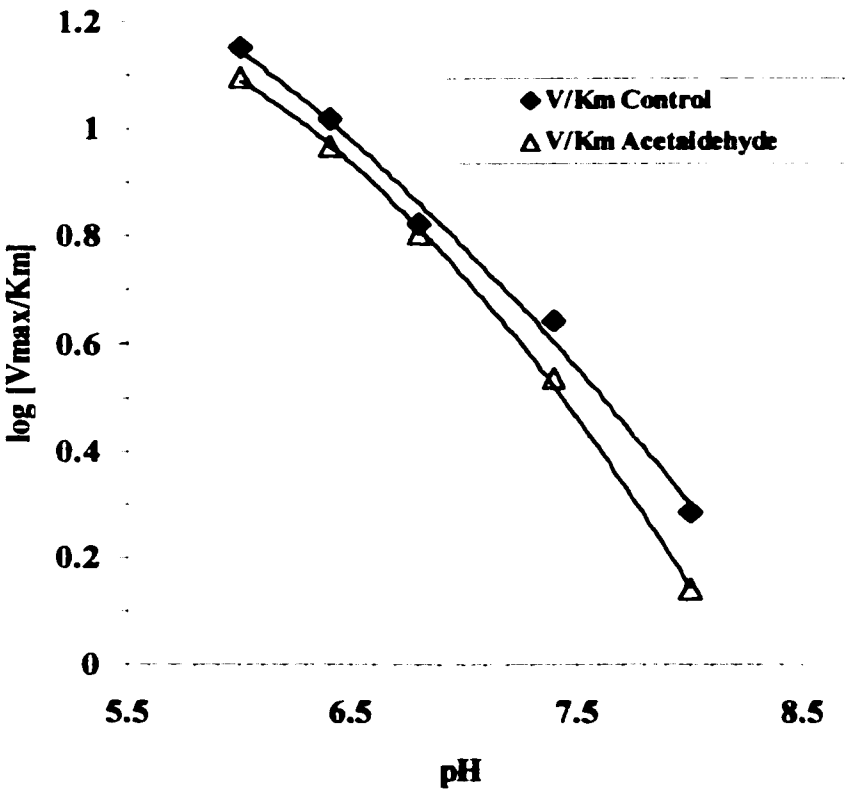

Fig. 4.8 pH-dependence of the catalytic efficiency (log V_{max}/K_M) for σ-ADH-dependent reduction of *p*NSP. Comparison of Control and 4.75 mM acetaldehyde inhibited reactions. Reaction conditions: 120 – 1000 μM *p*NSP; 3.75 mM NAD^+; and 0.1 M MES, 0.051 M NEA, 0.051 M DEA, pH 7.4. Enzyme concentration: 1.228 μg/ml σ-ADH.

If substrate binding does not affect the ionization constants, the effect will be truly noncompetitive, with V_{max} and the slope changed but K_M unaffected (101). In the simplest mechanism for inhibition, the inhibitor can bind both to the free enzyme to give an enzyme-inhibitor complex and to the enzyme-substrate complex to give an enzyme-substrate-inhibitor complex. If the inhibitor exhibits stronger effects on the enzyme than the enzyme-substrate complex both K_M and V_{max} will decrease with increasing concentrations of the inhibitor (101). In fig. 4.4, Lineweaver-Burk plots for HLADH, and χ-ADH catalyzed C-nitrosoreduction show just such a pattern, with pH-dependent lines intersecting below the x-axis. On the other hand, Lineweaver-Burk plots for the class I αα-, $\beta_1\beta_1$, $\beta_2\beta_2$-, and class IV σ-ADH, show pH-dependent lines intersecting above the x-axis, inferring that with these enzymes the inhibitor binds more strongly to the enzyme-substrate complex. As the concentration of NADH used in these studies was saturating, it can be assumed that the enzymes were present as enzyme-NADH binary complexes and pH effects associated with the free enzymes were in fact in the binary complex. Therefore, kinetic constants presented in Table 4.2 reflect changes in C-nitroso reduction due to ionizations of the ADH-NADH complex or the ADH-NADH-*p*NSP tertiary complex.

Many ionizable groups may be involved in an enzyme-catalyzed reaction. Typically, any given reaction mechanism requires that ionizable residues be in a particular ionic form for activity (101). The first residue to become protonated or deprotonated as the pH is adjusted from that which is optimum is the one that is reflected in a pH-dependent change in enzyme activity measurements (101). The ionizations of other groups at pH values farther from the pH optimum are undetectable

because they affect only the equilibrium between inactive forms of the enzyme. However, other groups present in the enzyme may influence the ionization of the reactive group (102).

Structural studies of HLADH with coenzyme and substrate or inhibitors (23, 88, 103) have indicated that the substrate binding site is lined with hydrophobic residues including Phe 93. Other amino acids that line the alcohol-binding cleft and that may affect substrate binding include Ser 48, Leu 57, Phe 110, Leu 116, Leu 141, and Ile 318 (23); of these residues, Ser 48 is the only one that is ionizable. The kinetic properties of human ADH with substitutions at residue 47 in the coenzyme-binding site are quite different. The differences in K_M and V_{max} of ethanol oxidation between the $\beta_1\beta_1$-ADH and $\beta_2\beta_2$-ADH isozymes has been attributed to the presence of the weaker base, His, at position 47 of $\beta_2\beta_2$ in place of Arg in $\beta_1\beta_1$; it is the only difference between $\beta_1\beta_1$-ADH and $\beta_2\beta_2$-ADH (6). Examination of the structure of HLADH reveals that Arg 47 interacts with one of the adenosine phosphate oxygens of NAD^+ (23). Both the horse EE and human $\beta_1\beta_1$ ADH have Arg at position 47 and bind coenzyme with high affinity. Class I $\alpha\alpha$- and class IV σ-ADH have either Gly at position 47, while the class I $\beta_2\beta_2$- and class III χ-ADH have His at this position (18, 104).

When studying the reduction of *p*-nitroso-N, N-dimethylanline (NDMA) by yeast ADH, Trivic and Leskovac (42) reported a pH profile that reflected a pK of 8.6 for a catalytically active enzyme group in the enzyme-NADH complex. This was concluded because the concentration of NDMA was less than K_M, rates of the reaction were proportional to V_{max}/K_M, and the pH-profile reflected the dissociation in the enzyme-NADH complex (42). Kvassman and Pettersson (105), have proposed that the

pH dependence of NADH binding is attributable to electrostatic effects of the coenzyme pyrophosphate group on the ionization of zinc-bound water. In the present studies, only ionization constants for the enzyme-substrate complex in reactions catalyzed by class I $\alpha\alpha$- and $\beta_2\beta_2$-ADH were found to be 8.4-8.8. The calculated pK values of the free enzyme found in our experiments do not approximate the value of 8.6. However, if we assume that the enzyme is present as enzyme-NADH complexes, then the wide range of pK_b^E values obtained for the ADH isozymes in our experiments might also reflect dissociation of the ADH-NADH complex. As stated previously, dissociation of NADH is dependent on the binding strength (basicity) of the amino acid at position 47. The 0.6 log unit change in the constants reflect changes in the amino acid, 7.8 for HLADH and $\beta_1\beta_1$-ADH (Arg 47), 7.5 for $\beta_2\beta_2$-ADH and χ-ADH (His 47), and 7.2 for $\alpha\alpha$-ADH and σ-ADH (Gly 47).

From the profiles of log V_{max}/K_M vs. pH (Fig. 4.5), a catalytically active enzyme group with a pK_b of 7.4 – 7.8 was implicated in catalysis. However, using deuterium isotope effects, Maskos and Winston have reported an enzymatic residue with a pK of 6.5-6.7 in the HLADH-NADH complex that is involved in the binding of *p*NSP (87). This later ionization constant is typical of an imidazole ligand; however, imidazoles may exhibit pK's in the range of 5-8 in proteins (102, 106).

The catalytic zinc atom is bound at the bottom of the substrate binding pocket by three protein ligands; two sulfur atoms from Cys 46 and Cys 174 and one nitrogen atom from His 67. A water molecule or hydroxyl ion, depending on the pH, completes a distorted tetrahedral coordination (70). The zinc-bound water molecule is involved in a system of hydrogen bonds which include Ser 48 (Thr 48 in most human and in yeast

isozymes) and His 51 which comprise an obligatory proton relay system for catalysis (13, 19, 70). Mutagenesis of any one of the residues of the proton relay system inactivates ADH (107). In the relay, the proton is transferred through a hydrogen bonded network from the alcohol to Ser 48, to the 2′-hydroxyl of the nicotinamide ribose, and finally to His 51 imidazole, which acts as the terminal general base catalyst that transfers the proton to solvent (88). Dissociation of the nicotinamide moiety follows.

Sekhar and Plapp (108) have reported that the pH dependence for binding of NAD^+ to HLADH may arise when deprotonation of His 51 reduces electrostatic repulsion with the charged nicotinamide ring or promotes ionization of the zinc-bound water through the connecting hydrogen bond network. The pH dependence for NAD^+ shows a bell-shaped pH dependence, with pK values of 6.3 – 6.9 and 9 – 9.7, and the maximal rate at pH 8 (108). The pK near 9 has been assigned to the zinc-bound water (109). Light *et al.* proposed that since both the HLADH and αα-ADH isozymes show pK values near 7, and both enzymes have His 51, it is likely that the pK at 7 involved the histidine residue linked in the hydrogen bonded system to the zinc-ligand (110). Jacobs *et al.* have suggested that the absence of a pH effect during the reduction of aromatic aldehydes as seen in previous studies is consistent with electrophilic catalysis of hydride transfer and that such catalysis could result from protonation of substrate by a protonic acid-base catalyst or of complexation by zinc (111). The data of McFarland and Chu (90) support this conclusion in that catalysis by protonic acid (with a pK between 6 and 10) would show strong pH dependence. While the pK_b^{ES} in Table 4.3 are not typical of His 51 when compared with previous data and may be the result of

other ionizing groups in the ADH active sites, the significant difference in values for the class III χ-ADH as compared to the other isozymes does imply that these ionizations reflect changes in the proton relay system.

CHAPTER 5 OXIDATION OF 2,2'-THIODIGLYCOL BY ALCOHOL DEHYDROGENASE: COMPARISON OF HUMAN LIVER ISOENZYMES

5.1 Introduction

Sulfur mustard is a poisonous chemical warfare agent. It was used as recently by Iraq to attack its own Kurdish population in the Iranian-occupied village of Halbja in 1988 (49). Public concern arises from possible exposure and potential health hazards resulting from destruction of stockpiles of these chemical agents. Scientific data are being accumulated concerning potential adverse effects, including toxicology, carcinogenicity, mutagenicity, and teratogenicity.

Soon after introduction into body tissues, hydrolysis of mustard occurs to form 2,2′-thiobis-ethanol (thiodiglycol) and semimustard, which are relatively nontoxic. Recent research has shown that sulfur mustard inhibits serine and threonine phosphatases and that this inhibition was more closely related to the concentration of thiodiglycol (TDG) than the mustard itself (52). Subsequent observations have shown TDG to be a substrate for horse liver alcohol dehydrogenase (HLADH) and ADH in human skin cytosol (53).

Mammalian zinc-containing ADH constitute an enzyme family of multiple isoforms. Of these, HLADH is the most widely studied. HLADH is a dimer composed of two 40 kDa monomers, each containing 374 amino acids and two zinc ions, one having a structural function and the other a catalytic function. Humans produce more than 20 ADH isozymes composed of as many as nine different subunits (4). The horse enzyme shares between 60% and 87% sequence homology with the human isozymes. The latter have been assigned to their respective classes based on their electrophoretic

mobilities and inhibition by pyrazole and its 4-alkylated derivatives. The overall residue identity shows 60% homology between classes; many residues at the active site are substituted, especially in the substrate-binding cleft, which is large and hydrophobic in the traditional ethanol-active liver enzyme of class I, but different in the enzymes of the other classes. These ADH classes also differ in their tissue distribution. However, individual ADH isozymes are identical regardless of their tissue localization.

The class I α–, β–, and γ-ADHs, with allelic variants of β and γ (5, 6), are effectively inhibited by 4-methylpyrazole. Primary and secondary alcohols are typically good substrates for class I ADHs. Patterns of class I ADH also vary because of allelic polymorphism within and among different racial groups. Variants involving the β subunit have been designated β_1 (Caucasian), β_2 (Oriental), and β_3 (African) (6). Homo- and heterodimers of α, β, and γ subunits of human class I ADH are present in liver, kidney, skin, gastrointestinal tract and to a lesser extent lung (112).

Class II and class III ADH consist solely of one isozyme, π-ADH and χ-ADH, respectively, and are relatively insensitive to pyrazole inhibition. Class II ADH acts on primary aliphatic alcohols and aromatic aldehydes (7). All human ADH catalyze the oxidation of ethanol; however, the K_M of class II ADH for ethanol oxidation is significantly higher than that of class I forms. Of the vertebrate ADHs that have been identified only class III ADH has been conserved in all organisms (8). Class III ADH functions *in vitro* as a glutathione-dependent formaldehyde dehydrogenase, which suggests that this was the original function that drove the evolution of ADH (10) and identifies the ADH family as part of the cellular defense system. The π and χ subunits

share about 60% sequence identity with respect to each other and the other isozymes; these have not been observed to form heterodimers.

Class IV consists of σ-ADH. The class IV σ-ADH has unique enzymatic properties, with exceptionally high K_M and k_{cat} values for ethanol and alcohols and aldehydes of physiological interest. Found predominately in the stomach, the σ-ADH is considered to have a significant role in retinol metabolism and first-pass ethanol metabolism (11-13).

There has been extensive research done to elucidate the catalytic properties, expression and localization of ADH in mammalian tissues (113-116). Recently, Cheung, *et al.* (117) characterized the ADH content of human skin. Heightened awareness of the biological threats imposed by chemical warfare agents has prompted the study of the metabolism of these compounds and their intermediates. Herein, we have compared and contrasted the catalytic activity of HLADH and purified αα, $\beta_1\beta_1$, $\beta_2\beta_2$, $\gamma_1\gamma_1$, χ, π, and σ human ADH isozymes to oxidize TDG.

5.2 Materials and Methods

5.2.1 Chemicals and Enzymes

Tris-maleate and β-nicotinamide adenine dinucleotide were obtained from Sigma Chemical Co. (St. Louis, MO). Thiodiglycol and pyrazole were from Aldrich Chemical Co. (Milwaukee, WI). Horse liver alcohol dehydrogenase was obtained from Boehringer-Mannheim (Indianapolis, IN). All other chemicals were of the highest grade commercially available. Purified human liver ADH isozymes were generously provided for these studies by Dr. Thomas Hurley, Department of Biochemistry and Molecular Biology, Indiana University School of Medicine.

5.2.2 Enzyme Assays

Thiodiglycol oxidation by alcohol ADH was determined according to Brimfield *et al.* (1998) with modifications. All solutions were prewarmed to 30°C. Aliquots of a 5 mM NAD^+ solution in 20 mM tris-maleate buffer, pH 7.6 was placed in the wells of a 96-well microtiter plate. A solution of the appropriate enzyme concentration diluted in 20 mM tris-maleate buffer, pH 7.6 was added to each well. The microtiter plates were baseline determined in a THERMOmax MAXline Molecular Dynamics Microplate Reader running SOFTmax™ software and equipped for constant temperature (preincubated for 2 min). At the end of the preincubation period, the appropriate concentration of substrate in 0.85% saline at 30°C was added. The reaction was followed by measuring the change in absorbance at 340 nm for 5 min with mixing before each reading. Under the described conditions the ADH-catalyzed reactions were linear for at least 15 min and first order with respect to enzyme concentration. In reactions containing pyrazole, the volume of the NAD^+ solution added was reduced by 10 µl, and 10 µl of the appropriate concentration of inhibitor in tris-maleate buffer was added before the 2 min incubation. The total reaction volume was 250 µl. Ethanol oxidation was measured by the method of Bonnichsen *et al.* (61), which is based on spectrophotometric measurement of NADH formation from NAD^+ in the presence of ethanol.

5.2.3 Data Analysis

Kinetic constants for TDG were determined by monitoring the production of NADH at 340 nm ($\varepsilon = 6.32\ mM^{-1}\ cm^{-1}$). K_M and V_{max} values for TDG were calculated using the statistical software *Enzyme Kinetics* (version 1.2) described by Cleland (96)

and from a fit of the kinetic data to the Lineweaver-Burk equation [$1/v = K_M/(V_{max}S) + 1/V_{max}$], where S is the concentration of TDG. k_{cat} (min^{-1}) was obtained by dividing V_{max} by the concentration of active sites assuming a subunit MW of 40,000. K_M and V_{max} were confirmed from Hanes-Woolf plots. Ki values for inhibition by pyrazole were calculated from Dixon plots (118)

5.3 Results

5.3.1 Oxidation of TDG by Purified Human ADH Isozymes

The specific activities of each of the purified ADH isozymes were determined at saturating concentrations of TDG. Of the ADH isozymes class IV σ-ADH exhibited the highest specific activity, which was 1632 nmol/min/mg in the presence of 400 mM TDG (Table 5.1). The specific activities of the class I ADH were, respectively 123, 79, 347 and 647 nmol/min/mg for the αα, $\beta_1\beta_1$, $\beta_2\beta_2$ and $\gamma_1\gamma_1$ isozymes. The class II π-ADH exhibited the lowest activity, 12 nmol/min/mg protein. The class III χ-ADH did not exhibit activity with this substrate even when followed for 1 hour with saturating levels of substrate and elevated levels of enzyme. Only long-chain aliphatic alcohols have been found to be good substrates of class III χ-ADH (83).

When compared with ethanol oxidation, the relative orders of activity were essentially the same, with the class I $\gamma_1\gamma_1$-ADH being 4-5 fold greater than the αα-ADH and the $\beta_1\beta_1$-ADH having notably lower activity. The specific activity for $\beta_2\beta_2$-ADH was about half that of the $\gamma_1\gamma_1$-ADH, whereas $\beta_2\beta_2$-ADH oxidized ethanol at a rate twice that of $\gamma_1\gamma_1$-ADH. HLADH, also a class I isozyme, had a slightly higher specific activity than that of the $\gamma_1\gamma_1$-ADH, 780 nmol/min/mg versus 647 nmol/min/mg, respectively. The specific activity of class IV σ-ADH was approximately three times

greater with respect to TDG oxidation and seven times greater with respect to ethanol oxidation than that of class I $\gamma_1\gamma_1$-ADH.

5.3.2 Kinetic Constants for ADH-Catalyzed Oxidation of TDG

Based on the specific activity measurements of Table 5.1, only the class I and class IV ADH were subjected to more detailed kinetic analysis. All enzymes tested exhibited classical Michaelis-Menten kinetics (Figure 5.1A-C). The class I isozymes, $\alpha\alpha$, $\beta_1\beta_1$, $\gamma_1\gamma_1$, and HLADH, exhibited K_M's for TDG from 1.3-8.7 mM (Table 5.2). The highest K_M value for TDG oxidation among the class I isozymes was for $\beta_2\beta_2$-ADH (48 mM). In these studies, HLADH was shown to catalyze the oxidation of TDG with a K_M of 6.1 mM and a V_{max} of 780 nmol/min/mg compared to Brimfield's (1998) values

Table 5.1 Specific activities of ADH-catalyzed oxidation of thiodiglycol and inhibition by pyrazole (1mM).

Class	ADH isozyme	Specific Activity (nmol/min/mg)	% Pyrazole Inhibition	Alcohol Oxidation (μmol/min/mg)
I	$\alpha\alpha$	123	83	0.58
	$\beta_1\beta_1$	79	100	0.11
	$\beta_2\beta_2$	347	56	5.64
	$\gamma_1\gamma_1$	647	90	2.06
II	π	12	0	0.11
III	χ	No Activity	-----	2.70[a]
IV	σ	1632	73	15.40

Activities are means of triplicate measurements. Specific Activities of TDG were determined at: 45 mM TDG with 2.8 μg/ml $\alpha\alpha$, 45 mM TDG with 6.83 μg/ml $\beta_1\beta_1$, 200 mM TDG with 6.9 μg/ml $\beta_2\beta_2$, 33.4 mM TDG with 1.6 μg/ml $\gamma_1\gamma_1$, 33.4 mM TDG with 4.4 μg/ml π, and 400 mM TDG with 0.21 μg/ml σ-ADH. [a]Alcohol oxidase activity measurements for χ-ADH were performed using cinnamyl alcohol. All alcohol oxidase activity measurements were in 100 mM Glycine, pH 10; except $\beta_2\beta_2$, which was in 100 mM Sodium Phosphate, pH 8.5.

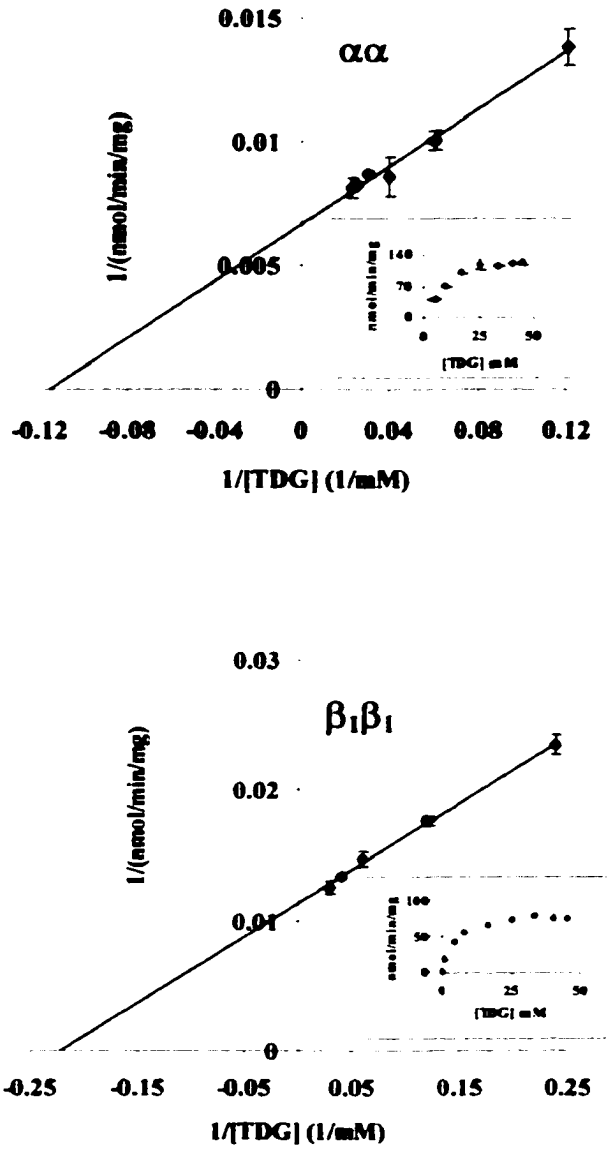

Fig. 5.1A Oxidation of 2,2'-Thiobis-ethanol by αα- and $\beta_1\beta_1$-ADH. The experiments were conducted as described under Materials and Methods under the following conditions: 4.2 mM – 45 mM TDG, 2.77μg/ml αα-ADH; 8.3 μM – 45mM TDG, 6.83 μg/ml $\beta_1\beta_1$-ADH. All reactions contained 5mM NAD^+in 20 mM tris-maleate buffer, pH 7.6. (Insert) Michaelis-Menten plot of V vs. S data for the oxidation of TDG by αα- and $\beta_1\beta_1$-ADH. Each data point represents the mean ± SD of at least three trials.

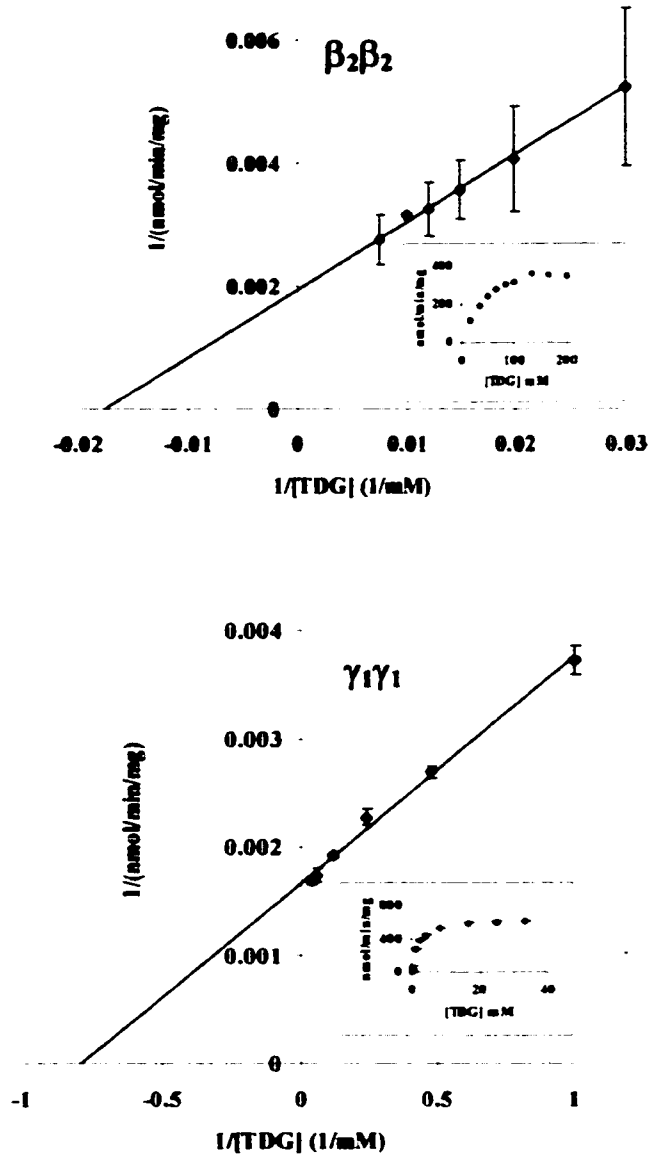

Fig. 5.1B Oxidation of 2,2'-Thiobis-ethanol by $\beta_2\beta_2$- and $\gamma_1\gamma_1$-ADH. The experiments were conducted as described under Materials and Methods under the following conditions: 16.7 mM – 200 mM TDG, 6.9 μg/ml $\beta_2\beta_2$-ADH; 4.2 mM – 45 mM TDG, 1.55 μg/ml $\gamma_1\gamma_1$-ADH. All reactions contained 5mM NAD^+in 20 mM tris-maleate buffer, pH 7.6. (Insert) Michaelis-Menten plot of V vs. S data for the oxidation of TDG by $\beta_2\beta_2$- and $\gamma_1\gamma_1$-ADH. Each data point represents the mean ± SD of at least three trials.

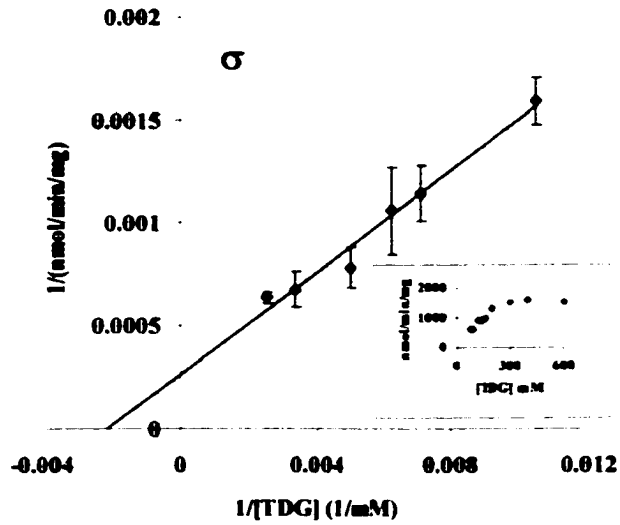

Fig. 5.1C Oxidation of 2,2'-Thiobis-ethanol by σ-ADH. The experiments were conducted as described under Materials and Methods under the following conditions: 75 mM – 600 mM TDG, 0.21 μg/ml σσ-ADH. All reactions contained 5mM NAD^+ in 20 mM tris-maleate buffer, pH 7.6. (Insert) Michaelis-Menten plot of V vs. S data for the oxidation of TDG by σ-ADH. Each data point represents the mean ± SD of at least three trials.

of 3.7 mM and 220 nmol/min/mg, respectively. The class IV σ isozyme, which has a K_M of 41 mM for ethanol oxidation (4), has a K_M for TDG that is two orders of magnitude higher than that of the class I ADHs at 255 mM. Michaelis-Menten plots for the σ isozyme showed a linear increase in activity up to approximately 200 mM approaching V_{max} at 300-400 mM TDG (Figure 5.1C). Above 600 mM the reaction was noticeably inhibited, for example, in the range of 800 mM – 1 M (data not shown) the oxidative activity of σ-ADH is reduced by half, probably due to ionic perturbations by these very high substrate concentrations. Exhibiting the highest activity of the ADH isozymes tested, V_{max} for σ-ADH was 2545 nmol/min/mg protein (k_{cat} = 1018 min^{-1}). Class I αα- and $\beta_1\beta_1$-ADH oxidize TDG with approximate k_{cat}/K_M values of 7-9 mM^{-1} min^{-1} and $\gamma_1\gamma_1$ had a value of about 187 mM^{-1} min^{-1}. The k_{cat}/K_M for σ-ADH was estimated at about 4 mM^{-1} min^{-1}. Caution needs to be exercised when interpreting the kinetic data of σ-ADH. We note that the reaction appears first order with respect to substrate concentration to above 200 mM. At such high concentrations ethanol displays substrate inhibition of other ADH (119). Therefore, we cannot be certain whether the plateau in the v vs. S plot for σ-ADH is a true reflection of saturation kinetics or substrate perturbation of the ADH activity. If the latter is true, then calculation of a K_M and hence catalytic efficiency may not be accurate. An equally valid interpretation may be that σ-ADH is highly efficient and may not be saturable by TDG even at high mM concentrations. That this hypothesis has credence is suggested by the relative efficiencies (k_{cat}/K_M) observed with longer chain (4-8 C) aliphatic alcohols and σ-ADH, which are more than two orders of magnitude greater than that obtained with ethanol

Table 5.2 Kinetic parameters for the oxidation of thiodiglycol and ethanol by ADH isozymes.

Class	Isozyme	TDG K_M	TDG k_{cat}	TDG k_{cat}/K_M	Ethanol K_M	Ethanol k_{cat}	Ethanol k_{cat}/K_M
I	HLADH	6.1	312	51	0.32	438	1369
	$\alpha\alpha$	8.7 (7.9 ± 1.2)	60	7	4.20	54	13
	$\beta_1\beta_1$	3.9 (4.7 ± 0.4)	36	9	0.05	18	376
	$\beta_2\beta_2$	48 (54 ± 5.3)	915	19	1.2	696	580
	$\gamma_1\gamma_1$	1.3 (1.4 ± 0.1)	244	187	1.10	140	130
IV	σ	255 (293 ± 87)	1018	4	41	1000	24

Units for kinetic constants: K_M, mM; k_{cat}, min^{-1}; k_{cat}/K_M, mM^{-1} min^{-1}. Enzyme concentrations used were: 2.8, 6.8, 6.9, 1.6 and 0.2 μg/ml respectively, for $\alpha\alpha$-, $\beta_1\beta_1$-, $\beta_2\beta_2$-, $\gamma_1\gamma_1$-, and σ-ADH. Values in parentheses are K_M values calculated from hyperbolic curve fits of the data with the software *Enzyme Kinetics* (version 1.2) by Cleland (96). Data for ethanol oxidation catalyzed by $\alpha\alpha$-, $\gamma_1\gamma_1$-, and σ-ADH were from Pares *et al.* (120), for $\beta_1\beta_1$ from Bosron *et al.* (121), for $\beta_2\beta_2$ from Kedishvili *et al.* (122), and for HLADH from Lee *et al.* (123).

(112). In this regard, TDG most closely resembles a 5C aliphatic alcohol in its structural motif.

5.3.3 Inhibition by Pyrazole of TDG Oxidation by Human ADH

Using the most active isozymes, we determined that 1 mM pyrazole, a potent inhibitor of ADH, inhibited the class I $\alpha\alpha$-, $\beta_1\beta_1$-, $\beta_2\beta_2$- and $\gamma_1\gamma_1$- ADH, and class IV σ-ADH by 83, 100, 56, 90, and 73%, respectively (Table 5.1). Both pyrazole and acetaldehyde competitively inhibited the ADH catalyzed oxidation of TDG. Inhibition by these competitive inhibitors with respect to the $\alpha\alpha$-ADH yielded apparent K_i values of 82 and 161 μM, respectively (Table 5.3). Under the experimental conditions employed in these studies, the $\beta_1\beta_1$ isozyme was inhibited 100 % by 0.4 mM pyrazole and 2.3 mM acetaldehyde. The apparent K_i values for class I $\beta_2\beta_2$-ADH was 430 μM.

The oxidation of TDG catalyzed by $\gamma_1\gamma_1$-ADH was also completely inhibited by pyrazole over the concentration range of 0.4 – 2 mM. By increasing the concentration of TDG to 40-75 mM, well above saturation of the enzyme, activity measurements were obtained that allowed for the determination of an apparent K_i for pyrazole inhibition from the slopes of double reciprocal plots of uninhibited reactions and reactions containing 1 mM pyrazole. Pyrazole inhibition of class I $\gamma_1\gamma_1$-ADH catalyzed TDG oxidation showed an apparent K_i of 3.2 μM. Determination of the apparent K_i's for pyrazole and acetaldehyde inhibition of the σ-ADH catalyzed oxidation was hampered due to the variations in the ability to saturate the enzyme as discussed previously. In this experiment, the higher activity of the σ isozyme may also lead to higher concentrations of NADH being formed from the oxidation of TDG. This higher concentration of NADH may drive the reduction of acetaldehyde, resulting in non-linear double reciprocal plots in these reactions.

Table 5.3 Apparent K_i constants for the inhibition of TDG oxidation by pyrazole and acetaldehyde.

Class	Isozyme	Pyrazole	Acetaldehyde
I	αα	82	161
	$\beta_2\beta_2$	430	ND
	$\gamma_1\gamma_1$	3.2	ND
IV	σ	878	ND

K_i units are μM. ND denotes Not Determined. The experiments were conducted as described in Materials and Methods and K_i values were calculated from Dixon plots. Enzyme concentrations used were: 2.8 μg/ml αα, 6.9 μg/ml $\beta_2\beta_2$, 1.6 μg/ml $\gamma_1\gamma_1$, and 0.21 μg/ml σ-ADH.

5.4 Discussion

Sulfur mustards are oily lipophilic liquids that penetrate skin and mucosal surfaces within 3 to 5 minutes after contact to provoke local discomfort both to the respiratory tract and to the skin (51). Employees in factories manufacturing mustard gas can become partially or totally disabled because of injury to the mucosa of the respiratory system after protracted exposure to small quantities of mustard gas vapor. Typically, such workers develop an aggregate of several symptoms, most notably problems of the eyes, respiratory tract, gastrointestinal tract, and the nervous system.

In previous incidents of exposure to mustard in solution, the lungs, kidneys, and skin sustained the most damage. In general, 80% of mustard making contact with skin will evaporate, and the 20% remaining will penetrate the skin; however, only 2% of the mustard becomes fixed, so that 18% is absorbed into the circulation to cause systemic intoxication (124). Nagy *et al.* (125) has estimated that as little as 6 $\mu g/cm^2$ of liquid sulfur mustard will cause lesions in human skin in most exposed sites. Of the three immediate target tissues of chemical warfare agents, namely, the skin, eyes and respiratory system, the ones that are immediately susceptible to the toxic action of mustard are the eyes (126). Mustard gas penetrates the cornea more rapidly than it does the skin, within 2 to 3 minutes after contact. The higher absorbance rate may lead to higher localized concentrations of TDG in the eyes. Next to eye lesions, the greatest discomfort produced by exposure to mustard gas is that resulting from irritation and injury of the respiratory system (51).

Human gastric mucosa contains only the class I $\gamma_1\gamma_1$-ADH and the ubiquitous class III χ-ADH (11). As discussed above, gastrointestinal problems have been

identified in workers at factories that manufacture mustard gas from protracted exposure to small quantities of mustard gas vapor. Therefore, if TDG oxidation is relevant to sulfur mustard toxicity as has been proposed by Brimfield et al. (1998), then the class I $\gamma_1\gamma_1$-ADH is indicated, based on our studies with purified enzymes, as a major catalyst in the sequelae of toxic action. Again, the present data indicate that TDG is not a substrate of class III χ-ADH.

Duester *et al.* (16, 127) has reported that the ADH3 gene, which encodes class I γ-ADH, is inducible by certain chemicals. The ADH3 gene was found to possess a retinoic acid response element in its promoter region that may function in some tissues to regulate the amount of ADH activity in response to retinoic acid. It remains to be established whether or not $\gamma_1\gamma_1$-ADH is induced by TDG, but if this substrate behaves similarly to others for this isoenzyme it may account, at least in part, for the deleterious effects of TDG. We are not aware of any studies to indicate induction of class I $\gamma_1\gamma_1$-ADH by TDG; nevertheless, its marked catalytic efficiency toward TDG suggests that such a study would be of importance in regard to TDG exposure. To the best of our knowledge class I $\gamma_1\gamma_1$-ADH is the only human ADH that has been shown to be inducible by xenobiotic agents.

Recent immunohistochemical studies have shown the presence of class I ADH and class III ADH enzymes in human skin, predominantly in the epidermis, with very little expression of the class II protein in the epidermis and dermis (117). The severity of skin lesions as a consequence of exposure to mustard is dependent upon the dose of the agent, the humidity, and the length of exposure (128). It has also been shown that sweaty human skin incurred greater damage from mustard exposure because its

sensitivity to the compounds was enhanced by a film of moisture on the skin surface (129). In this regard class I ADH was observed primarily in the microvasculature and sweat duct moisture (117).

The class I isozymes show significant differences in their abilities to catalyze the oxidation of TDG. One difference is $\beta_2\beta_2$-ADH catalyzes a 5-fold greater rate of TDG oxidation compared to that of $\beta_1\beta_1$-ADH; the former is found in 65% of Japanese and Chinese populations (130). These polymorphic variants are the result of a single amino acid substitution, Arg 47 for His in β_2 (6), which is located in the coenzyme binding cleft and provides electrostatic stabilization for coenzyme binding (91, 92). Thus, the difference seen in the activity of these β variants may be attributed to the ability of the β_1 isozyme to bind NAD^+ in a more stable conformation, which may translate into slower release of NADH as product (91). We are unaware of the existence of data suggesting significant differences in the toxicity of sulfur mustards amongst different ethnic groups. Nevertheless, the above indicates that such a study of ADH-dependent oxidation of TDG in different ethnic groups is of heuristic value.

The class III χ-ADH is expressed in most organ systems. Despite its presence in most tissues χ-ADH does not catalyze TDG oxidation with up to 30 mM TDG thus, it is unlikely that χ-ADH plays a role in TDG metabolism. χ-ADH has a unique substrate binding site that encloses twice the volume of the $\beta_1\beta_1$ substrate binding site (86). Cinnamyl alcohol, a preferred substrate of χ-ADH, has a large phenyl ring bound to a propenol moiety, which favors formation of productive interactions within the active site. Also, the dihydric nature of the TDG molecule may favor unproductive associations with amino acid side chains lining the substrate binding site. Brimfield *et*

al. (1998) found no evidence to suggest oxidation by ADH of both hydroxyl groups of TDG. One possibility is that through its associations with amino acid side chains the hydroxyl moiety that is not directly involved in oxidation may hinder the TDG from obtaining a productive orientation in the substrate binding site.

Class IV σ-ADH is the extrahepatic form of ADH found in the epithelial cells, especially the lining of the stomach and esophagus (131). mRNA for σ-ADH has also been detected in human cornea and skin. Assuming that localized TDG concentrations in the eyes following sulfur mustard exposure may be high due to the fast absorption rate, TDG may achieve its apparent high K_M (122). However, even at TDG concentrations well below its K_M, the class IV σ-ADH catalyzed oxidation of TDG can exceed that of the other human ADH isozymes. Based on the v vs. [S] plot for TDG oxidation by σ-ADH (Fig. 5.1) we estimated the K_M at greater than 200 mM, which translates to an enzyme with an efficiency (k_{cat}/K_M) for TDG oxidase of about 4 - 5 mM^{-1} min^{-1}. The substrate binding site of σ-ADH is enlarged near the catalytic zinc ion and the middle region of the substrate binding pocket is narrow. This enlarged active site would not restrict the binding modes of relatively small substrates, thus more non-productive encounters between the enzyme and such small substrates will occur, which is reflected in higher K_M values (86). In general, oxidation of primary aliphatic alcohols by σ-ADH presents increasing catalytic efficiencies as the chain length increases, primarily a result of decreasing K_M values (4, 11). σ-ADH is unable to oxidize steroid alcohols and secondary alcohols efficiently. At pH 7.4, σ-ADH has a K_M of 120 mM for S(+)-2-Butanol (4). At pH 10, a K_M of 140 mM is noted for cyclohexanol (11). Hurley and Vessell (132) have suggested that the enlarged entrance to the σ-ADH

alcohol-binding site may yield fewer productive versus unproductive encounters between the enzyme and secondary alcohols.

The highest efficiency for TDG catalysis by the various purified human ADH studied was observed with the class I $\gamma_1\gamma_1$-ADH (>180 mM^{-1} min^{-1}). ADH classes I, II and III are constitutively expressed in human skin, a major target of sulfur mustard toxicity, with localization in specific regions of the epidermis. We note that class I γ-, α- and the β-ADHs all catalyze TDG oxidation. $\gamma_1\gamma_1$-ADH was clearly the most efficient of these; the value of k_{cat}/K_M was at least an order of magnitude greater than that of the others (see Results) suggesting a marked potential for involvement in TDG oxidation by the skin. Although the class I isozymes can form heterodimers *in vivo* and the α, β_1, and β_2 isozymes show significant TDG oxidase activity, implying that these isozymes may have a role in oxidizing TDG *in vivo*, their limited tissue distribution and the high catalytic efficiency of the γ_1 isozyme would seem to limit any significant participation of these isozymes in the action of sulfur mustards in the primary target tissues. The class I α- and β-ADH isozymes are not expressed in the eyes nor gastrointestinal tract. Class III χ-ADH does not catalyze TDG oxidation; thus, it seems unlikely that this isoenzyme has a role in the oxidation of TDG by human skin cytosol (53). Class II π-ADH catalyzed low level TDG oxidation (12 nmol/min/mg); however, because both liver and skin NADH-dependent cytosolic oxidation of TDG was potently inhibited by pyrazole and class II ADH is pyrazole-insensitive a minor role for this class of ADH in TDG oxidation is suggested.

The low K_i value obtained for pyrazole inhibition with $\gamma_1\gamma_1$-ADH suggests a possible therapeutic role for pyrazole and 4-substituted pyrazoles in sulfur mustard

toxicity if indeed ADH-dependent TDG metabolism is part of the toxic sequelae of sulfur mustard. The high activity of the σ-ADH, although less efficient than the $\gamma_1\gamma_1$-ADH, may account for sulfur mustard action in eyes, however, the apparent high K_i of pyrazole inhibition may limit the effectiveness of pyrazole therapy. The exact role that the ADH-catalyzed oxidation of TDG plays in sulfur mustard toxicity has not been established. However, these studies may prove important in the interpretation of the interactions between sulfur mustard and metabolic systems of humans.

CHAPTER 6 SUMMARY

Liver cytosolic fractions are known to catalyze the reduction of certain C-nitroso compounds to their corresponding hydroxylamines and amines. C-nitroso compounds are highly reactive intermediates in the toxic sequelae of nitroarene metabolism. Alcohol dehydrogenase, NAD(P)H: quinone oxidoreductase and xanthine and aldehyde oxidase have been implicated as C-nitroso reductases. To probe the role of these cytosolic enzymes in the reduction of C-nitroso compounds we have studied the effects of classical inhibitors of these enzymes on the ability of liver cytosolic fractions from ADH^+ and ADH^- deermice to reduce *p*-nitrosophenol (pNSP) to *p*-aminophenol (pAP). Pyrazole, a potent inhibitor of ADH, inhibited NADH- pNSP reduction by ADH^+ cytosol by > 85%. Thus, ADH contributes substantially to NADH-C-nitroso reduction by cytosol from ADH^+ deermice. The NAD(P)H: quinone oxidoreductase inhibitor, dicumarol, inhibited NADH-dependent pAP formation about 25%; however, dicumarol potently inhibited the NADPH-dependent formation (90-95%). As expected, cytosol from ADH^- deermice did not catalyze pyrazole-sensitive (ADH-dependent) C-nitroso reduction with NADH as the cofactor. Both NADPH- and NADH- pNSP reduction by ADH^- cytosol was inhibited >90% by dicumarol. The xanthine oxidase/aldehyde oxidase inhibitor, allopurinol, was without effect on NAD(P)H cytosolic *p*-nitrosophenol reduction from ADH^- and ADH^+ deermice under either aerobic or anaerobic conditions. Our findings suggest that in the ADH^+ animal, ADH contributes significantly to NADH-dependent C-nitroso reduction by cytosol relative to NAD(P)H: quinone oxidoreductase. NADPH-dependent pNSP reduction by liver cytosol of ADH^+ animals is mostly dicumarol-sensitive which implicates NAD(P)H: quinone

oxidoreductase as the major NADPH-dependent activity. In ADH$^-$ deermice, both NADH- and NADPH-dependent *p*-nitrosophenol reduction is essentially all dicumarol-sensitive (NAD(P)H: quinone oxidoreductase-dependent). Because the toxic expression of C-nitroso compounds are mediated by hydroxylamine intermediates, the present data indicate the importance of considering the role of ADH in the toxic sequelae of nitro and nitroso arenes.

ADH is a Zn-containing metalloenzyme. Although, extensive structural homology between horse and different isozymes of human liver ADH exist, significant differences occur within the active site, which account for great variability among substrate specificities, kinetic constants, and response to inhibitors. We have studied the metabolic activity of horse liver alcohol dehydrogenase (HLADH), purified class I $\alpha\alpha$, $\beta_1\beta_1$, and $\beta_2\beta_2$, class II π, class III χ and class IV σ human isozymes, and human liver cytosol (HLC) towards the model C-nitroso substrate pNSP. Significant differences in the reaction rates of pNSP reduction and the sensitivity to pyrazole inhibition were observed between HLADH and the human isozymes. Class II π-ADH catalyzed pNSP reduction at a rate ~10 times greater than did class I $\beta_2\beta_2$-ADH and was relatively insensitive to pyrazole. The relative order of the rates of *p*NSP reduction by these ADH isozymes was HLADH > $\alpha\alpha$ > π > σ > χ > $\beta_2\beta_2$ > $\beta_1\beta_1$. Interestingly, while pNSP reduction by HLADH proceeds via an observable spectral intermediate between 252-257 nm, such a spectral intermediate is not apparent with the human isozymes. *p*NSP reduction catalyzed by HLADH, purified class I $\alpha\alpha$, $\beta_1\beta_1$, and $\beta_2\beta_2$, class III χ and class IV σ human isozymes show pH dependence with maxima greater than or

equal to pH 6. These pH dependence seemingly reflects a protein moiety involved in the proton relay system.

Sulfur mustard is a poisonous chemical agent that exerts local action on the eyes, skin, and respiratory tissues, with subsequent systemic action on the nervous, cardiac, and digestive systems in humans. This toxic action is thought to be related to the generation of 2,2'-thiodiglycol (TDG; also known as 2,2'-*bis*-thiodiethanol), the hydrolysis product of sulfur mustard. TDG subsequently can undergo oxidation catalyzed by ADH. Human ADH isozymes differ in their tissue distribution. Therefore, we have compared the catalytic activity of purified human liver class I α, β_1, β_2 and γ_1 ADH, class II π ADH, class III χ ADH, and class IV σ ADH with respect to TDG oxidation. Specific activities with respect to TDG were 123, 79, 7, 647, and 8 nmol/min/mg for the class I α, β_1, β_2 and γ_1 ADH and class II π ADH, respectively. Class III χ ADH did not exhibit activity with this substrate. The specific activity of class IV σ ADH was estimated at about 2545 nmol/min/mg. 1 mM pyrazole, a potent inhibitor of class I and class II ADH, inhibited the class I α, β_1 and γ_1 ADH and class IV σ ADH by 83, 100, 90, and 73%, respectively. The class I α and β_1 ADH oxidized TDG with k_{cat}/K_M values of 8-9 mM^{-1} min^{-1}, and class I γ_1 ADH with a value of 154 mM^{-1} min^{-1}. The k_{cat}/K_M value for class IV σ ADH was estimated at 4 mM^{-1} min^{-1}. The activities of class IV σ and class I γ_1 ADH are of significant interest because of their prevalence, respectively, in the eyes, lungs, stomach and skin, all potential target organs of sulfur mustard toxicity.

REFERENCES

1. C. S. Lieber (1991). Hepatic metabolic and toxic effects of ethanol: 1991 -- update. *Alcohol Clin. Exp. Res.*, **25**, 573-592.

2. E. Cederlund, J. M. Peralba, X. Parés and H. Jörnvall (1991). Amphibian alcohol dehydrogenase, the major frog liver enzyme. Relationships to other forms and asessment of an early gene duplication separating vertebrate class I and class III alcohol dehydrogenases. *Biochemistry*, **30**, 2811-2816.

3. O. Danielsson and H. Jörnvall (1992). Enzymogenesis: classical liver alcohol dehydrogenase. Origin from the glutathione-dependent formaldehyde dehydrogenase line. *Proc. Natl. Acad. Sci. USA*, **89**, 9247-9251.

4. N. Y. Kedishvili, W. F. Bosron, C. L. Stone, T. D. Hurley, C. F. Peggs, H. R. Thomasson, K. M. Popov, L. G. Carr, H. J. Edenberg and T.-K. Li (1995). Expression and Kinetic Characterization of Recombinant Human Stomach Alcohol Dehydrogenase: Active-site amino acid sequence explains substrate specificity compared with liver isozymes. *J. Biol. Chem.*, **270**, 3625-3630.

5. T. Ehrig, W. F. Bosron and T.-K. Li (1990). Alcohol and aldehyde dehydrogenase. *Alcohol Alcohol*, **25**, 105-116.

6. H. Jörnvall, J. Hempel, B. L. Vallee, W. F. Bosron and T.-K. Li (1984). Human liver alcohol dehydrogenase: Amino acid substitution in the β2β2 Oriental isozyme explains functional properties, establishes an active site structure, and parallels mutational exchanges in the yeast enzyme. *Proc. Natl. Acad. Sci. USA*, **81**, 3024-3028.

7. K. Engeland and W. Maret (1993). Extrahepatic, Differential Expression of Four Classes of Human Alcohol Dehydrogenase. *Biochem. Biophys. Res. Commun.*, **193**, 47-53.

8. O. Danielsson, S. Atrian, T. Luque, L. Hjelmqvist, R. González-Duarte and H. Jörnvall (1994). Fundamental molecular differences between alcohol dehydrogenase classes. *Proc. Natl. Acad. Sci. USA*, **91**, 4980-4984.

9. J. Shafqat, M. El-Ahmad, O. Danielsson, M. C. Martinez, B. Persson, X. Parés and H. Jörnvall (1996). Pea formaldehyde-active class III alcohol dehydrogenase: Common derivation of the plant and animal forms but not of the corresponding ethanol-active forms (classes I and P). *Proc. Natl. Acad. Sci. USA*, **93**, 5595-5599.

10. M. H. Foglio and G. Duester (1996). Characterization of the functional gene encoding mouse class III alcohol dehydrogenase (glutathione-dependent formaldehyde dehydrogenase) and an unexpressed processed pseudogene with an intact open reading frame. *Eur. J. Biochem.*, **237**, 496-504.

11. A. Moreno and X. Parés (1991). Purification and Characterization of a New Alcohol Dehydrogenase from Human Stomach. *J. Biol. Chem.*, **266**, 1128-1133.

12. X. Parés, I. Cederlund, A. Moreno, N. Saubi, J.-O. Höög and H. Jörnvall (1992). Class IV alcohol dehydrogenase (the gastric enzyme): structural analysis of human σσ-ADH reveals class IV to be variable and confirms the presence of a fifth mammalian alcohol dehydrogenase class. *FEBS Lett.*, **303**, 69-72.

13. M. A. Satre, M. Zgombic-Knight and G. Duester (1994). The complete structure of human class IV alcohol dehydrogenase (retinol dehydrogenase) determined from the ADH7 gene. *J. Biol. Chem.*, **269**, 15606-15612.

14. C. C. Ditlow, B. Holmquist, M. M. Morelock and B. L. Vallee (1984). Physical and Enzymatic Properties of a Class II Alcohol Dehydrogenase Isozyme of Human Liver: π-ADH. *Biochemistry*, **23**, 6363-6368.

15. B. Persson, J. S. J. Zigler and H. Jörnvall (1994). A super-family of medium-chain dehydrogenases/reductases (MDR). Sub-lines including ζ-crystallin, alcohol and poyol dehydrogenases, quinone oxido-reductases, enoyl reductases, VAT-1 and other proteins. *Eur. J. Biochem.*, **226**, 15-22.

16. G. Duester, M. L. Shean, M. S. McBride and M. J. Stewart (1991). Retinoic acid response element in the human alcohol dehydrogenase gene ADH3: Implications for regulation of retinoic acid synthesis. *Mol. Cell. Biol.*, **11**, 1638-1646.

17. M. Smith, D. A. Hopkinson and H. Harris (1971). Developmental changes and polymorphism in human alcohol dehydrogenase. *Ann. Hum. Genet.*, **34**, 251-271.

18. H. Eklund, E. Horjales, B. L. Vallee and H. Jörnvall (1987). Computer-graphics interpretations of residue exchanges between the α, β, and γ subunits of human-liver alcohol dehydrogenase class I isoenzymes. *Eur. J. Biochem.*, **167**, 185-193.

19. H. Eklund, P. Müller-Wille, E. Horjales, O. Futer, B. Holmquist, B. L. Vallee, J.-O. Höög, T. Kaiser and H. Jörnvall (1990). Comparison of three classes of human liver alcohol dehydrogenase. Emphasis on different substrate binding pockets. *Eur. J. Biochem.*, **193**, 303-310.

20. B. Persson, T. Bergman, W. M. Keung, U. Waldenström, B. Holmquist, B. L. Vallee and H. Jörnvall (1993). Basic features of class-I alcohol dehydrogenase: variable and constant segments coordinated by inter-class and intra-class variability. Conclusions from characterization of the alligator enzyme. *Eur. J. Biochem.*, **216**, 49-56.

21. C.-I. Brändén and H. Eklund (1978). Coenzyme-induced conformational changes and substrate binding in liver alcohol dehydrogenase. *Ciba Found. Symp.*, **60**, 63-80.

22. C.-I. Brändén and H. Eklund (1980). Structure and Mechanism of Liver Alcohol Dehydrogenase, Lactate Dehydrogenase and Blyceraldehyde-3-phosphate Dehydrogenase. In *Dehydrogenases Requiring Nicotinamide Coenzymes*. J. Jeffrey, ed., pp. 40-84, Birkhauser Verlag, Basel and Boston.

23. H. Eklund, J.-P. Samama, L. Wallén, C.-I. Brändén, Å. Åkeson and T. A. Jones (1981). Structure of a triclinic ternary complex of horse liver alcohol dehydrogenase at 2.9 Å resolution. *J. Mol. Biol.*, **146**, 561-587.

24. B. V. Plapp, H. Eklund and C.-I. Brändén (1978). Crystallography of Liver Alcohol Dehydrogenase Complexed with Substrates. *J. Mol. Biol.*, **122**, 23-32.

25. D. L. Sloan, J. M. Young and A. S. Mildvan (1975). Nuclear magnetic resonance studies of substrate interactions with cobalt substituted alcohol dehydrogenase from liver. *Biochemistry*, **14**, 1998-2008.

26. B.-E. Drysdale and D. P. Hollis (1980). A Nuclear Magnetic Resonance Study of Cobalt II Alcohol Dehydrogenase: Substrate Analog-Metal Interactions. *Arch. Biochem. Biophys.*, **205**, 267-279.

27. T. D. Hurley, W. F. Bosron, J. A. Hamilton and L. M. Amzel (1991). Structure of human β1β1 alcohol dehydrogenase: Catalytic effects of non-active-site substitutions. *Proc. Natl. Acad. Sci. USA*, **88**, 8149-8153.

28. M. O. Amdur, J. Doull and C. D. Klaassen (1991). Casarett and Doull's Toxicology: The Basic Science of Poisons. , , McGraw-Hill, Inc., New York.

29. C. S. Lieber (1990). Interaction of ethanol with drugs, hepatotoxic agents, carcinogens and vitamins. *Alcohol. Clin. Exp. Res.*, **25**, 157-176.

30. A. Abbondanza, M. B. Batelli, M. Soffritti and C. Cessi (1989). Xanthine oxidase status in ethanol-intoxicated rat liver. *Alcoholism Clin. Exp. Res.*, **13**, 841-844.

31. T. Cronholm (1993). Ethanol metabolism in isolated hepatocyte. *Biochem. Pharmacol.*, **45**, 553-558.

32. D. E. Rickert (1985). Mammalian and bacterial metabolism of nitroaromatic compounds. In *Toxicity of Nitroaromatic Compounds*. D. E. Rickert, ed., pp. 87-102, Hemisphere Publishing Co., Washington.

33. A. B. Shah, R. D. Combes and I. R. Rowland (1990). Activation and detoxification of 1,8-dinitropyrene by mammalian hepatic fractions in the *Salmonella* mutagenicity assay. *Mutagenesis*, **5**, 45-49.

34. G. W. Winston, C. A. Traynor, B. S. Shane and A. K. D. Hajos (1992). Modulation of the mutagenicity of three dinitropyrene isomers *in vitro* by rat-liver S9, cytosolic, and microsomal fractions following chronic ethanol ingestion. *Mutat. Res.*, **279**, 289-298.

35. F. F. Kadlubar, L. E. Uhruh, F. A. Beland, K. M. Straub and F. E. Evans (1980). In vitro reaction of the carcinogen, N-hydroxy-2-naphthylamine, with DNA at the C-8 and N^2 atoms of quanine and at the N^6 atom of adenine. *Carcinogenesis*, **1**, 139-150.

36. Z. Maskos and G. W. Winston (1993). Alcohol Dehydrogenase-Dependent Reduction of 2-Nitrosofluorene and Rearrangement of N-Hydroxy-2-aminofluorene. *Biochemistry*, **32**, 12768-12773.

37. Z. Maskos and G. W. Winston (1994). Mechanism of p-Nitrosophenol Reduction Catalyzed by Horse Liver and Human π-Alcohol Dehydrogenase (ADH): Human π-ADH as a Quinone Reductase. *J. Biol. Chem.*, **269**, 31579-31584.

38. H. S. Rosenkranz and R. Mermelstein (1983). Mutagenicity and genotoxicity of nitroarenes: All nitro-containing chemicals were not created equal. *Mutat. Res.*, **114**, 217-267.

39. H. Tokiwa, R. Nadagawa, K. Itorikawa and A. Ohkuko (1987). The nature of the mutagenicity and carcinogenicity of nitrated aromatic compounds in the environment. *Environ. Health Persp.*, **73**, 191-199.

40. M. F. Dunn and S. A. Bernhard (1971). Rapid kinetic evidence for adduct formation between the substrate analog *p*-nitroso-N,N-dimethylaniline and reduced nicotinamide-adenine dinucleotide during enzymic reduction. *Biochemistry*, **10**, 4569-4575.

41. S. C. Koerber, P. Schack, A. M.-J. Au and M. F. Dunn (1980). Investigation of a Novel Liver Alcohol Dehydrogenase Catalyzed Redox-Elimination Reaction Involving Arylnitroso Substrate Analogues. *Biochemistry*, **19**, 731-738.

42. S. Trivic and V. Leskovac (1991). Redox-elimination reaction catalyzed by yeast alcohol dehydrogenase. *Biochem. Internat.*, **25**, 669-675.

43. M. L. C. Bernhiem (1973). The reduction of certain C-nitroso compounds by rat liver cytosol. *Res. Commun. Chem. Pathol. Pharmacol.*, **6**, 151-165.

44. S. Horie, T. Watanabe and Y. Ogura (1980). Studies on the Enzymatic Reduction of C-Nitroso Compounds: I. Distribution of C-nitrosoreductase Activity in Animal Tissues and Partial Purification of the Enzyme from Porcine Liver. *J. Biochem.*, **88**, 847-857.

45. Y. Ogura and S. Horie (1980). Studies on the Enzymatic Reduction of C-Nitroso Compounds. III. The Kinetic Analysis of C-Nitrosoreductase Reaction Catalyzed by the Cytoplasmic Enzyme from Porcine Liver. *J. Biochem.*, **88**, 1135-1139.

46. S. Horie and Y. Ogura (1980). Studies on the Enzymatic Reduction of C-Nitroso Compounds. IV. Partial Purification and Kinetic Properties of Porcine Heart C-Nitrosoreductase. *J. Biochem.*, **88**, 1141-1150.

47. S. Horie, T. Watanabe and A. Ohta (1982). Studies on the Enzymatic Reduction of C-Nitroso Compounds. V. Molecular Properties of Porcine Heart C-Nitrosoreductase and Identity of This Enzyme with NAD(P)H Dehydrogenase. *J. Biochem.*, **92**, 661-671.

48. A. K. D. Hajos and G. W. Winston (1992). Role of cytosolic NAD(P)H-quinone oxidoreductase and alcohol dehydrogenase in the reduction of *p*-nitrosophenol following chronic ethanol ingestion. *Arch. Biochem. Biophys.*, **295**, 223-229.

49. S. Dickman (1988). Nerve gas cloud hangs over West German farms. *Nature*, **332**, 573.

50. D. H. Rosenblatt, T. A. Miller, J. C. Dacre, I. Muul and D. R. Cogley (1975). Problem definition studies of potential environmental pollutants. II. Physical, chemical, toxicological and biological properties of 16 substances. In *Technical Report 7509, AD A030428*, pp. , U. S. Army Medical Bioengineering Research and Development Laboratory, Fort Detrick, Frederic, MD.

51. J. C. Dacre and M. Goldman (1996). Toxicology and Pharmacology of the Chemical Warfare Agent Sulfur Mustard. *Pharmacol. Rev.*, **48**, 289-320.

52. A. A. Brimfield (1995). Possible protein phosphatase inhibition by bis(hydroxyethyl)sulfide, a hydrolysis product of mustart gas. *Toxicology Letters*, **78**, 43-48.

53. A. A. Brimfield, L. M. Zweig, M. J. Novak and D. M. Maxwell (1998). *In Vitro* Oxidation of the Hydrolysis Product of Sulur Mustard, 2,2'-Thiobis-ethanol, by Mammalian Alcohol Dehydrogenase. *J. Biochem. Mol. Toxicol.*, **12**, 361-369.

54. M. L. C. Bernhiem (1972). The non-enzymic oxidation of NADH by nitrosobenzene. *Biochem. Biophys. Res. Commun.*, **46**, 1598-1602.

55. A. R. Becker and L. A. Sternson (1980). Nonenzymatic Reduction of Nitrosobenzene to Phenylhydroxylamine by NAD(P)H. *Bioorg. Chem.*, **9**, 305-312.

56. K. G. Burnett and M. R. Felder (1980). Ethanol metabolism in *Peromyscus* genetically deficient in alcohol dehydrogenase. *Biochem. Pharmacol.*, **29**, 125-130.

57. Y. Shigeta, F. Nomura, S. Iida, M. A. Leo, M. R. Felder and C. S. Lieber (1984). Ethanol metabolism *in vivo* by the microsomal ethanol-oxidizing system in deermice lacking alcohol dehydrogenase (ADH). *Biochem. Pharmacol.*, **33**, 807-814.

58. S. Kato, J. Alderman and C. S. Lieber (1987). Respective roles of the microsomal ethanol oxidizing system and catalase in ethanol metabolism by deermice lacking alcohol dehydrogenase. *Arch. Biochem. Biophys.*, **254**, 586-591.

59. B. G. Lake (1987). Preparation and characterization of microsomal fractions for studies on xenobiotic metabolism. In *Biochemical Toxicology- A Practical Approach*. K. Snell and B. Mullock, eds., pp. 183-215, IRL Press, Washington, DC.

60. L. Ernster (1967). DT Diaphorase. In *Methods in Enzymology*, Vol. 10. R. W. Estabrook and M. E. Pullman, eds., pp. 309-317, Academic Press, San Diego.

61. R. K. Bonnichsen and N. G. Brink (1955). Liver Alcohol Dehydrogenase. In *Methods in Enzymology*, Vol. 1. S. P. Colowick and N. O. Kaplan, eds., pp. 495-500, Academic Press, New York.

62. I. Fridovich and P. Handler (1962). Xanthine Oxidase: V. Differential inhibition of the reduction of various electron acceptors. *J. Biol. Chem.*, **237**, 916-921.

63. M. F. Dunn and S. J. Hutchison (1973). Roles of Zinc Ion and Reduced Coenzyme in the Formation of a Transient Chemical Intermediate During the Equine Liver Alcohol Dehydrogenase Catalyzed Reduction of an Aromatic Aldehyde. *Biochemistry*, **12**, 4882-4892.

64. M. V. Orna and R. P. Mason (1989). Correlation of Kinetic Parameters of Nitroreductase Enzymes with Redox Properties of Nitroaromatic Compounds. *J. Biol. Chem.*, **264**, 12379-12384.

65. Z. Djuric, D. W. Potter, R. H. Heflich and F. A. Beland (1986). Aerobic and anaerobic reduction of nitrated pyrenes *in vitro*. *Chem.-Biol. Interact.*, **59**, 309-324.

66. C. A. Traynor, B. S. Shane, A. K. D. Hajos and G. W. Winston (1991). Arylamine activation following chronic ethanol ingestion by rats: Studies on the liver S9 microsomal and cytosolic fractions and comparison with Aroclor 1254-pretreatment. *Mutat. Res.*, **247**, 153-166.

67. A. K. D. Hajos and G. W. Winston (1991). DT-diaphorase-dependent nitroreduction of dinitropyrenes: Stereoselectivity and induction by Aroclor 1254 pretreatment. *Carcinogenesis*, **12**, 697-702.

68. J. B. Williams, A. Y. H. Lu, R. G. Cameron and C. B. Picket (1986). Rat Liver NAD(P)H:Quinone Reductase. Construction of a Quinone Reductase cDNA Clone and Regulation of Quinone Reductase mRNA by 3-Methylcholanthrene and in Persistent Hepatocyte Nodules Induced by Chemical Carcinogens. *J. Biol. Chem.*, **261**, 5524-5528.

69. C. A. Metosh-Dickey, D. F. Church and G. W. Winston (1994). Superoxide radical anion production resulting from reduction of 4-nitroquinoline-N-oxide by the purified flavo-enzymes cytochrome P450 reductase, DT-diaphorase and xanthine oxidase: a spin trapping study. *The Toxicologist*, **14**, 175 (abstract).

70. C.-I. Brändén, H. Jörnvall, H. Eklund and B. Furugren (1975). Alcohol Dehydrogenases. In *The Enzymes*, Vol. 11A. P. D. Boyer, ed., pp. 103-190, Academic Press, New York.

71. J. P. Klinman (1981). Probes of Mechanism and Transition-State Structure in the Alcohol Dehydrogenase Reaction. *CRC Crit. Rev. Biochem.*, **10**, 39-78.

72. E. K. Weisburger (1981). N-2-Fluorenylacetamide and derivatives. In *Carcinogens in Industry and the Environment*. J. M. Sontag, ed., pp. 583-666, Marcel Dekker, New York.

73. B. F. Dudley and G. W. Winston (1995). *p*-Nitrosophenol Reduction by Liver Cytosol from ADH-Positive and -Negative Deermice (*Peromyscus maniculatus*). *Arch. Biochem. Biophys.*, **316**, 879-885.

74. V. Leskovac, S. Trivic and B. M. Anderson (1996). Yeast Alcohol Dehydrogenase Catalyzed Reduction of *p*-Nitroso-N,N-dimethylaniline by NADH. *Italian J. Biochem.*, **45**, 9-18.

75. M. Pantelic, S. Trivic and V. Leskovac (1996). Reduction of *p*-nitrosophenol by NADH catalyzed by equine liver alcohol dehydrogenase. *J. Serb. Chem. Soc.*, **61**, 859-863.

76. L. Ernster, L. Danielson and M. Ljunggren (1962). DT Diaphorase: I. Purification from the soluble fraction of rat-liver cytoplasm, and properties. *Biochim. Biophys. Acta*, **58**, .

77. M. Novak and K. A. Martin (1991). Steric effects on the pKa of N-protonated N-acetyl-p-benzoquinone imines: evidence for hydration via N-protonation. *J. Org. Chem.*, **56**, 1585-1590.

78. W. W. Cleland (1977). Determining the Chemical Mechanisms of Enzyme-Catalyzed Reactions by Kinetic Studies. In *Adv. Enzymol.*, Vol. 45. A. Meister, ed., pp. 273-387, Interscience, New York.

79. T.-K. Li, W. F. Bosron, W. P. Dafeldecker, L. G. Lange and B. L. Vallee (1977). Isolation of π-alcohol dehydrogenase of human liver: Is it a determinant of alcoholism? *Proc. Natl. Acad. Sci. USA*, **74**, 4378-4381.

80. H. Sund and H. Theorell (1963). Alcohol dehydrogenases. In *The Enzymes*, Vol. 7. P. D. Boyer, H. A. Lardy and K. Myrback, eds., pp. 25-83, Academic Press, New York.

81. W. F. Bosron, T.-K. Li and B. L. Vallee (1980). New molecular forms of human liver alcohol dehydrogenase: Isolation and characterization of $ADH_{Indianapolis}$. *Proc. Natl. Acad. Sci. USA*, **77**, 5784-5788.

82. F. W. Wagner, A. R. Burger and B. L. Vallee (1983). Kinetic Properties of Human Liver Alcohol Dehydrogenase: Oxidation of Alcohols by Class I Isoenzymes. *Biochemistry*, **22**, 1857-1863.

83. F. W. Wagner, X. Parés, B. Holmquist and B. L. Vallee (1984). Physical and enzymatic properties of a class III isoenzyme of human liver alcohol dehydrogenase; χ-ADH. *Biochemstry*, **23**, 2193-2199.

84. G. Mårdh and B. L. Vallee (1986). Human Class I Alcohol Dehydrogenases Catalyze the Interconversion of Alcohols and Aldehydes in the Metabolism of Dopamine. *Biochemistry*, **25**, 7279-7282.

85. W. F. Bosron, T.-K. Li, W. P. Dafeldecker and B. L. Vallee (1980). Human Liver π-Alcohol Dehydrogenase: Kinetic and Molecular Properties. *Biochemistry*, **18**, 1101-1105.

86. T. D. Hurley, C. G. Steinmetz, P. Xie and Z.-N. Yang (1997). Three-dimensional structures of human alcohol dehydrogenase isoenzymes reveal the molecular basis for their functional diversity. In *Molecular Biology and Enzymology of Carbonyl Metabolism*, Vol. 6. H. Weiner, B. Wermuth and D. Crabb, eds., pp. , Plenum Press, NY.

87. Z. Maskos, W. H. Welch and G. W. Winston (2000). Reduction of *p*-Nitrosophenol Catalyzed by Horse Liver Alcohol Dehydrogenase: Evidence for a Mechanism Involving Dual Pathways. *(Unpublished Results)*, .

88. H. Eklund, B. V. Plapp, J.-P. Samama and C.-I. Brändén (1982). Binding of substrate in a ternary complex of horse liver alcohol dehydrogenase. *J. Biol. Chem.*, **257**, 14349-14358.

89. R. L. Brooks and J. D. Shore (1971). Effect of Substrate Structure on the Rate of the Catalytic Step in the Liver Alcohol Dehydrogenase Mechanism. *Biochemistry*, **10**, 3855-3858.

90. J. T. McFarland and Y.-H. Chu (1975). Effect of pH on the Liver Alcohol Dehydrogenase Reaction. *Biochemistry*, **14**, 1140-1146.

91. C. L. Stone, W. F. Bosron and M. F. Dunn (1993). Amino Acid Substitutions at Position 47 of Human $\beta_1\beta_1$ and $\beta_2\beta_2$ Alcohol Dehydrogenases Affect Hydride Transfer and Coenzyme Dissociation Rate Constants. *J. Biol. Chem.*, **268**, 892-899.

92. T. D. Hurley, W. F. Bosron, C. L. Stone and L. M. Amzel (1994). Structures of three human β alcohol dehydrogenase variants: correlations with their functional differences. *J. Mol. Biol.*, **239**, 415-429.

93. U. K. Laemmli (1970). Cleavage of structural proteins during the assembly of the head of bacteriophage T4. *Nature*, **227**, 680-684.

94. H. Towbin, T. Staehelin and J. Gordon (1979). Electrophoretic transfer of proteins from polyacrylamide gels to nitrocellulose sheets, procedure and some applications. *Proc. Natl. Acad. Sci. U.S.A.*, **76**, 4350-4355.

95. M. M. Bradford (1976). A Rapid and Sensitive Method for the Quantitation of Microgram Quantities of Protein Utilizing the Principle of Protein-Dye Binding. *Anal. Biochem.*, **72**, 248-254.

96. W. W. Cleland (1979). Statistical analysis of enzyme kinetic data. *Methods Enzymol.*, **63**, 103-138.

97. I. H. Segel (1993). Enzyme Kinetics. Behavior and Analysis of Rapid Equilibrium and Steady-State Enzyme Systems., 957 pp., John Wiley & Sons, Inc., New York.

98. R. K. Norris and S. Sternhell (1966). N.M.R. Spectra of "*p*-Nitrosophenol" and its methyl derivatives. *Aust. J. Chem.*, **19**, 841-860.

99. W. R. Voughan and G. K. Finch (1956). The Effect of Alkyl Groups on 4-Nitro- and 4-Nitroso-phenols. *J. Org. Chem.*, **21**, 1201-1210.

100. Z. Maskos and G. W. Winston (2000). The Coupled Reduction of *p*-Nitrosophenol with Ethanol Oxidation Catalyzed by Horse Liver Alcohol Dehydrogenase: Toxicological Implications of the Recyyling of NAD^+/NADH. *(Unpublished Results)*, .

101. K. F. Tipton and H. B. F. Dixon (1979). Effects of pH on Enzymes. In *Methods in Enzymology*, Vol. 63. D. L. Purich, ed., pp. 183-234, Academic Press, New York.

102. T. E. Creighton (1993). Proteins. Structures and Molecular Properties, W. H. Freeman, New York.

103. E. Horjales, H. Eklund and C.-I. Brändén (1987). Comparison of computer modelling and X-ray results of the binding of a pyrazole derivative to liver alcohol dehydrogenase. *J. Mol. Biol.*, **197**, 685-694.

104. J.-O. Höög, M. Estonius and O. Danielsson (1994). Site-directed mutagenesis and enzyme properties of mammalian alcohol dehydrogenases correlated with their tissue distribution. In *Toward a Molecular Basis of Alcohol Use and Abuse*. B. Jansson, H. Jörnvall, U. Rydberg, L. Terenius and B. L. Vallee, eds., pp. 301-308, Birkhauser Verlag Basel, Switzerland.

105. J. Kvassman and G. Pettersson (1980). Unified mechanism for proton-transfer reactions affecting the catalytic activity of liver alcohol dehydrogenase. *Eur. J. Biochem.*, **103**, 565-575.

106. A. Fersht (1985). Enzyme Structure and Mechanism, 155-175 pp., W. H. Freeman, New York.

107. V. Leskovac, S. Trivic and B. M. Anderson (1999). Comparison of the chemical mechanisms of action of yeast and equine liver alcohol dehydrogenase. *Eur. J. Biochem.*, **264**, 840-847.

108. V. C. Sekhar and B. V. Plapp (1988). Mechanism of Binding of Horse Liver Alcohol Dehydrogenase and Nicotinamide Adenine Dinucleotide. *Biochemistry*, **27**, 5082-5088.

109. G. Pettersson (1987). Liver alcohol dehydrogenase. *CRC Crit. Rev. Biochem.*, **21**, 349-389.

110. D. R. Light, M. S. Dennis, I. J. Forsythe, C.-C. Liu, D. W. Green, D. A. Kratzer and B. V. Plapp (1992). α-Isoenzyme of Alcohol Dehydrogenase from Monkey Liver. Cloning, Expression, Mechanism, Coenzyme, and Substrate Specificity. *J. Biol. Chem.*, **267**, 12592-12599.

111. J. W. Jacobs, J. T. McFarland, I. Wainer, D. Jeanmaier, C. Ham, K. Hamm, M. Wnuk and M. Lam (1974). Electronic substituent effects during the liver alcohol dehydrogenase catalyzed reduction of aromatic aldehydes. *Biochemistry*, **13**, 60-64.

112. H. J. Edenberg and W. F. Bosron (1997). Alcohol Dehydrogenases. In *Comprehensive Toxicology*, Vol. 3 Biotransformation. F. P. Guengerich, ed., pp. 119, Pergamon Press, New York.

113. T. B. Beisswenger, B. Holmquist and B. L. Vallee (1985). χ-ADH is the sole alcohol dehydrogenase isozyme of mammalian brains: Implications and inferences. *Proc. Natl. Acad. Sci. USA*, **82**, 8369-8373.

114. R. Buehler, M. Hess and J. P. Von-Wartburg (1982). Immunohistochemical localization of human liver alcohol dehydrogenase in liver tissue, cultured fibroblasts, and HeLa cells. *Am. J. Pathol.*, **108**, 89-99.

115. M. Estonius, O. Danielsson, C. Karlsson, H. Persson, H. Jörnvall and J.-O. Höög (1993). Distribution of alcohol and sorbitol dehydrogenases: Assessment of mRNAs in rat tissues. *Eur. J. Biochem.*, **215**, 497-503.

116. B. J. Petersen, N. W. Cornell and R. L. Veech (1980). Alcohol dehydrogenase in cultured human skin fibroblasts. Human fibroblast alcohol dehydrogenase. *Adv. Exp. Med. Biol.*, **132**, 533-541.

117. C. Cheung, C. K. Smith, J.-O. Höög and S. A. M. Hotchkiss (1999). Expression and Localization of Human Alcohol and Aldehyde Dehydrogenase Enzymes in Skin. *Biochem. Biophys. Res. Commun.*, **261**, 100-107.

118. M. Dixon (1953). The determination of enzyme inhibitor constants. *Biochem. J.*, **55**, 170-171.

119. K. Dalziel and F. M. Dickinson (1966). The Kinetics and Mechanism of Liver Alcohol Dehydrogenase with Primary and Secondary Alcohols as Substrates. *Biochem. J.*, **100**, 34-46.

120. X. Parés, E. Cederlund, A. Moreno, H. L., J. Farrés and H. Jörnvall (1994). Mammalian class IV alcohol dehydrogenase (stomach alcohol dehydrogenase): Structure, origin, and correlation with enzymology. *Proc. Natl. Acad. Sci. USA*, **91**, 1893-1897.

121. W. F. Bosron, L. J. Magnes and T.-K. Li (1983). Kinetics and electrophoretic properties of native and recombined isoenzymes of human liver alcohol dehydrogenase. *Biochemistry*, **22**, 1852-1857.

122. N. Y. Kedishvili, W. H. Gough, W. I. Davis, S. Parsons, T.-K. Li and W. F. Bosron (1998). Effect of Cellular Retinol-Binding Protein on Retinol Oxidation by Human Class IV Retinol/Alcohol dehydrogenase and Inhibition by Ethanol. *Biochem. Biophys. Res. Comm.*, **249**, 191-196.

123. K. M. Lee, K. F. Dahlhauser and B. V. Plapp (1988). Reactivity of Horse Liver Alcohol Dehydrogenase with 3-Methylcyclohexanols. *Biochemistry*, **27**, 3528-3532.

124. B. A. Pruit (1987). Treatment of the cutaneous injury. In *Proceedings of the Vesicant Workshop*, pp. pp.39-43, AD A188222, USAM-RICD-SP-87-09, U.S. Army Medical Research Institute of Chemical Defense, Aberdeen Proving Ground, MD, Columbia, MD.

125. S. M. Nagy, C. Golumbic, W. H. Stein, J. S. Fruton and M. Bergmann (1946). The penetration of vesicant vapors into human skin. *J. Gen. Physiol.*, **29**, 441-469.

126. B. P. McNamara (1960). Medical aspects of chemical warfare., , U.S. Army Chemical Research and Development Laboratories, Army Chemical Center, Edgewood Arsenal, MD.

127. P. P. Harding and G. Duester (1992). Retinoic Acid Activation and Thyroid Hormone Repression of the Human Alcohol Dehydrogenase gene ADH3. *J. Biol. Chem*, **267**, 14145-14150.

128. B. P. McNamara, E. J. Owens, M. K. Christensen, F. J. Vocci, D. F. Ford, H. Rozimarek and others (1975). Toxicological basis for controlling levels of mustard in the environment. In *Edgewood Arsenal Special Publication EB-SP-74020, AD A011260*, , Edgewood Arsenal Biomedical Laboratory, Aberdeen Proving Ground, MD.

129. B. Renshaw (1945). Observations on the role of water in the susceptibility of human skin to vesicant vapors. In *National Defense Research Committee*, Vol. Report OSRD No. 5169, pp. , Washington, DC, Division 9.

130. W. F. Bosron and T.-K. Li (1986). Genetic polymorphism of human liver alcohol and aldehyde dehydrogenase, and their relationship to alcohol metabolism and alcoholism. *Hepatology*, **6**, 502-510.

131. S.-J. Yin, F.-J. Chou, S.-F. Tsai, C.-S. Liao, S.-L. Wang, C.-W. Wu and S.-C. Lee (1993). Alcohol and Aldehyde Dehydrogenases in Human Esophagus - Comparison with the Stomach Enzyme Activities. *Alcohol. Clin. Exp. Res.*, **17**, 376-381.

132. T. D. Hurley and L. D. Vessell (1995). The role of leucine 116 in determining the substrate specificity in human β1 alcohol dehydrogenase. In *Enzymology and Molecular Biology of Carbonyl Metabolism*, Vol. 5. H. Weiner, Wermuth, B., and Holmes, R., ed., pp. 321-325, Plenum Press, New York.

133. W. A. Deutsch (1987). Enzymatic studies of DNA repair in Drosophila melanogaster. *Mutat. Res.*, **184**, 209-215.

134. B. K. Duncan and B. Weiss (1982). Specific Mutator Effects of *ung* (Uracil-DNA Glycosylase) Mutations in *Escherichia coli*. *J. Bacteriol.*, **151**, 750-755.

135. E. C. Friedberg, T. Bonura, R. Cone, R. Simmons and C. Anderson (1978). Base excision repair of DNA. In *DNA Repair Mechanisms*, Vol. 163-173. P. C. Hanawalt, E. C. Friedberg and C. F. Fox, eds., pp. , Academic Press, New York.

136. W. A. Deutsch and A. L. Spiering (1982). A New Pathway Expressed during a Distinct Stage of *Drosophila* Development for the Removal of dUMP Residues in DNA. *J. Biol. Chem.*, **257**, 3366-3368.

137. L. H. Breimer (1986). A DNA Glycosylase for Oxidized Thymine Residues in *Drosophila melanogaster*. *Biochem. Biophys. Res. Comm.*, **134**, 201-204.

138. L. E. Giroir and W. A. Deutsch (1987). *Drosophila* Deoxyuridine Triphosphatase. Purification and Characterization. *J. Biol. Chem.*, **262**, 130-134.

139. M. D. Nation, S. N. Guzder, L. E. Giroir and W. A. Deutsch (1989). Control of *Drosophila* deoxyuridine triphosphatase. Existence of a developmentally expressed protein inhibitor. *Biochem. J.*, **259**, 593-596.

140. A. R. Morgan and J. Chelbek (1989). Uracil-DNA Glycosylase in Insects. *Drosophila* and the Locust. *J. Biol. Chem.*, **264**, 9911-9914.

141. A. W. Johnson and B. Demple (1988). Yeast DNA Diesterase for 3'-Fragments of Deoxyribose: Purification and Physical Properties of a Repair Enzyme for Oxidative DNA Damage. *J. Biol. Chem.*, **263**, 18009-18016.

142. W. A. Franklin and T. Lindahl (1988). DNA deoxyribophosphodiesterase. *EMBO J.*, **7**, 3617-3622.

143. F. T. Gates III and S. Linn (1977). Endonuclease V of *Escherichia coli*. *J. Biol. Chem.*, **252**, 1647-1653.

144. H. W. Fescemyer and A. M. Hammond (1986). Effect of density and plant age on color phase variation and development of larval velvetbean caterpillar, Anticarsia *gemmatalis* Hubner (*Lepidoptera: Noctuidae*). *Environ. Entomol.*, **15**, 784-789.

145. S. D. Hensley and A. M. Hammond (1968). Laboratory techniques for rearing the sugarcane borer on an artificial diet. *J. Econ. Entomol.*, **61**, 1742-1743.

146. R. M. Roe, A. M. Hammond and T. C. Sparks (1982). Growth of larval *Diatraea saccharalis (Lepidoptera: Pyralidae)* on an artificial diet and synchronization of the last larval stadium Sugarcane borer. *Ann. Entomol. Soc. Am.*, **75**, 421-429.

147. C. W. Clifford, R. M. Roe and J. P. Woodring (1977). Rearing methods for obtaining house crickets, *Acheta domesticus*, of known age, sex, and instar. *Ann. Entomol. Soc. Am.*, **70**, 69-74.

148. C. U. Wittwer and H. Krokan (1985). Uracil-DNA glycosylase in HeLa S_3 cells: interconvertibility of 50 and 20 kDa forms and similarity of the nuclear and mitochondrial form of the enzyme. *Biochim. Biophys. Acta*, **832**, 308-318.

149. W. G. Burton, C. T. Grabowy and R. Sager (1979). Tole of methylation in the modification and restriction of chloroplast DNA in *Chlamydomonas*. *Proc. Natl. Acad. Sci. USA*, **76**, 1390-1394.

150. P. D. Sadowski and J. Hurwitz (1969). Enzymatic Breakage of Deoxyribonucleic Acid. II. Purification and Properties of endonuclease IV from T4 Phage-infected *Escherichia coli*. *J. Biol. Chem.*, **244**, 6192-6198.

151. T. A. Bickle (1982). The ATP-dependent Restriction Endonucleases. In *Nucleases*. S. M. Linn and R. J. Roberts, eds., pp. 85-108, Cold Spring Harbor Laboratory, New York.

152. A. R. Price and J. Frato (1975). *Bacillus subtilis* Deoxyuridinetriphosphatase and its Bacteriophage PBS2-induced Inhibitor. *J. Biol. Chem.*, **250**, 8804-8811.

153. H. M. Ellis and H. R. Horvitz (1986). Genetic Control of Programmed Cell Death in the Nematode *C. elegans*. *Cell*, **44**, 817-829.

154. A. H. Wylie (1980). Glucocorticoid-induced thymocyte apoptosis is associated with endogenous endonuclease activation. *Nature*, **284**, 555-556.

APPENDIX A THE PRESENCE OF URACIL-DNA GLYCOSYLASE IN INSECTS IS DEPENDENT UPON DEVELOPMENTAL COMPLEXITY[2]

A.1 Abstract

The metamorphosis of insects can, in a general way, be divided between those organisms that undergo pupation accompanied by cellular histolysis and those that gradually develop into adults without an intervening pupal stage of development. In the former case, the death of a cell population is an integral part of development that is tightly associated with massive DNA degradation during pupation. In that regard, it has been suggested that uracil-containing DNA acts as a target for the nucleolytic breakdown of DNA during histolysis in insects (133), thus placing into question how compatible the existence of uracil-DNA glycosylases would be for this form of developmental signal. As a result, we tested for the presence of a uracil-DNA glycosylase in insects representative of those having an intervening pupal stage of development and those that do not. We show here that a nonpupating insect contains a uracil-DNA glycosylase activity. Conversely, crude extracts of *Drosophila melanogaster*, as well as three other insect populations that undergo pupation similar to that found in *Drosophila*, do not contain detectable levels of this DNA repair activity. Thus, there appears to be a consistent correlation between cellular destruction during development and the absence of a uracil-DNA glycosylase, which supports the possibility that uracil-containing DNA may play an important role in those cells targeted for death.

[2] Reprinted by permission of the Journal of Biological Chemistry.

A.2 Introduction

Uracil is found in DNA either as the consequence of misincorporation during DNA synthesis or, alternatively, as the result of cytosine deamination. The latter event has been shown to be mutagenic, causing GC:AT transition mutations in bacterial strains lacking uracil-DNA glycosylase activity (*ung*$^-$), thus demonstrating the importance of this enzyme (134). Indeed, uracil-DNA glycosylases were assumed to exist in virtually all organisms. However, the ubiquitous nature of this activity eventually came into some doubt when a number of laboratories failed to detect the repair of uracil-containing DNA in extracts from *Drosophila melanogaster* (135-137). On the other hand, *Drosophila* was found to contain a nuclease that preferentially acts on uracil-containing DNA, but only in developmental stages prior to the cellular destruction observed during histolysis (136). In view of this, a closer examination of uracil metabolism in *Drosophila* was undertaken. These studies revealed that the dUTPase activity responsible for keeping cellular dUTP levels low in relationship to TTP is also developmentally expressed and limited to embryonic stages coincident to the production of cells ultimately destroyed during pupation (138). Finally, an inhibitor of dUTPase activity was also detected in these early stages of *Drosophila* development, where it was presumed that it acted to moderate dUTPase activity, thereby providing a greater opportunity for uracil incorporation into DNA (133, 139).

The novel features associated with uracil metabolism in *Drosophila* provided an experimental basis for suggesting that perhaps insects as a whole were deficient in uracil-DNA glycosylase activity (136). Recently, however, it was shown that *Drosophila*, as well as the locust *Locusta migratoria*, contains this DNA repair activity (140). Notably, the developmental pathways used by these two organisms are vastly

different (see Table A.1), giving us reasons to reinspect insects with regard to those that pupate like *Drosophila* as opposed to those insects like locusts that emerge from the egg and pass through immature stages of development (nymph) until they become sexually mature. In this paper, we confirm, using another nonpupating organism similar to the locust, the existence of a uracil-DNA glycosylase activity. On the other hand, we were unable to find this activity in *Drosophila* or in three other insect populations that undergo pupation. The absence of uracil-DNA glycosylase activity may therefore be unique to only those insects that undergo pupation.

A.3 Materials and Methods

A.3.1 Materials

Deoxy[5-^{3}H]uridine 5'-triphosphate and deoxycytidine 5'-[α-^{32}P]triphosphate were purchased from Amersham Corp. [α-^{32}P] dUTP was prepared from [α-^{32}P]dCTP by deamination of 1 N NaOH as described by Johnson and Demple (141).

A.3.2 Preparation of [uracil-^{3}H, ^{32}P]Poly(dA-dT)

Poly(dA-dT) containing [*uracil*-^{3}H,α-^{32}P]dUMP was made essentially as described by Johnson and Demple (141).

A.3.3 Assay of Uracil-DNA Glycosylase Activity

Reaction conditions were as described by Morgan and Chlebek (140), except for the manner in which assays were terminated and radioactive material was measured. Briefly, reactions (50μl) contained 40 mM Tris-HCl, 1 mM EDTA, 70 mM NaCl, and radioactive poly(dA-dT). Incubations were generally for 20 min at 37°C, at which time assays were precipitated by the addition of 20 μg of calf thymus DNA, 110 μl of 10% trichloroacetic acid, and 30 μl of 5% Norit suspension and were centrifuged in a

microcentrifuge for 15 min at 4°C (142). Radioactive material in the supernatant was determined by removing an aliquot and measuring for radioactive material.

Norit-nonabsorbed reaction products were determined by ascending polyethyleneimine-cellulose thin-layer chromatography as described by Gates and Linn (143).

A.3.4 Insect Populations

Insects chosen for this study are identified in Table A.1. *Anticarsia gemmatalis* eggs were from a colony kept in the Department of Entomology, Louisiana State University, Agricultural Experiment Station, and were maintained according to previously described methods (144). *Apis mellifera* eggs were obtained from an active bee hive maintained by personnel of the Bee Breeding Laboratory, United States Department of Agriculture (Baton Rouge, La.). *Diatraea saccharalis* eggs were obtained from a laboratory colony maintained according to previously described procedures (145, 146). *Acheta domesticus* eggs and nymphs were collected from a colony maintained by the techniques described by Clifford *et al.* (147). *D. Melanogaster* (Oregon-R) embryos were collected and stored as described by Deutsch and Spiering (136) and Giroir and Deutsch (138). *Drosophila* embryos that had not been subjected to dechorionation were a generous gift of Dr. M. R. Kelley (Loyola Medical School, Maywood, Ill.).

A.3.5 Preparation of Extracts

Organisms identified in Table A.1 were placed in 40 mM Tris-HCl, pH 8, 1 mM dithiothreitol, 4 mM EDTA, 1 mM phenylmethylsulfonyl fluoride, and 0.2 M NaCl and

were homogenized in a glass homogenizer as described by Morgan and Chlebek (140). Cellular debris was generally removed by centrifugation at 12,000 × *g*.

A.3.6 Other Methods

Protein was measured by the technique of Bradford (95) using the Bio-Rad protein kit. Buffer pH values were routinely checked at 50 mM and room temperature.

A.4 Results

The search for a uracil-DNA glycosylase activity in insects originally focused on an organism that closely parallels the type of developmental life cycle found in locusts (Table A.1). The organism chosen was the cricket *A. domesticus*, which is a representative member of a group of insects that lack a pupal stage of development. Initial experiments did reveal some activity in this organism that was considerably enhanced when the pH optimum for the uracil-DNA glycosylase activity was subsequently discovered to be acidic and sharply centered around 6.0 (Fig.A.1).

Table A.1 Types of insect populations tested for uracil-DNA glycosylase activity.

Endopterygota[a]	Exopterygota[b]
A. gemmatalis (velvetbean caterpillar)	*A. domesticus* (house cricket)
A. mellifera (honeybee)	
D. saccharalis (sugarcane borer)	
D. melanogaster	

[a]These insects undergo larval and pupal stages of development and develop their wings internally until they are externalized at the pupal molt. [b]These insects lack a pupal stage and develop their wings externally. The locust *L. migratoria*, which was previously identified as having uracil-DNA glycosylase activity (140), is also a representative member of this group of insects.

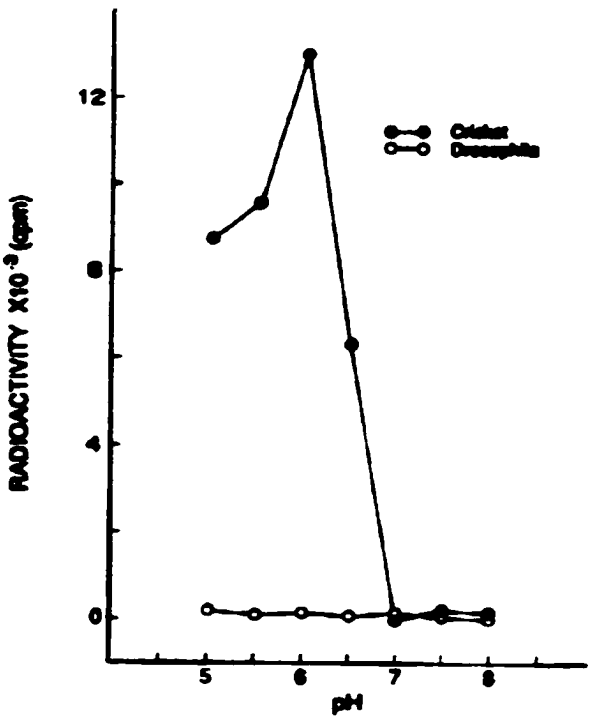

Fig. A.1 Determination of pH optimum. Reactions (50 µl) contained 5 or 2 µg of *Drosophila* or cricket protein, respectively, and ~100,000 cpm of [*uracil*-^{3}H]poly(dA-dT). Assays were terminated with 144 µl of Norit suspension and centrifuged, and the supernatant (50 µl) was determined for radioactivity.

A common characteristic shared by uracil-DNA glycosylases found in other organisms is their inhibition by free uracil (135, 148). The activity detected in crickets was also inhibited by uracil (Table A.2), suggesting that the liberation of Norit-nonabsorbed material was due to the presence of an authentic uracil-DNA glycosylase protein. This was verified by separating the products of the reaction by polyethyleneimine chromatography (Fig. A.2), in which 95% of the Norit-nonabsorbed radioactivity was detected coincident with authentic uracil. The remainder of radioactive material migrated close to the origin of the polyethyleneimine chromatogram and most likely was oligonucleotides produced by nonspecific nucleases.

Table A.2 Uracil-DNA glycosylase activity in the house cricket (*A. domesticus*).

Organism	Activity
	pmol/min
A. domesticus	43
A. domesticus + 2.5 mM uracil	<1
A. domesticus + *D. melanogaster*	42
D. melanogaster	<1

Each reaction received 4 μg of crude extract protein. In the mixing experiment, a protein extract (4 μg) of *Drosophila* was incubated for 5 min prior to the addition of a crude extract (4 μg) of *A. domesticus*.

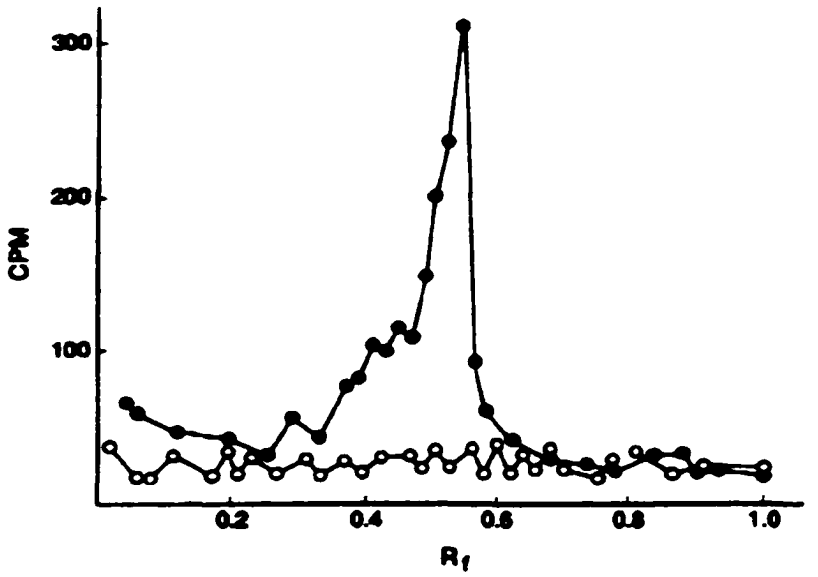

Fig. A.2 Thin-layer chromatography of reaction products. Complete reactions indicated that ~3500 cpm of ^3H were liberated by extracts (2 μg) of 1-day-old crickets. Thirty-two μl were applied to a polyethyleneimine-impregnated cellulose thin-layer plate along with authentic uracil and developed as described by Gates and Linn (143). Roughly 60% of the radioactivity applied to the chromatogram was recovered, with the majority as free uracil. ●, plus extract; ○, minus extract.

The above experiments were conducted using 1-day-old crickets (nymphs), which appear to have more uracil-DNA glycosylase activity than do embryos (Table A.3). Furthermore, there is not a sharp and distinctive pH optimum for the DNA glycosylase activity observed in embryos (data not shown). Thus, it may be that different forms of uracil-DNA glycosylase reside in crickets, one of which is originally expressed at emergence from the embryo.

Table A.3 Uracil-DNA glycosylase activity in different insects.

Organism	Activity
	pmol/min
A. gemmatalis	<1
A. mellifera	<1
A. saccharalis	<1
D. saccharalis first instar larvae	<1
D. melanogaster	<1
A. domesticus	
Embryos, with chorion	15
Embryos, chorion removed	3
1-Day-old adult (nymph)	29
E. coli uracil-DNA glycosylase	84
E. coli uracil-DNA glycosylase + *Drosophila* extract	77

Reactions were conducted at pH 6.0, except for those using purified *E. coli* uracil-DNA glycosylase, which were assayed at pH 7.5. Incubations were for 20 min at 37°C. Each reaction received 5 μg of crude extract protein or 2 units of *E. coli* uracil-DNA glycosylase capable of releasing 1 nmol of free uracil in 1 h at 37°C. Unless otherwise stated, extracts were produced from organisms in the embryonic stage of development.

Somewhat puzzling was the finding that there appears to be a relationship between the levels of uracil-DNA glycosylase activity detected and whether the insect was exposed to conditions to remove its chorion, as originally suggested by Morgan and

Chlebek (140). As seen in Table A.3, roughly 5-fold more uracil-DNA glycosylase activity was observed in cricket embryos retaining intact chorions.

Having established the presence of a uracil-DNA glycosylase in crickets, we then turned to evaluating *Drosophila*, which is an example of an organism that undergoes pupation. We originally attempted to determine if, like crickets, the DNA glycosylase activity may also have an acidic pH optimum. However, tests performed at pH 5-8 failed to reveal detectable amounts of activity (Fig. A.1). Eliminating sonication proved to be an unsatisfactory means of revealing any activity, as did toluene treatment of embryos or the use of nondechorionated embryos (140). Thus, the use of a variety of conditions failed to show detectable amounts or uracil-DNA glycosylase activity in *Drosophila.*

An obvious distinction can be made between *Drosophila* and crickets as to the manner in which they develop after embryogeneses toward the onset of adulthood (Table A.1). It therefore seemed reasonable to question whether insects that undergo pupation such as *Drosophila* also lack uracil-DNA glycosylase activity. As seen in Table A.3, three additional organisms that share the common feature of undergoing pupation also lacked detectable amounts of activity on uracil-containing DNA. The extraction procedures or assay conditions were once again varied for experiments with the three other pupating species of insects identified in Tables A.1 and A.3, with the same unsuccessful results as for *Drosophila.*

One last question regarding the apparent absence of uracil-DNA glycosylase activity in *Drosophila* is whether there might be certain inhibitory factors present in their cells that could mask its detection. To test this, *Drosophila* extracts were

combined with labeled uracil-containing DNA for 5 min, and then purified *Escherichia coli* uraci-DNA glycosylase was added and allowed to incubate for the normal 20 min. As seen in Table A.3, the presence of *Drosophia* extracts had virtually no effect on the ability of the *E. coli* enzyme to liberate uracil residues from DNA. Similar results were obtained when *Drosophila* extracts failed to inhibit the uracil-DNA glycosylase activity present in *Bacillus subtilis* (135). Likewise, combining extracts of *Drosophila* and *A. domesticus* also failed to change the amount of activity revealed by the cricket protein (Table A.2). Taken together, the inability to detect uracil-DNA glycosylase activity in *Drosophila* does not appear to be due to some endogenous protease or inhibitory factor.

A.5 Discussion

After the formation of the cellular blastoderm in *Drosophila* embryogenesis, segregation of cells takes place; some of these cells are earmarked for their eventual destruction through a process known as histolysis. One of the characteristics associated with cellular death is DNA degradation, which could be mediated through a random nucleolytic attack on DNA or, perhaps instead, through a more selective pathway of DNA degradation. For example, the inheritance of paternal *versus* maternal chloroplasts in *Chlamydomonas* is dictated by DNA modifications in which the maternal chloroplast is methlylated and stably inherited. Notably, paternal chloroplasts, which are degraded, contain the nonconventional base uracil in their DNA (149). Other examples exist in which the existence of modified or nonconventional bases in DNA is important for directing the breakdown or preserving the integrity of DNA molecules (150, 151).

For the four insect populations examined in this study that undergo pupation (Table A.1), we found that they all share the same characteristic of also lacking

detectable levels of an enzyme necessary for the removal of uracil residues in DNA. One may explain these results by hypothesizing that these insects utilize uracil-containing DNA as a target for initiating the DNA degradation associated with pupation. This interpretation of the data is reinforced by the previous finding of a protein inhibitor for *Drosophila* embryonic dUTPase (139), in which dUTPase is the main safety valve for preventing dUMP incorporation in DNA. Inhibition of dUTPase by a protein inhibitor has been identified in only one other organism, in which *B. subtilis* phage PBS2 induces an inhibitor of host-cell dUTPase, resulting in PBS2 having the only known genome that contains uracil instead of thymine in its DNA (152).

The presence of a pathway that moderates dUTPase activity, thus providing a greater opportunity for uracil incorporation into DNA, suggests a strategy that in all likelihood is part of a programed cycle that ultimately leads to the death of certain cells. Programed cellular death is known to exist in *Caenorhabditis elegans* (153) and in the glucocorticoid-mediated cytolysis of thymocytes (154). In *Drosophila*, and perhaps in other insects that pupate, this program could involve the incorporation of uracil into the DNA of cells targeted for destruction, most likely through the moderation of dUTPase activity (139). Subsequently, a nuclease expressed as part of the histolyzation process would selectively degrade the uracil-containing DNA (136). Clearly, the presence of a uracil-DNA glycosylase would be incompatible with this form of instructed cellular death.

APPENDIX B LETTERS OF PERMISSION

10/15/99 15:17

ACADEMIC PRESS

Academic Press, Inc.
6277 Sea Harbor Drive
Orlando, FL 32887
Tel 407-345-2000
Fax 407-345-4058

Dear Requestor:

Thank you for your request to use material from your work published in an Academic Press publication.

It is now the policy of Academic Press that authors need not obtain permission in the following cases: (1) to use their original figures or tables in their future works; (2) to make copies of their papers for their classroom teaching; and (3) to include their papers as part of their dissertations/thesis.

Sincerely,

Ana Merced 10/15/99

Ana Merced
Paralegal Department
Academic Press - Permissions
407 345 3994
407 345 4058
amerced@harcourtbrace.com

A Division of Harcourt Brace & Company

Subj: Copyright Permission
Date: 3/26/99 3:55:51 PM Central Daylight Time
From: jmezger@asbmb.faseb.org (Juana Mezger)
To: bfdudley@aol.com

Dear Dr. Dudley:

Please note your recent request for copyright permission has been granted for the following:

Volume: Page, Year

267: 11964-11967, 1992

Please note your original will follow by mail only if requested. For future requests, we can be contacted by e-mail at jbc@asbmb.faseb.org. If you have any questions, please contact us at the number listed above.

Sincerely yours,

PERMISSION GRANTED
contingent upon obtaining that of the author

JUANA MEZGER

for the copyright owner
THE AMERICAN SOCIETY FOR BIOCHEMISTRY
AND MOLECULAR BIOLOGY

---------- Headers ----------
Return-Path: <jmezger@asbmb.faseb.org>
Received: from rly-ya01.mx.aol.com (rly-ya01.mail.aol.com [172.18.144.193]) by air-ya03.mx.aol.com (v58.16) with SMTP; Fri, 26 Mar 1999 15:55:51 -0500
Received: from fw.faseb.org (fw.faseb.org [12.17.12.66])
by rly-ya01.mx.aol.com (8.8.8/8.8.5/AOL-4.0.0)
with ESMTP id PAA02946 for <bfdudley@aol.com>;
Fri, 26 Mar 1999 15:55:48 -0500 (EST)
Received: from asbmb.faseb.org (asbmb.faseb.org [192.0.209.253])
by fw.faseb.org (8.9.1a/8.9.1) with SMTP id QAA09669
for <bfdudley@aol.com>; Fri, 26 Mar 1999 16:02:17 -0500 (EST)
Received: by asbmb.faseb.org(Lotus SMTP MTA v1.06 (346.8 3-18-1997)) id 85256740.0072FE3C ;
Fri, 26 Mar 1999 15:56:01 -0400
X-Lotus-FromDomain: ASBMB
From: "Juana Mezger"<jmezger@asbmb.faseb.org>
To: bfdudley@aol.com
Message-ID: <85256740.0072974D.00@asbmb.faseb.org>
Date: Fri, 26 Mar 1999 15:52:55 -0400
Subject: Copyright Permission
Mime-Version: 1.0
Content-type: text/plain; charset=US-ASCII

HYPERBOLIC CURVE FIT

****

FIT TO v = Vm*A/(K + A)

****

#	[A]	1/[A]	Vobs	1/Vobs	Vcal	1/Vcal	Diff
1	1.670E+01	5.988E-02	1.170D+02	8.544E-03	1.185E+02	8.442E-03	-1.411D+00
2	3.340E+01	2.994E-02	1.914D+02	5.226E-03	1.921E+02	5.206E-03	-7.382D-01
3	5.010E+01	1.996E-02	2.458D+02	4.069E-03	2.423E+02	4.127E-03	3.476D+00
4	6.680E+01	1.497E-02	2.809D+02	3.560E-03	2.787E+02	3.587E-03	2.139D+00
5	8.350E+01	1.198E-02	3.085D+02	3.242E-03	3.064E+02	3.264E-03	2.068D+00
6	1.002E+02	9.980E-03	3.168D+02	3.156E-03	3.281E+02	3.048E-03	-1.123D+01
7	1.336E+02	7.485E-03	3.653D+02	2.738E-03	3.599E+02	2.778E-03	5.335D+00

CONST.	VALUE	S.E.	Weight
K=	5.4894D+01	4.0851D+00	5.9922E-02
V=	5.0781D+02	1.6027D+01	3.8930E-03
K/V=	1.0810D-01	4.8369D-03	4.2743E+04
1/V=	1.9692D-03	6.2151D-05	2.5888E+08
V/K=	9.2508D+00	4.1393D-01	5.8365E+00

SIGMA= 5.967630D+00

VARIANCE= 3.561261D+01

HYPERBOLIC CURVE FIT-PNSP 01-16-2000

HYPERBOLIC CURVE FIT

****

FIT TO v = Vm*A/(K + A)

****

#	[A]	1/[A]	Vobs	1/Vobs	Vcal	1/Vcal	Diff
1	8.300E+00	1.205E-01	7.240D+01	1.381E-02	7.467E+01	1.339E-02	-2.271D+00
2	1.670E+01	5.988E-02	9.972D+01	1.003E-02	9.899E+01	1.010E-02	7.289D-01
3	2.500E+01	4.000E-02	1.170D+02	8.547E-03	1.108E+02	9.023E-03	6.170D+00
4	3.340E+01	2.994E-02	1.148D+02	8.710E-03	1.180E+02	8.477E-03	-3.158D+00
5	4.000E+01	2.500E-02	1.210D+02	8.263E-03	1.218E+02	8.209E-03	-8.018D-01
6	4.500E+01	2.222E-02	1.232D+02	8.119E-03	1.241E+02	8.058E-03	-9.362D-01

CONST.	VALUE	S.E.	Weight
K=	7.9217D+00	1.1669D+00	7.3435E-01
V=	1.4595D+02	5.2708D+00	3.5996E-02
K/V=	5.4278D-02	6.2315D-03	2.5752E+04
1/V=	6.8519D-03	2.4745D-04	1.6331E+07
V/K=	1.8424D+01	2.1151D+00	2.2352E-01

SIGMA= 3.716732D+00

VARIANCE= 1.381409D+01

HYPERBOLIC CURVE FIT

****

FIT TO v = Vm*A/(K + A)

****

#	[A]	1/[A]	Vobs	1/Vobs	Vcal	1/Vcal	Diff
1	4.200E+00	2.381E-01	4.269D+01	2.343E-02	4.195E+01	2.384E-02	7.361D-01
2	8.300E+00	1.205E-01	5.679D+01	1.761E-02	5.684E+01	1.759E-02	-4.255D-02
3	1.670E+01	5.988E-02	6.798D+01	1.471E-02	6.955E+01	1.438E-02	-1.571D+00
4	2.500E+01	4.000E-02	7.454D+01	1.342E-02	7.506E+01	1.332E-02	-5.205D-01
5	3.340E+01	2.994E-02	7.973D+01	1.254E-02	7.820E+01	1.279E-02	1.533D+00

CONST.	VALUE	S.E.	Weight
K=	4.7398D+00	3.6789D-01	7.3885E+00
V=	8.9294D+01	1.7619D+00	3.2215E-01
K/V=	5.3081D-02	3.2353D-03	9.5534E+04
1/V=	1.1199D-02	2.2097D-04	2.0481E+07
V/K=	1.8839D+01	1.1483D+00	7.5845E-01

SIGMA= 1.370347D+00

VARIANCE= 1.877850D+00

HYPERBOLIC CURVE FIT-PNSP 01-16-2000

HYPERBOLIC CURVE FIT

****

FIT TO v = Vm*A/(K + A)

****

#	[A]	1/[A]	Vobs	1/Vobs	Vcal	1/Vcal	Diff
1	9.500E+01	1.053E-02	6.317D+02	1.583E-03	7.001E+02	1.428E-03	-6.837D+01
2	1.400E+02	7.143E-03	8.877D+02	1.127E-03	9.244E+02	1.082E-03	-3.674D+01
3	1.600E+02	6.250E-03	9.736D+02	1.027E-03	1.010E+03	9.903E-04	-3.613D+01
4	2.000E+02	5.000E-03	1.295D+03	7.723E-04	1.160E+03	8.623E-04	1.351D+02
5	3.000E+02	3.333E-03	1.503D+03	6.655E-04	1.446E+03	6.915E-04	5.656D+01
6	4.000E+02	2.500E-03	1.577D+03	6.342E-04	1.650E+03	6.062E-04	-7.281D+01

CONST.	VALUE	S.E.	Weight
K=	2.9261D+02	8.7307D+01	1.3119E-04
V=	2.8564D+03	4.6740D+02	4.5774E-06
K/V=	1.0244D-01	1.4486D-02	4.7651E+03
1/V=	3.5008D-04	5.7285D-05	3.0474E+08
V/K=	9.7621D+00	1.3805D+00	5.2469E-01

SIGMA= 9.229716D+01

HYPERBOLIC CURVE FIT

****

FIT TO v = Vm*A/(K + A)

****

#	[A]	1/[A]	Vobs	1/Vobs	Vcal	1/Vcal	Diff
1	1.000E+00	1.000E+00	2.694D+02	3.713E-03	2.561E+02	3.905E-03	1.328D+01
2	2.100E+00	4.762E-01	3.722D+02	2.687E-03	3.693E+02	2.708E-03	2.913D+00
3	4.200E+00	2.381E-01	4.405D+02	2.270E-03	4.622E+02	2.164E-03	-2.166D+01
4	8.300E+00	1.205E-01	5.214D+02	1.918E-03	5.277E+02	1.895E-03	-6.325D+00
5	1.670E+01	5.988E-02	5.770D+02	1.733E-03	5.693E+02	1.756E-03	7.610D+00
6	2.500E+01	4.000E-02	5.922D+02	1.689E-03	5.845E+02	1.711E-03	7.770D+00

CONST.	VALUE	S.E.	Weight
K=	1.4112D+00	1.2095D-01	6.8362E+01
V=	6.1745D+02	1.1735D+01	7.2618E-03
K/V=	2.2856D-03	1.6499D-04	3.6735E+07
1/V=	1.6196D-03	3.0780D-05	1.0555E+09
V/K=	4.3753D+02	3.1585D+01	1.0024E-03

SIGMA= 1.425037D+01

VARIANCE= 2.030731D+02

HYPERBOLIC CURVE FIT-PNSP 01-16-2000

VITA

Billy Fred Dudley was born in Shreveport, Louisiana, on November 27, 1968. He is the son of Billy F. Dudley, Sr. and Betty J. Dudley. He graduated from Captain Shreve High School in Shreveport, Louisiana in June 1986 and spent the summer working in the Medical Toxicology Department of Louisiana State University Medical School in Shreveport. In the Fall of 1986 Billy enrolled at Louisiana State University in Baton Rouge where he completed his bachelor of science degree in Biochemistry in August 1991. He was then accepted in the graduate program of the Biochemistry Department at Louisiana State University. He will receive a doctor of philosophy degree in biochemistry with a minor in physiology at spring commencement 2000.

DOCTORAL EXAMINATION AND DISSERTATION REPORT

Candidate: Billy F. Dudley, Jr.

Major Field: Biochemistry

Title of Dissertation: Activation and Metabolism of p-Nitrosophenol and 2,2'-Thiobis-ethanol by Horse Liver and Human Alcohol Dehydrogenase: Toxicological Implications

Approved:

Major Professor and Chairman

Dean of the Graduate School

EXAMINING COMMITTEE:

Date of Examination:

March 16, 2000